THE LAMINAR BOUNDARY LAYER ON SPINNING BODIES OF REVOLUTION

By

Ralph John Muraca

Thesis submitted to the Graduate Faculty of the
Virginia Polytechnic Institute
in partial fulfillment for the degree of

DOCTOR OF PHILOSOPHY

in

Aerospace Engineering

APPROVED: _____

Chairman, Dr. R. T. Davis

_____ _____

Dr. F. R. DeJarnette Dr. F. Lutze

_____ _____

Dr. Yau Wu Dr. J. C. Smith, Jr.

June 1970

Blacksburg, Virginia

TABLE OF CONTENTS

LIST OF FIGURES

LIST OF TABLES

CHAPTER I. INTRODUCTION

1. Statement of the Problem

The goal of this effort is the solution of the differential equations describing the laminar boundary layer on a spinning body of revolution immersed in a steady oncoming stream. The bodies of revolution to be considered must be analytic, and must have inviscid solutions available. The flow may be compressible or imcompressible and the only limitation on spin rate involves the assumption that the pressures through the boundary layer normal to the body are essentially constant. The order of magnitude of the limiting value of spin rate will be defined as a function of the oncoming stream velocity. The equations describing the boundary layer on a spinning body are presented in nondimensional form. The Mangler and Howarth-Dorodnitsyn transformations are utilized to transform the governing physical equations to a similarity form.

The boundary conditions required to solve the set of differential equations cannot always be expressed in algebraic form, consequently, in some instances a set of ordinary differential equations must be solved along with the partial differential equations, to obtain the necessary boundary conditions.

The resulting set of differential equations are reduced to a set of difference equations using central differences to approximate

derivatives in the direction normal to the body and a two-point backward difference to approximate derivatives in the meridional direction. The use of a backward difference to replace derivatives in the meridional directions places this method in the implicit category. As such a simpler method of solution can be utilized than those associated with explicit finite difference methods.

The accuracy of the solutions obtained herein is demonstrated by comparing these results with data obtained by other investigators for a variety of cases.

The effect of variations in step size in the normal and meridional direction on the solutions obtained for a few geometries and flow conditions are also investigated along with the convergence properties of the method.

The characteristics of the boundary layers associated with spinning bodies are presented in the form of the shear stress in both the meridional and circumferential directions; the heat transfer at the body surface, and the total frictional moment and drag coefficients.

2. Literature Survey

The problems of flow about nonrotating bodies, and flow about bodies rotating in a still medium have been considered and in many instances the equations describing the boundary layers for these situations have been solved. However, the combined problem of forced flow about a spinning body has not received nearly so much attention. One of the earliest references on the subject is by Hannah[1], who considered the

incompressible flow about a spinning disc. The solution of Cochran[2] for the flow due to an infinite rotating lamina, and Homann[3] for flow about an infinite stationary lamina were used to obtain the form of the solution for the entire viscid/inviscid flow field. Utilizing these known solutions similarity variables were found which transformed the partial differential equations into ordinary differential form. The resulting ordinary differential equations were numerically integrated. The equations derived by Hannah are not restricted in any way and reduce to either Homann's or Cochran's equations for either Ω, the spin rate, or U_∞, the free-stream velocity, equal to zero. Tifford and Chu[4], and Schlicting and Truckenbrodt[18] consider the same problem as Hannah. Tifford and Chu give no details of their method of solution and imply that it is similar to Hannah's. Schlicting and Truckenbrodt use the Karman-Polhausen method to obtain their results.

Illingworth[5] considered the problem of compressible flow about a spinning body of revolution and in particular presented the solution for the case of a spinning cone. He used the von Mises and Mangler transformations to obtain an "incompressible" planar form for the describing differential equation. A series solution involving a parameter containing spin rate, edge velocity and radius is assumed and a set of ordinary differential equations result. Second-order solutions have been obtained in this manner. The solutions thus

presented are restricted to small values of the spin parameter. A Prandtl number of unity is assumed in this analysis.

Schlicting[6] presents a method for solving the incompressible laminar boundary layer equations for arbitrary bodies of revolution. This method consists of applying momentum integral methods in both the meridional and circumferential directions. Fourth-order polynomials are used to represent the velocity profiles and solutions for the two resulting ordinary differential equations involving displacement thickness are obtained. In this formulation the form constant K which determines separation includes a spin term, consequently, this analysis is limited in spin. Results are presented for a sphere (with potential edge velocity), a body with a blunt base, and a streamlined body.

Illingsworth[7] also considered the problem of the boundary layer growth on a spinning body at low velocities and spin rates. As a first-order solution only diffusion terms are considered and in the second and third-order solution convection and pressure terms are considered. He obtains a solution for the shear stress in both the meridional and circumferential directions as a function of time, spin rate, and edge velocity.

Schmidt[8] presents some experimental results for cones and cone cylinders at various Mach numbers and spin rates. These were obtained from gun firings in a spark photography range. The data presented includes drag, normal forces and moments on the bodies.

Kelly[9] considers the problem of spinning bodies with small yaw angles. As such Kelly's paper is representative of a group of papers

which deal with the problem of spin and yaw in an effort to better define Magnus forces. Kelly considers a hollow cylinder spinning about its axis of revolution in an incompressible stream at small angle of attack, α. A perturbation solution in both angle of attack and spin rate is utilized. Carrying terms to order α^2, Ω^2, and $\alpha\Omega$ yields ultimately a set of forty-five ordinary differential equations which are solved numerically. Kelly's report represents an extension of and correction to Martin's work[11]. Sedney[13] applies this technique to a cone in compressible flow and it is noted that his zero angle of attack case reproduces Illingsworth's cone results for spin only. Fieberg[15] also solves the case of compressible flow over a cone using the same basic approach but with slightly different transformations thereby eliminating Mach number and cone angle as parameters. Of major importance in Kelly's work is the identification of the primary causes of Magnus forces on spinning bodies.

Yamaga[19] uses the same approach as Schlicting to solve the problem for compressible flow over a spinning sphere. He assumes Prandtl number of unity and a linear viscosity temperature relationship. This analysis is also spin and Mach number limited.

Siekmann[20] presents a method for determining the thermal boundary layer on a spinning sphere. The velocity profiles are obtained from Hoskin's[24] work which involves a series solution in powers of arc length along the body. These calculations were for the incompressible boundary layer on a sphere. The resulting differential equations are numerically integrated.

Tien and Tsuei[29] utilize a series solution in spin rate to obtain solutions for a spinning cone in incompressible flow. Two distinctive regions are considered. The first is slow spin rates and a solution is postulated which to zeroth order matches the solution for flow about a stationary cone. For a case of high spin rates an entirely different expansion is postulated. The zeroth order solution obtained by this approximation matches the case of a cone spinning with no forced flow. Although the solutions cannot be easily matched in the boundary layer due to the differently defined normal coordinates the solution at the surface can be matched directly.

Rubinow and Keller[22] consider the problem of a spinning sphere moving in an incompressible fluid with small Reynolds number. The Navier-Stokes equations were reduced to tractable form through the use of the Stokes expansion for the inner solution and the Oseen expansion for the outer solution. First and second-order inner and outer solutions were obtained and matching was used to obtain a complete solution.

Rott and Lewellen[26] presented a survey of the work done on incompressible rotating boundary layers on axisymmetric bodies. They discuss similar solutions and their limitations with respect to transverse pressure gradients and body curvature. A general momentum integral solution is presented which is applicable to both laminar and turbulent flows. Results of this method applied to a power law body are also presented. In addition, the interaction of the boundary layer with the

outer flow for the case of enclosed flows is discussed. Limitations involved with the pressure gradients across the boundary layer are also discussed.

Koh and Price[28] were the first to consider direct integration of the partial differential equations describing the boundary layer on a spinning body. They consider the incompressible flow on a spinning cone. An implicit finite difference scheme is used to integrate the equations. Since this is not an approximate method the results are not restricted except by the assumption that the pressure is constant across the boundary layer. This imposes a restriction on the maximum rate of spin for which solutions are valid.

3. List of Symbols

a^*, b^*	parameters in hyperbola equation
A,B,C,D	coefficients in the polynomial representations to determine derivatives at the wall (eq. (III-14))
A_n, B_n, C_n, D_n	coefficient in the finite difference formulation (eq. (III-8))
BC_1, BC_2, BC_3	coefficients in the general boundary condition equation (eq. (III-13))
B1 to B11	coefficients (eqs. (II-101(a) to (k))
C_p^*	specific heat of constant pressure
C_{D_f}	viscous drag coefficient (eq.(II-99)

C_{M_ϕ} viscous moment coefficient (eq.(II-100))

D^* viscous drag (eq. (II-86))

E dimensionless quantity $\frac{U_\infty^{*2}}{C_p^* T_\infty^*}$

E_n, G_n quantities in the finite difference solution (eq. (III-21))

F meridional velocity function u/u_e

j parameter related to cone angle in the Falkner-Skan inviscid solution

K form constant from Schlicting

k^* local curvature of the body ($1/R^*$)

l $(\rho\mu)/(\rho\mu)_e = \psi/\theta$

m,n subscripts denoting the mth and nth steps related ξ to η, respectively

M_ϕ^* viscous moment (eq. (II-87))

M_∞ Mach number free-stream

n^* normal coordinate

N $n/\sqrt{Rey}$ - transformed normal coordinate

p^* parameter in parabola equation

p^* pressure

P_r Prandtl number $\frac{\mu^* C_p^*}{\kappa^*}$

q_w^* heat transfer at the wall

r' dr/ds

r^* local radius from axis of symmetry

r_b^*	radius at upper limit of surface integration
R^*	radius of curvature
R_{es}	local Reynolds number $\frac{\rho_e u_e s}{\mu_e}$
Rey	Reynolds number $\frac{\rho_\infty^* U_\infty^* L^*}{\mu_\infty^*}$
R_N^*	radius of curvature of a tangent ogive
R_o	spin parameter $(L^*\Omega^*/U_\infty^*)^2$
s^*	arc length
S_{ref}^*	surface area of attached boundary layer flow
S	constant in Sutherland viscosity law
$\bar{S}$	S/T_e
T^*	temperature
u^*	velocity, meridional
U_∞^*	free-stream velocity
v^*	velocity, normal
V	$v/\sqrt{Rey}$ - transformed normal velocity
$\bar{V}$	transformed normal velocity function (eq. (II-44))
w	circumferential velocity function $\frac{w^*}{r^*\Omega^*}$
XK1,XK2,XK3	defined by (eqs. (III-28), (29), (30))
α	coefficient (eq. (II-55(e))
α	angle of attack
$\alpha_1,\alpha_2,\alpha_3,\alpha_4$	coefficients in the finite difference formulation (eq. (III-7))
β	local slope of the body with respect to the axis of symmetry
β	coefficient (eq. (II-55(a))

γ	ratio of specific heats
δ	coefficient (eq. (II-55(d))
δ_1^*	displacement thickness (eq. (II-97))
$\delta\eta$	step size in η direction
$\delta\xi$	step size in ξ direction
ϵ	convergence criteria
ϵ	coefficient (eq. II-55(c))
η	similarity variable (eq. (II-40))
Θ	temperature function T/Te
κ^*	coefficient of thermal conductivity
μ^*	viscosity
ξ	similarity variable (eq. (II-39))
ρ^*	density
σ	coefficient (eq. (II-55(b))
τ^*	shear stress
ϕ	circumferential angular coordinate
ψ	μ/μ_e

Subscripts

w	wall condition
o	stagnation point
e	edge condition
∞	free-stream

Superscripts

'	derivative with respect to η, $\frac{\partial}{\partial\eta}$

CHAPTER II. PRESENTATION OF EQUATIONS

1. Introduction

In this chapter the equations describing the boundary layer on a spinning body of revolution, and their associated boundary conditions are presented. The nondimensionalizing quantities are also shown along with the transformations used to reduce the physical equations to similarity form. The expressions for the boundary layer characteristics are also presented. Coefficients which appear in the equations and which are functions of edge values only are defined and similarity values of these functions for each case are presented.

2. Presentation of the Flow Field Equations and Boundary Conditions

The coordinate system upon which the flow field equations are based is shown in figure II-1. s^* is the arc length measured from the origin along a meridian. The associated velocity is defined as u^*. n^* is the coordinate normal to the body surface at s^* and extending into the boundary layer. The associated velocity is v^*. r^* is the radius of the body measured from the axis of symmetry. ϕ is the circumferential coordinate with associated velocity w^*. R^* is the transverse radius of curvature, and β is the slope of the body surface with respect to the axis of symmetry. k^* is the curvature $(1/R^*)$, and Ω^* is the spin rate in radians per second.

Based upon the coordinate system shown on figure II-1, the equations describing the boundary layer on a spinning body of revolution are:[30]

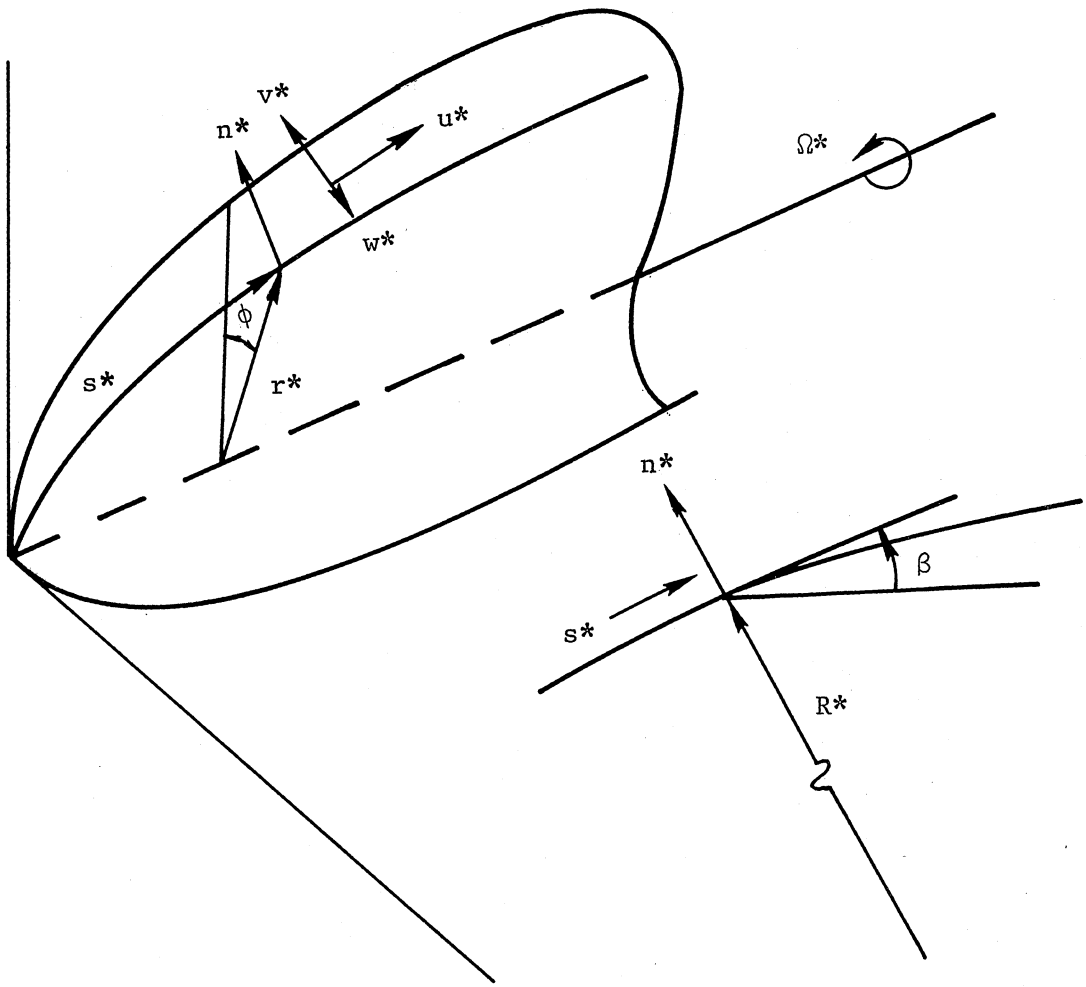

FIGURE II-1.- Coordinate System.

Continuity:

$$\frac{\partial}{\partial s}(\rho r u) + \frac{\partial}{\partial n}(\rho r v) = 0, \tag{II-1}$$

s momentum:

$$\rho\left[u\frac{\partial u}{\partial s} + v\frac{\partial u}{\partial n} - R\ rw^2\frac{dr}{ds}\right] = -\frac{\partial p}{\partial s} + \frac{1}{Rey}\frac{\partial}{\partial n}\left(\mu\frac{\partial u}{\partial n}\right), \tag{II-2}$$

ϕ momentum:

$$\rho\left[u\frac{\partial(rw)}{\partial s} + v\frac{\partial(rw)}{\partial n} + uw\frac{dr}{ds}\right] = \frac{1}{Rey}\frac{\partial}{\partial n}\left(\mu\frac{\partial(rw)}{\partial n}\right), \tag{II-3}$$

n momentum:

$$\rho\left[\cos\beta w^2 r R_o + u^2 k\right] = \frac{\partial p}{\partial n}, \tag{II-4}$$

Energy:

$$\rho\left[u\frac{\partial T}{\partial s} + v\frac{\partial T}{\partial n}\right] = \left(u\frac{\partial p}{\partial s} + v\frac{\partial p}{\partial n}\right) + \frac{1}{P_r Rey}\frac{\partial}{\partial n}\left(\mu\frac{\partial T}{\partial n}\right)$$

$$+ \frac{1}{Rey}\left[\mu\left(\frac{\partial u}{\partial n}\right)^2 + \mu R_o\left(\frac{\partial(rw)}{\partial n}\right)^2\right], \tag{II-5}$$

State:

$$p = \frac{\rho T(\gamma - 1)}{\gamma}, \tag{II-6}$$

and

Viscosity Law (Sutherland's):

$$\mu = \frac{T^{3/2}E^{3/2}(1/E + S)}{(T + S)} . \qquad \text{(II-7)}$$

The usual boundary-layer assumptions have been made in obtaining these equations with the exception that all terms containing the spin parameter, R_o, have been retained. In addition, the Prandtl number, P_r, and specific heats, C_p^* and C_v^*, are assumed to be constant. The boundary conditions associated with these equations at the wall where $n = 0$ are:

$$u = 0, \qquad \text{(II-8)}$$

$$v = 0, \qquad \text{(II-9)}$$

$$w = 1, \qquad \text{(II-10)}$$

and either

$$T = T(s), \qquad \text{(II-11)}$$

or

$$\frac{\partial T}{\partial n} = T'(s). \qquad \text{(II-12)}$$

At the edge of the boundary layer where $n = n_e$ the boundary conditions are:

$$u = u_e, \tag{II-13}$$

$$w = 0, \tag{II-14}$$

and

$$T = T_e. \tag{II-15}$$

The dimensionless coefficients appearing in equations (II-1) through (II-7) are:

$$Rey = \frac{\rho_\infty^* U_\infty^* L^*}{\mu_\infty^*}, \tag{II-16}$$

$$P_r = \frac{\mu^* C_p^*}{\kappa^*}, \tag{II-17}$$

$$E = \frac{U_\infty^{*2}}{C_p^* T_\infty^*}, \tag{II-18}$$

and

$$R_o = \left(\frac{L^* \Omega^*}{U_\infty^*}\right)^2 \tag{II-19}$$

Equations (II-1) through (II-15) have been nondimensionalized using the following scheme:

$$u^* = uU_\infty^*, \tag{II-20}$$

$$v^* = vU_\infty^*, \tag{II-21}$$

$$w^* = wr\Omega^* L^*, \tag{II-22}$$

$$r^* = rL^*, \tag{II-23}$$

$$k^* = k/L^*, \tag{II-24}$$

$$n^* = nL^*, \tag{II-25}$$

$$s^* = sL^*, \tag{II-26}$$

$$\mu^* = \mu\ \mu_\infty^*, \tag{II-27}$$

$$\kappa^* = \kappa\ \kappa_\infty^*, \tag{II-28}$$

$$\rho^* = \rho\ \rho_\infty^*, \tag{II-29}$$

$$p^* = p\rho_\infty^* U_\infty^{*2}, \tag{II-30}$$

and

$$T^* = TU_\infty^{*2}/C_p^* \tag{II-31}$$

Equations (II-1) through (II-7) represent the set of equations for which solutions will be determined using the boundary conditions given by equations (II-8) through (II-15).

Equations (II-1) through (II-5) are transformed to variables which are of order unity in the boundary layer where,

$$n = N\Big/\sqrt{Re_y}\ , \tag{II-32}$$

and

$$v = V\Big/\sqrt{Rey}\ , \tag{II-33}$$

with all other variables remaining unchanged. This transformation yields the following set of equations:

Continuity:

$$\frac{\partial}{\partial s}(\rho u r) + \frac{\partial}{\partial N}(\rho V r) = 0, \tag{II-34}$$

s-momentum:

$$\rho\left[u\frac{\partial u}{\partial s} + V\frac{\partial u}{\partial N} - R\ rw\ \frac{dr}{ds}\right] = -\frac{\partial p}{\partial s} + \frac{\partial}{\partial N}\left(\mu\frac{\partial u}{\partial N}\right), \tag{II-35}$$

ϕ-momentum:

$$\rho\left[u\frac{\partial(rw)}{\partial s} + V\frac{\partial(rw)}{\partial N} + uw\frac{dr}{ds}\right] = \frac{\partial}{\partial N}\mu\left(\frac{\partial(rw)}{\partial N}\right), \tag{II-36}$$

n momentum:

$$\frac{\partial p}{\partial N} = R_o r\cos\beta\ \rho w^2\Big/\sqrt{Rey}, \tag{II-37}$$

and

energy:

$$\rho\left[u\frac{\partial T}{\partial s} + V\frac{\partial T}{\partial N}\right] = u\frac{\partial p}{\partial s} + V\frac{\partial p}{\partial N} + \frac{1}{P_r}\frac{\partial}{\partial N}\left(\mu\frac{\partial T}{\partial N}\right) + \mu\left[\left(\frac{\partial u}{\partial N}\right)^2 + R_o\left(\frac{\partial(rw)}{\partial N}\right)^2\right]. \tag{II-38}$$

The state equation and viscosity law remain unchanged. Note in the n momentum equation the term u^2k is small with respect to the other terms and has been dropped. This restricts these equations to bodies whose curvature is small. These equations are now transformed to similarity variables using the Mangler and Howarth-Dorodnitsyn transformations[31] where,

$$\xi = \int_o^s (\rho\mu)_e u_e r^2 \, ds, \tag{II-39}$$

and

$$\eta = \frac{u_e r}{\sqrt{2\xi}} \int_o^N \rho \, dN. \tag{II-40}$$

The derivative operators are:

$$\frac{\partial}{\partial s} = \frac{\partial \xi}{\partial s}\frac{\partial}{\partial \xi} + \frac{\partial \eta}{\partial s}\frac{\partial}{\partial \eta}, \tag{II-41}$$

or

$$\frac{\partial}{\partial s} = (\rho\mu)_e u_e r^2 \frac{\partial}{\partial \xi} + \frac{\partial \eta}{\partial s}\frac{\partial}{\partial \eta}, \tag{II-42}$$

and

$$\frac{\partial}{\partial N} = \frac{u_e r \rho}{\sqrt{2\xi}}\frac{\partial}{\partial \eta}. \tag{II-43}$$

If the continuity equation is integrated in the N direction and the following quantities defined, the following transformed equations result:

$$\bar{V} \equiv -\sqrt{2\xi}\,\frac{\partial}{\partial \xi}\left(\sqrt{2\xi}\int_{o}^{\eta} F\, d\eta\right), \tag{II-44}$$

or

$$\frac{\partial \bar{V}}{\partial \eta} + 2\xi\,\frac{\partial F}{\partial \xi} + F = 0, \tag{II-45}$$

where

$$F = \frac{u}{u_e}, \tag{II-46}$$

and $\bar{V}$ is related to the transformed normal velocity as,

$$\rho V r = \frac{(\rho\mu)_e u_e r^2 \bar{V}}{\sqrt{2\xi}} - \sqrt{2\xi}\,\frac{\partial \eta}{\partial s}\,F. \tag{II-47}$$

From this transformation and using equation (II-47) the following operator's can be defined:

$$\rho u\,\frac{\partial}{\partial s} + \rho V\,\frac{\partial}{\partial N} = \rho u\left[(\rho\mu)_e u_e r^2\,\frac{\partial}{\partial \xi}\right] + \frac{(\rho\mu)_e u_e^2 r^2 \rho \bar{V}}{2\xi}\,\frac{\partial}{\partial \eta}, \tag{II-48}$$

and

$$\frac{\partial}{\partial N}\left(\mu\,\frac{\partial}{\partial N}\right) = \frac{u_e^2 r^2 \rho}{2\xi}\,\frac{\partial}{\partial \eta}\left(\rho\mu\,\frac{\partial}{\partial \eta}\right). \tag{II-49}$$

Applying these operators to the momentum and energy equations yields: for the s-momentum equation

$$\frac{\partial}{\partial\eta}\left(l\,\frac{\partial F}{\partial\eta}\right) - \bar{V}\,\frac{\partial F}{\partial\eta} + \beta(\Theta - F^2) + R_o\sigma w^2 - 2\xi F\,\frac{\partial F}{\partial\xi} = 0, \qquad \text{(II-50)}$$

for the ϕ-momentum equation

$$\frac{\partial}{\partial\eta}\left(l\,\frac{\partial w}{\partial\eta}\right) - \bar{V}\,\frac{\partial w}{\partial\eta} - 2\xi F\,\frac{\partial w}{\partial\xi} - \epsilon F w = 0, \qquad \text{(II-51)}$$

and for the energy equation

$$\frac{\partial}{\partial\eta}\left(l\,\frac{\partial\Theta}{\partial\eta}\right) - P_r\bar{V}\,\frac{\partial\Theta}{\partial\eta} + l\delta\left(\frac{\partial F}{\partial\eta}\right)^2 + R_o\alpha l\left(\frac{\partial w}{\partial\eta}\right)^2 - 2\xi P_r F\,\frac{\partial\Theta}{\partial\xi} = 0. \qquad \text{(II-52)}$$

The N momentum equation shows that pressure is constant across the boundary layer since $\partial p/\partial N$ will be of order 1 only if R_o is of the order of $\sqrt{Rey}$. For this to be true would require

$$\frac{L^*\Omega^*}{U_\infty^*} = O(Rey^{1/4}). \qquad \text{(II-53)}$$

In equations (II-49), (II-50), and (II-51), the following quantities appear:

$$l = \frac{\rho\mu}{(\rho\mu)_e} = \frac{\psi}{\Theta}, \qquad \text{(II-54(a))}$$

$$\Theta = \frac{T}{T_e}, \qquad \psi = \frac{\mu}{\mu_e} \qquad \text{(II-54(b,c))}$$

and

$$F = \frac{u}{u_e} . \qquad \text{(II-54(d))}$$

Also, the following coefficients are defined.

$$\beta = \frac{2\xi}{u_e} \frac{\partial u_e}{\partial \xi}, \qquad \text{(II-55(a))}$$

$$\sigma = \frac{2\xi r'}{(\rho\mu)_e r u_e^3}, \qquad \text{(II-55(b))}$$

$$\epsilon = \frac{4\xi r'}{(\rho\mu)_e u_e r^3}, \qquad \text{(II-55(c))}$$

$$\delta = \frac{u_e^2 P_r}{T_e}, \qquad \text{(II-55(d))}$$

and

$$\alpha = \frac{r^2 P_r}{T_e}. \qquad \text{(II-55(e))}$$

The following inviscid surface relations have also been used:

$$\frac{du_e}{d\xi} = - \frac{1}{\rho u} \frac{dp_e}{d\xi} \qquad \text{(II-56(a))}$$

and

$$\frac{dT_e}{d\xi} = - u_e \frac{du_e}{d\xi} \qquad \text{(II-56(b))}$$

The state and viscosity relations become,

$$p = \rho T_e \Theta \left(\frac{\gamma - 1}{\gamma} \right), \tag{II-57}$$

and

$$\mu = \Theta^{3/2} T_e^{3/2} \left(\frac{1/E + S}{\Theta T_e + S} \right) E^{3/2} \tag{II-58}$$

or

$$\psi = \frac{\mu}{\mu_e} = \frac{\Theta^{3/2}(1 + \bar{S})}{(\Theta + \bar{S})}. \tag{II-59}$$

$\bar{S}$ is related to the constant in Sutherland's viscosity law as follows:

$$\bar{S} = \frac{S}{T_e}, \tag{II-60}$$

where

$$S = \frac{S^* C_p^*}{U_\infty^{*2}}, \tag{II-61}$$

and $S^* = 198.6^\circ$ R.

Using the preceding transformations on the boundary conditions at the wall, where $n = 0$, yields

$$\eta = 0, \tag{II-62}$$

$$F = 0, \tag{II-63}$$

$$\overline{V} = 0, \tag{II-64}$$

$$w = 1, \tag{II-65}$$

and

$$\Theta = \Theta(\xi), \tag{II-66}$$

or

$$\Theta' = \Theta'(\xi). \tag{II-67}$$

The boundary condition at the edge of the boundary layer where $n = n_e$ become:

$$\eta_e = \frac{u_e r}{\sqrt{2\xi}} \int_o^{N_e} \rho \, dN, \tag{II-68}$$

$$F = 1, \tag{II-69}$$

$$w = 0, \tag{II-70}$$

and

$$\Theta = 1. \tag{II-71}$$

Equation (II-45), (II-50), (II-51), and (II-52) with auxiliary equations (II-6) and (II-7) and with the appropriate boundary conditions form the final set of equations for which numerical solutions will be obtained.

3. Edge Conditions

Determination of solutions for the set of equations (II-45), (II-50), (II-51), and (II-52), require knowledge of the conditions at the outer edge of the boundary layer. The relationship between pressure, temperature and velocity in differential form are,

$$\frac{dp_e^*}{ds^*} = - \rho_e^* u_e^* \frac{du_e^*}{ds^*}, \qquad \text{(II-72)}$$

and

$$\frac{dT_e^*}{ds^*} = - \frac{u_e^*}{C_p^*} \frac{du_e^*}{ds^*}. \qquad \text{(II-73)}$$

Thus, either the temperature, pressure or the velocity distribution along the edge of the boundary layer must be specified.

With the assumption that entropy is conserved along the edge of the boundary layer equations (II-72) and (II-73) take the following form:

$$T_e = T_o \left(\frac{p_e}{p_o}\right)^{\gamma-1/\gamma} \qquad \text{(II-72(a))}$$

$$u_e = \sqrt{2(T_o - T_e)} \qquad \text{(II-73(a))}$$

where T_o and p_o are the values of T_e and p_e at stagnation conditions.

4. Body Geometries

In some instances it is necessary to specify the body radius, r^*, and the transformation variable, ξ, in differential form. In the case of ξ this occurs when the specified velocity, temperature or pressure distribution do not lend themselves to analytical description. In particular the cases of compressible flow over bodies with stagnation points, and flow over a tangent ogive are examples of this.

In the case of r^* one is faced with difficult computational problems for bodies such as parabolas, hyperbolas, and tangent ogives. These difficulties arise from the relationship between the arc length s^* and the local radius r^*. For a parabola this relationship in differential form is

$$ds^* = \sqrt{1 + \frac{r^{*2}}{p^*}}\, dr^*, \qquad \text{(II-74)}$$

where p^* is a constant. Although this can be integrated it results in a transcendental relationship of the form $s^* = s^*(r^*)$. However, in the integration scheme the step size δs^* is specified, thus the expression must be inverted to give $r^* = r^*(s^*)$. In the case of a hyperbola the relationship between dr^* and ds^* is

$$ds^* = \sqrt{1 + \frac{(a^*/b^*)^2 r^{*2}}{b^{*2} + r^{*2}}}\, dr^*, \qquad \text{(II-75)}$$

where the slope of the asymptotes of the hyperbola are given by $\pm b^*/a^*$.

The exact solution to this equation involves elliptic integrals. For a tangent ogive the relationship between ds^* and dr^* is

$$ds^* = R_N^* \left[R_N^{*2} - (r^* - r_b^* + R_N^*)^2 \right]^{-1/2} dr^*, \qquad \text{(II-76)}$$

where R_N^* is the radius of curvature and r_b^* is the local radius at the point of tangency. To eliminate the aforementioned problems the following equations are included along with (II-74) and (II-75) to form a set of ordinary differential equations which can be numerically solved to yield the necessary edge conditions. Nondimensionalizing yields

$$\frac{dr}{ds} = \cos s \text{ (sphere)}, \qquad \text{(II-77)}$$

$$\frac{dr}{ds} = \left[1 + \frac{r^2}{p} \right]^{-1/2}, \text{ (parabola)} \qquad \text{(II-78)}$$

$$\frac{dr}{ds} = \left[1 + \frac{(a/b)^2 r^2}{b^2 + r^2} \right]^{-1/2}, \text{ (hyperbola)} \qquad \text{(II-79)}$$

and

$$\frac{dr}{ds} = \frac{\left\{ -2(r - r_b)R_N - (r - r_b)^2 \right\}^{1/2}}{R_N} \text{ (tangent ogive)} \qquad \text{(II-80)}$$

The relationship between ξ and s is given by

$$\frac{d\xi}{ds} = \rho_e \mu_e u_e r^2. \qquad \text{(II-81)}$$

In the case of incompressible flow over either a cone or a sphere the edge velocity can be obtained from potential theory, as a function or arc length. This introduces considerable simplification into the evaluation of the transformed variable ξ.

For the case of incompressible flow over a cone $u_e = s^j$, and $r = s \sin \beta$, thus

$$\xi = \frac{\sin^2\beta \; s^{j+3}}{j+3}. \qquad \text{(II-82)}$$

For the case of incompressible flow over a sphere $u_e = 3/2 \sin s$ and $r = \sin s$, thus

$$\xi = 1 - \frac{3}{2}\cos s + \frac{1}{2}\cos^3 s. \qquad \text{(II-83)}$$

In the cone solution the quantity j is related to the cone semivertex angle[32].

5. Boundary Layer Characteristics

In addition to the flow variables u, v, w, ρ, and T other quantities exist which are of interest. These include the shear stress, τ^*, the heat transfer, q_w^*, the displacement thickness, δ_1^*, and the frictional drag and moment on the body.

The shear stress at the wall in the s direction is given by

$$\tau_s^* = \mu_w^* \left(\frac{\partial u^*}{\partial n^*} \right)_w , \tag{II-84}$$

and in the ϕ direction by

$$\tau_\phi^* = \mu_w^* \left(\frac{\partial w^*}{\partial n^*} \right)_w \tag{II-85}$$

The drag force due to shear is

$$D^* = \int \int \tau^* (\cos \beta) dA^*, \tag{II-86}$$

and the moment about the axis of symmetry is

$$M_\phi^* = \int \int r^* \tau_\phi^* \, dA^* . \tag{II-87}$$

The heat transfer is given by

$$q_w^* = - \kappa_w^* \left(\frac{\partial T^*}{\partial n^*} \right)_w . \tag{II-88}$$

Nondimensionalizing and transforming equations (II-84) to (II-88) yields:

$$\frac{\tau_s^*}{\frac{\mu_\infty^* U_\infty^*}{L^*}} \equiv \tau_s = \frac{\mu_w \sqrt{Re_y} \, u_e^2 r \rho_w}{\sqrt{2\xi}} \left(\frac{\partial F}{\partial \eta} \right)_w , \tag{II-89}$$

$$\frac{\tau_\phi^*}{\mu_\infty^* \Omega_\infty^*} \equiv \tau_\phi = \frac{\mu_w \sqrt{Rey}\, u_e r^2 \rho_w \left(\frac{\partial w}{\partial \eta}\right)_w}{\sqrt{2\xi}}, \tag{II-90}$$

$$\frac{D^*}{\mu_\infty^* U_\infty^* L^*} \equiv D = 2\pi \int_o^\xi \frac{\tau_s \cos\beta}{(\rho\mu)_e u_e r}\, d\xi, \tag{II-91}$$

$$\frac{M_\phi^*}{L^{*3} \mu_\infty^* \Omega^*} \equiv M_\phi = 2\pi \int_o^\xi \frac{\tau_\phi}{(\rho\mu)_e u_e}\, d\xi, \tag{II-92}$$

and

$$\frac{q_w^*}{\mu_\infty^* U_\infty^{*2}/L^*} \equiv q_w = \frac{r u_e T_e \sqrt{Rey}(\rho\kappa)_w \left(\frac{\partial \Theta}{\partial \eta}\right)_w}{\sqrt{2\xi}\, P_r}. \tag{II-93}$$

Defining a local Reynolds number

$$R_{es} = \frac{\rho_e u_e s}{\mu_e}, \tag{II-94}$$

and multiplying τ_s and q_w by $\sqrt{R_{es}}$ and dividing by $\sqrt{Rey}$ one obtains

$$\tau_s \sqrt{\frac{R_{es}}{Rey}} = \sqrt{\frac{\rho_e u_e s}{2\xi\mu_e}}\, (\rho\mu)_w u_e^2 r_o \left(\frac{\partial F}{\partial \eta}\right)_w, \tag{II-95}$$

and

$$q_w \sqrt{\frac{R_{es}}{Rey}} = \sqrt{\frac{\rho_e u_e s}{2\xi\mu_e}}\, \frac{r u_e T_e (\rho\kappa)_w}{P_r} \left(\frac{\partial \Theta}{\partial \eta}\right)_w. \tag{II-96}$$

The displacement thickness, δ_1, is given by

$$\delta_1 = \frac{\delta_1^*}{L^*} = \int_o^n \left(1 - \frac{\rho u}{\rho_e u_e}\right) dn \qquad \text{(II-97)}$$

Transforming equation (II-97) yields

$$\sqrt{Rey}\ \delta_1 = \frac{\sqrt{2\xi}}{u_e r\ \rho_e} \int_o^\eta \Theta \left(1 - \frac{F}{\Theta}\right) d\eta \qquad \text{(II-98)}$$

The following coefficients are also defined for the frictional drag and moment. The frictional drag coefficient, C_{D_f}, is defined as

$$C_{D_f} \equiv \frac{D^*}{\frac{S^*_{ref}\mu^*_\infty U^*_\infty}{L^*}\sqrt{1 + R_o}}. \qquad \text{(II-99)}$$

The frictional moment coefficient, C_{M_ϕ}, is defined as

$$C_{M_\phi} \equiv \frac{M^*_\phi}{S^*_{ref} r^*_b \mu^*_\infty \Omega^*}. \qquad \text{(II-100)}$$

6. Evaluation of Outer Inviscid Quantities

A. Edge Coefficients

In addition to the coefficients defined by equations (II-55(a) to (e) other groups of terms appear in equations (II-90), (II-95), (II-96), and (II-98) which are functions of the body geometry and the specified edge quantity (either p_e or u_e). These quantities are listed below and are redefined as the following coefficients:

$$\beta = B1 = \frac{2\xi}{u_e}\frac{du_e}{d\xi},$$

$$\sigma = B2 = \frac{2\xi r'}{\rho_e \mu_e u_e r^3},$$

$$\epsilon = B3 = \frac{4\xi r'}{\rho_e \mu_e u_e r^3},$$

$$\delta = B4 = \frac{u_e^2}{T_e},$$

$$\alpha = B5 = \frac{r^2}{T_e},$$

$$B6 = \frac{\sqrt{2\xi}}{u_e r T_e}, \qquad \text{(II-101 (a)-(k))}$$

$$B7 = \sqrt{\frac{\rho_e u_e s}{2\xi\mu_e}}\, r\, u_e^2,$$

$$B8 = \frac{u_e r^2}{\sqrt{2\xi}},$$

$$B9 = \frac{\sqrt{2\xi}}{\rho_e u_e r},$$

$$B10 = \frac{\sqrt{2\xi}}{u_e r},$$

$$B11 = r u_e T_e \sqrt{\frac{\rho_e u_e s}{2\xi\mu_e}}.$$

B. Similarity Values of the Edge Coefficients

The similarity values of certain of equations (II-101(a) to (k)) appear to be indeterminate, and must be evaluated. To evaluate these quantities the transformation variable ξ must be evaluated as s approaches zero. For compressible flow over blunt bodies the edge variables can be represented as

$$p_e = p_o(1 + p_2 s^2 + p_4 s^4 + \ldots), \tag{II-102}$$

$$u_e = u_1 s + u_3 s^3 + \ldots, \tag{II-103}$$

$$(\rho\mu)_e = (\rho\mu)_o(1 + (\rho\mu)_2 s^2 + (\rho\mu)_4 s^4 + \ldots), \tag{II-104}$$

and the radius by

$$r = s + r_3 s^3 + r_5 s^5 + \ldots \tag{II-105}$$

Thus ξ takes on a value of

$$\xi = (\rho\mu)_o u_1 \frac{s^4}{4} + O(s^5), \tag{II-106}$$

where

$$u_1 = \left(\frac{du_e}{d\xi}\right)_{s=0}. \tag{II-107}$$

For the case of compressible flow over a pointed body as s approaches zero u_e is constant and $r \approx s \sin\beta$ yielding

$$\xi \approx \frac{1}{3}(\rho\mu)_e u_e \sin^3\beta \, s^3 \tag{II-108}$$

For incompressible flow over a pointed body ξ is given by equation (II-82), and for incompressible flow over a sphere ξ is given by equation (II-83). Using equation (II-82), (II-83), (II-106), and (II-108) and the appropriate expressions for u_e, r, T_e, and p_e in equation (II-100(a) to (k)), and evaluating these expressions as s approaches zero yields their similarity values. These values are shown in table II-1. In addition to the quantities given by equation (II-101 (a)-(k)), for the case of compressible flow over a blunt body, equation (II-72) has a limiting value given by[31]

$$\lim_{s \to 0}\left(-\frac{1}{\rho_e^* u_e^*}\frac{dp_e^*}{ds^*}\right) = -\frac{1}{R_N^*}\sqrt{\frac{2(p_o^* - p_\infty^*)}{\rho_o^*}}, \qquad \text{(II-109)}$$

where R_N^* is the radius of curvature at the stagnation point and p_o^* and ρ_o^* are evaluated at the stagnation point.

TABLE II-1.- SIMILARITY VALUES OF THE EDGE COEFFICIENTS DEFINED BY EQUATIONS (II-101(a) to (k)).

	Compressible flow over blunt bodies	Compressible flow over pointed bodies	Incompressible flow over a sphere	Incompressible flow over a pointed body	
				$j \neq 1.0$	$j = 1.0$
B1	0.5	0	0.5	$2j/(j+3)$	0.5
B2	$0.5\ u_1^2$	0	2/9	0	0.5
B3	1.0	4/3	1.0	$4/(j+3)$	2.0
B4	0	u_e^2/T_e	0	0	0
B5	0	0	0	0	0
B6	$1/T_o\sqrt{2u_1}$	0	$1/\sqrt{3T_e}$	0	$1/2\ T_e$
B7	0	$\sqrt{3/2}\ u_e^2/\mu_e$	0	0	0
B8	0	0	0	0	0
B9	$\sqrt{(\rho\mu)_o}/\rho_o\sqrt{2u_1}$	0	$1/\sqrt{3}$	0	$1/\sqrt{2}$
B10	$\sqrt{(\rho\mu)_o}/\sqrt{2u_1}$	0	$1/\sqrt{3}$	0	$1/\sqrt{2}$
B11	0	$\sqrt{3/2}\ u_e T_e/\mu_e$	0	0	0

Note: Subscript o denotes stagnation point values, and $u_1 = (du_e/d\xi)_o$. For pointed bodies the values of u_e and T_e are obtained at the vertex of the body.

CHAPTER III. METHOD OF SOLUTION

1. Introduction

In this chapter the reduction of the differential equations describing the boundary layer on a spinning body of revolution to difference equations in the similarity variables will be presented. An implicit finite difference technique is outlined, and applied to a general difference equation representative of the momentum and energy equations. The method used to accommodate a general boundary condition is derived, along with the recurrence formulas associated with the implicit method. The computational procedure is outlined and the other numerical integration schemes used to solve the continuity equation and to obtain the similarity variable ξ and body radius r for certain bodies is also presented. Several methods for the determination of derivatives of edge quantities are also discussed.

2. Determination of the Difference Equations

The method used to solve the set of nonlinear second-order parabolic partial differential equations (II-49) - (50) and (51) consists of replacing the differentials by differences and proceeding to solve the resulting set of difference equations step by step downstream using an implicit finite difference scheme[33][34][35].

Basically the differentials are replaced by differences obtained by repeated use of Taylor series expansions. Consider the domain shown in figure III-1. This domain is subdivided by a grid in which the

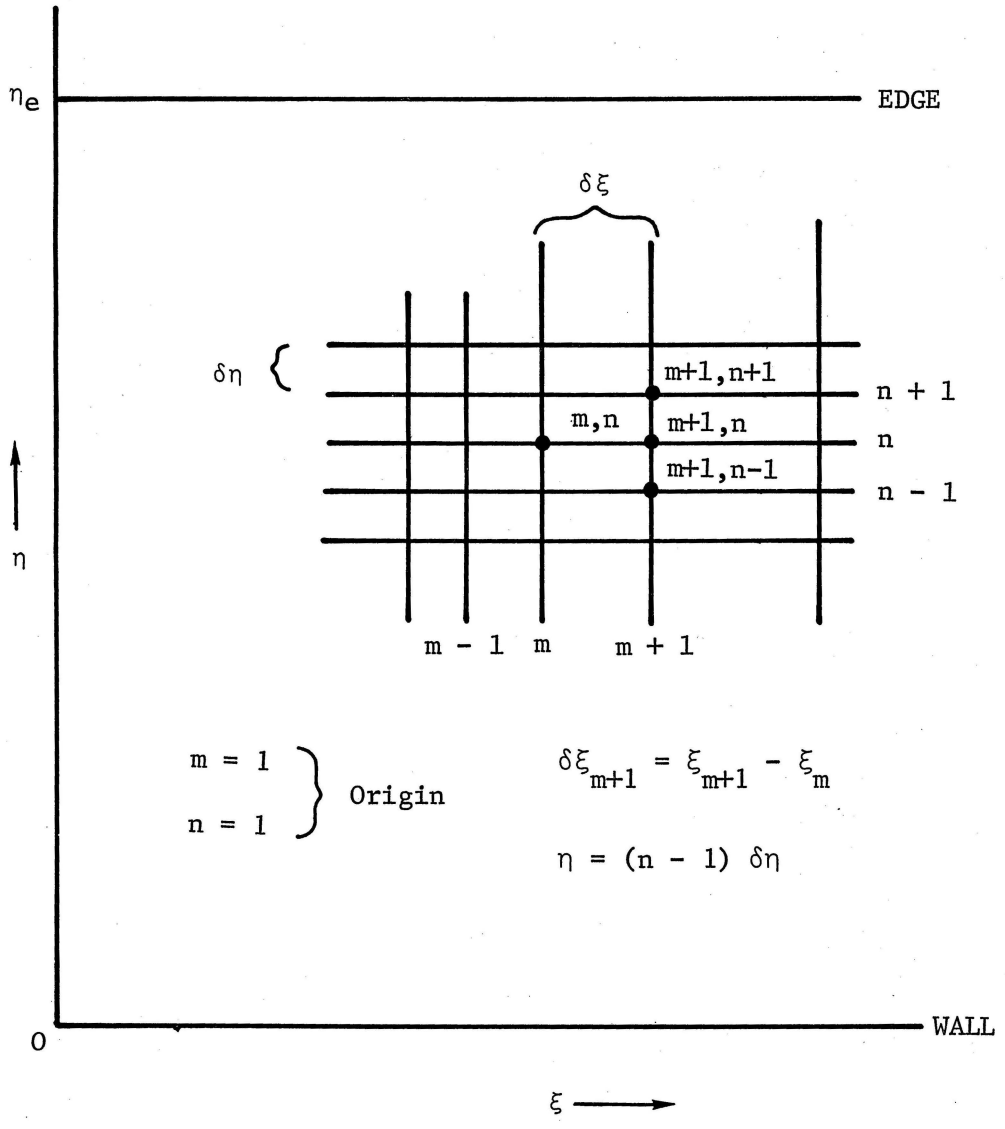

Figure III-1 Finite Difference Grid.

spacing along the ordinate is equal and the spacing along the abscissa is arbitrary. With these conditions

$$\eta = (n - 1)\delta\eta, \tag{III-1}$$

$$\delta\xi_m = \delta\xi(\xi) = \xi_m - \xi_{m-1}, \tag{III-2}$$

and

$$P(\xi,\eta) = P_{m,n}. \tag{III-3}$$

With these definitions in mind we can write

$$\frac{\partial^2 P}{\partial\eta^2} = \frac{P_{m+1,n+1} - 2P_{m+1,n} + P_{m+1,n-1}}{(\delta\eta)^2} - \left(\frac{\partial^4 P}{\partial\eta^4}\right)_{m+1,n} \frac{\delta\eta^2}{12}, \tag{III-4}$$

$$\frac{\partial P}{\partial\eta} = \frac{P_{m+1,n+1} - P_{m+1,n-1}}{2\delta\eta} - \left(\frac{\partial^3 P}{\partial\eta^3}\right)_{m+1,n} \frac{\delta\eta^2}{6}, \tag{III-5}$$

and

$$\frac{\partial P}{\partial\xi} = \frac{P_{m+1,n} - P_{m,n}}{\delta\xi_m} + \left(\frac{\partial^2 P}{\partial\eta^2}\right)_{m+1,n} \frac{\delta\xi}{2}. \tag{III-6}$$

the energy and both momentum equations reduce to a general form as follows

$$\frac{\partial^2 P}{\partial\eta^2} + \alpha_1 \frac{\partial P}{\partial\eta} + \alpha_2 P + \alpha_3 + \alpha_4 \frac{\partial P}{\partial\xi} = 0, \tag{III-7}$$

where P is either u/u_e, w, or T/T_e. Substituting equations (III-4) (5), and (6) into equation (III-7) yields an equation of the form

$$A_n P_{m+1,n+1} + B_n P_{m+1,n} + C_n P_{m+1,n-1} + D_n = 0. \qquad \text{(III-8)}$$

Where

$$A_n = \frac{1}{\delta\eta^2}\left(1 + \frac{\alpha_1 \delta\eta}{2}\right), \qquad \text{(III-9)}$$

$$B_n = \frac{1}{\delta\eta^2}\left(-2 + \alpha_2 P_n \delta\eta^2 + \alpha_4 P_n \frac{\delta\eta^2}{\delta\xi_m}\right), \qquad \text{(III-10)}$$

$$C_n = \frac{1}{\delta\eta^2}\left(1 - \frac{\alpha_1 \delta\eta}{2}\right), \qquad \text{(III-11)}$$

and

$$D_n = \alpha_3 - \frac{\alpha_4 P_n^2}{\delta\xi_m}. \qquad \text{(III-12)}$$

The α's are evaluated at the nth grid point. Note since in equation (III-8) only terms along the $(m + 1)$ grid line are involved, and the equation is valid at any point along the ξ axis, equation (III-8) can be considered as independent of $m(\xi)$ and it reduces to a recurrence equation in $n(\eta)$.

3. Boundary Equations

Consider a general equation

$$BC_1 \frac{\partial P}{\partial n} + BC_2 P + BC_3 = 0, \qquad \text{(III-13)}$$

where BC_1, BC_2, and BC_3 are coefficients which are dependent on the boundary conditions. The dependency of the BC's and the possible boundary conditions on P are shown in table III-1.

TABLE III-1.- RELATIONSHIP BETWEEN BC'S AND ACTUAL BOUNDARY CONDITIONS

	BC_1	BC_2	BC_3
$P(0,\xi) = 0$	0	1.0	0
$\frac{\partial P(0,\xi)}{\partial \eta} = P_1(\xi)$	-1.0	0	$P_1(\xi)$
$P(0,\xi) = P_2(\xi)$	0	-1.0	$P_2(\xi)$

4. Derivation of Derivative Expressions at the Solid Boundary.

Assume $P(\eta,\xi)$ can be described by a polynomial in η, at any position ξ

$$P(\eta) = A + B\eta + C\eta^2 + D\eta^3. \tag{III-14}$$

Solving for the coefficients A, B, C, and D yields

$$A = P_1, \tag{III-15}$$

$$B = \frac{36P_2 - 18P_3 + 4P_4 - 22P_1}{12\delta\eta}, \tag{III-16}$$

$$C = \frac{24P_3 - 6P_4 - 30P_2 + 12P_1}{12\delta\eta^2}, \tag{III-17}$$

and

$$D = \frac{P_4 - 3P_3 + 3P_2 - P_1}{6\delta\eta^3}, \tag{III-18}$$

where the subscripts refer to the finite difference solution grid points. Thus we have

$$\frac{\partial P(0,\xi)}{\partial \eta} = \frac{18P_2 - 9P_3 + 2P_4 - 11P_1}{6\delta\eta}, \qquad \text{(III-19)}$$

and

$$\frac{\partial^2 P(0,\xi)}{\partial \eta^2} = \frac{4P_3 - P_4 - 5P_2 + 2P_1}{2\delta\eta^2}. \qquad \text{(III-20)}$$

5. Recurrence Formulas - Initial Values of E and G

Assume a solution to equation (III-8) of the form[36]

$$P_n = E_n P_{n+1} + G_n. \qquad \text{(III-21)}$$

Substituting equation (III-21) into equation (III-8) yields the following recurrence formulas for E and G,

$$E_n = - \frac{A_n}{B_n + C_n E_{n-1}}, \qquad \text{(II-22)}$$

and

$$G_n = - \frac{D_n G_{n-1} + D_n}{B_n + C_n E_{n-1}}. \qquad \text{(III-23)}$$

The initial values of E_n and G_n are obtained from the boundary conditions at the wall as follows. Representing P by a 2nd-order polynomial of the form

$$P = A + B\eta + C\eta^2, \qquad \text{(III-24)}$$

yields for P'

$$P'_{n-1} = \frac{-3P_{n-1} + 4P_n - P_{n+1}}{2\delta\eta}. \qquad \text{(III-25)}$$

Thus we have three equations (III-8), (III-13), and (III-21) involving three unknowns P_{n-1}, P_n, P_{n+1}. Substituting equation (III-25) into equation (III-13) yields

$$\frac{BC_1}{2\delta\eta}(-3P_{n-1} + 4P_n - P_{n+1}) + BC_2P_{n-1} + BC_3 = 0 \qquad \text{(III-26)}$$

Solving equation (III-26) for P_{n+1} and substituting this into (III-8) yields

$$XK_1\, P_n + XK_2\, P_{n+1} + XK_3 = 0 \qquad \text{(III-27)}$$

In equation (III-27)

$$XK_1 = BC_2 + \frac{BC_1}{2\delta\eta}\left(-3 + \frac{C_n}{A_n}\right), \qquad \text{(III-28)}$$

$$XK_2 = \frac{BC_1}{2\delta\eta}\left(4 + \frac{B_n}{A_n}\right), \qquad \text{(III-29)}$$

and

$$XK_3 = \frac{BC_1}{2\delta\eta}\left(\frac{D_n}{A_n}\right) + BC_3, \qquad \text{(III-30)}$$

where A_n, B_n, C_n, and D_n are evaluated using equations (III-9) through (III-12). However, comparing equation (III-27) with equation (III-21) we have

$$P_1 = - \frac{XK_2}{XK_1} P_2 - \frac{XK_3}{XK_1}, \qquad \text{(III-27)}$$

and

$$P_1 = E_1 P_2 + G_1 \qquad \text{(III-21)}$$

Thus

$$E_1 = - \frac{XK_2}{XK_1}, \qquad \text{(III-31)}$$

and

$$G_1 = - \frac{XK_3}{XK_1}. \qquad \text{(III-32)}$$

6. Discussion of the Computational Procedure

The actual numerical method proceeds as follows: Values for F, w, and Θ are assumed at the origin of the system ($\xi = 0$) where a similarity solution is assumed to exist. At this point the governing equations reduce to ordinary differential equation since $\partial/\partial\xi$ of all functions equals zero. With these assumed values, and with the geometric coefficients evaluated, the α's in equation (III-7) can be determined. From these A_n, B_n, C_n, and D_n can be determined. From equations (III-31) and (32) and knowledge of the boundary conditions E_1 and G_1 can be determined. The recurrence equations for E and G in conjunction with the assumed solutions for P can then be

used to determine all of the E and G values; that is, the values of E and G from the body out to the edge of the boundary layer can be consecutively determined. From the boundary condition at the edge P_{IE} will be known, thus equation (III-21) can be used to work back into the boundary layer to the body and calculate new values of P. This procedure is repeated until convergence occurs. Once convergence has been achieved the solution obtained is used as the assumed solution at the next point on the body. In this way the solution progresses until the entire body has been covered or until some limiting value of s is reached.

In this numerical technique the derivatives at the body and at the edge are defined assuming a polynomial variation for the functions F, Θ, and w. Using a 3rd-order polynomial at the body yields equations (III-19) and (20). Using a 2nd-order polynomial at the edge yields

$$\left(\frac{\partial P}{\partial \eta}\right)_{edge} = \frac{3P_{IE} - 4P_{IE-1} - P_{IE-2}}{2\delta\eta}, \qquad \text{(III-33)}$$

and

$$\left(\frac{\partial^2 P}{\partial \eta^2}\right)_{edge} = \frac{P_{IE} - 2P_{IE-1} + P_{IE-2}}{\delta\eta^2}, \qquad \text{(III-34)}$$

where subscripts denote grid points in the η direction. The continuity equation (II-44) is solved by direct integration in the η direction using a trapezoidal rule. The similarity variable ξ is obtained

through numerical integration utilizing Simpson's rule. That is

$$\xi_{m+1} = \xi_m + \frac{\delta S}{6}(f_{e_m} + 4f_{e(m-1/2)} + f_{e(m-1)}), \qquad \text{(III-35)}$$

where

$$f_e = (\rho\mu)_e \, u_e r^2. \qquad \text{(III-36)}$$

The local radius r for hyperboloids, paraboloids, and tangent ogives is obtained using a 4th-order Runge-Kutta method[37].

7. Derivatives of Edge Quantities

Note that $B1$ in equation (II-101(a)), requires the evaluation of a derivative $du_e/d\xi$. In those instances where u_e is defined exactly (potential flow solutions for a cone and sphere in incompressible flow) the evaluation of this derivative presents no problems. However, for the compressible flow over blunt bodies, and over the tangent ogive only numerical solutions exist; consequently, the derivative must be determined numerically. The best results in terms of smoothness of the coefficient $B1$ are obtained by using a polynomial to represent one of the edge quantities. Usually this quantity is the edge pressure and since this is an even function of arc length, s, an even polynomial in either arc length or body radius can be used to represent the edge pressure. To obtain the inviscid solutions, the method of Lomax and Inouye[38] is used. This consists of an inverse method to determine the subsonic solution, and the method of characteristics to obtain the

supersonic solution. For the tangent ogive, the method of characteristics is used.

For a spherical shape, the results of the inviscid solution are fitted with a polynomial in arc length s, using the method of least squares to evaluate the coefficients. An eight-term even polynomial of the form

$$p_e = p_o(1 + P_2 s^2 + P_4 s^4 + P_6 s^6 + P_8 s^8 + P_{10} s^{10} + P_{12} s^{12} + P_{14} s^{14}), \tag{III-37}$$

is used for spheres. The value of the coefficients used in the polynomial for sphere edge pressure for $M_\infty = 10$ are given as follows:

$P_2 = -1.2039186$ $\qquad$ $P_{10} = -0.48498085 \times 10^{-1}$

$P_4 = +0.63597393$ $\qquad$ $P_{12} = 0.16454986 \times 10^{-1}$

$P_6 = -0.20600574$ $\qquad$ $P_{14} = 0.21268077 \times 10^{-2}$

$P_8 = +0.84633473 \times 10^{-1}$

For a hyperbola, parabola and tangent ogive, it was found that although smooth derivatives of the edge pressure could be obtained other problems arose. As the independent variable increased the higher order terms in the polynomial became more predominant and oscillations appeared in the derivatives of p_e. Attempts to patch together polynomials eliminated this problem but resulted in discontinuities in the derivatives at the points where the polynomial changes occur. The method which was finally used to insure smooth derivatives was spline fitting[39] of the data. A subroutine written by Mr. R. E. Smith, Jr., of Langley Research Center and based upon the work of reference 39 was used.

CHAPTER IV. ACCURACY AND COMPARISONS

1. Introduction

The accuracy of the solutions obtained herein are established in this chapter by comparison with previous efforts and also by an analysis of the effect of step sizes, and convergence criteria, in the numerical method. The effect of step size is determined by holding all quantities fixed and allowing first $\delta\eta$ and then δs to decrease until the "exact" value of a given quantity can be estimated. The quantity which is most sensitive to step size and convergence criteria is Θ_w', and the case which requires the most effort to obtain accurate solutions is compressible flow over a sphere. Once the appropriate values of step size are determined the effect of iterating on the value of Θ_w' can be established. Thus for a given accuracy requirement minimum values of $\delta\eta$ and δs can be determined and the minimum number of iterations for acceptable convergence can also be determined. These solutions are also compared with previous results from various sources and these comparisons are presented. The agreement with previous work is in most instances very good.

2. Effect of Step Size on Accuracy of the Numerical Solution

Two cases were considered in this part of the study. The incompressible flow about a disc and the compressible flow about a sphere. Since the incompressible disc case is included in the class of problems which have similar solutions the only quantity of interest is the step size in the η direction. Table IV-1 shows values of shear parameter at the body

for various step sizes and also the results of Hannah.[1] These results are for the case of $R_o = 0$.

TABLE IV-1.- MERIDIONAL SHEAR PARAMETER VERSUS STEP SIZE IN THE η DIRECTION FOR THE CASE OF INCOMPRESSIBLE FLOW OVER A DISC WITH ZERO SPIN

$\delta\eta$	$F'_w/\sqrt{2}(1 + R_o)^{3/4}$
Hannah	0.656
0.025	0.65597
0.05	0.65599
0.10	0.65605
0.20	0.65628
0.40	0.65655

As can be seen for this case step size in the η direction as large as 0.20 yields three place agreement with Hannah. However, when $R_o \gg 1.0$ the effect of step size becomes much more critical. In particular step size causes the derivatives of F and w at the surface to change markedly. This is due to the large gradients which the high spin rate induces in the F and w profiles. A study of F'_w and w'_w as functions of step size and ϵ show that as η decreases from a value of 0.2 to 0.025 the values of F'_w and w'_w approach Hannah's values.

For the case of compressible flow over a sphere the most sensitive quantity is Θ'_w as s approaches $\pi/2$. Consequently, this quantity was investigated at $s = 1.5$ as $\delta\eta$ and δs varied. Table IV-2 (figs. IV-1, 2) shows the values of F'_w and Θ'_w at $s = 1.5$ as a

TABLE IV-2.- VARIATION OF F'_w AND Θ'_w AT $s = 1.5$ FOR THE CASE OF COMPRESSIBLE FLOW OVER A SPHERE, WITH STEP SIZE IN THE s AND η DIRECTIONS, AND WITH ITERATIONS, $M_\infty = 10$, $\Theta_w = 0.6\ T_o/T_e$

(a) η step size varied.				
δs	$\delta\eta$	Iterations	Θ'_w	F'_w
0.01	0.1	5	1.33055	2.0070
0.01	0.05	5	1.32818	1.9945
0.01	0.025	5	1.32465	1.9920
0.01	0.0375	5	1.32671	1.9930
0.01	0.0125	5	1.31714	1.99029
0.01	0.008	5	1.30997	1.98905
(b) s step size varied.				
$\delta\eta$	δs	Iterations	Θ'_w	F'_w
0.1	0.01	5	1.33055	2.0070
0.1	0.005	5	1.31349	2.0023
0.1	0.0025	5	1.30223	1.9996
0.1	0.0030	5	1.30508	2.0002
0.1	0.00125	5	1.29508	1.99818
(c) number of iterations varied.				
$\delta\eta$	δs	Iterations	Θ'_w	F'_w
0.008	0.002	1	0.66968	1.79960
0.008	0.002	5	1.28438	1.98197

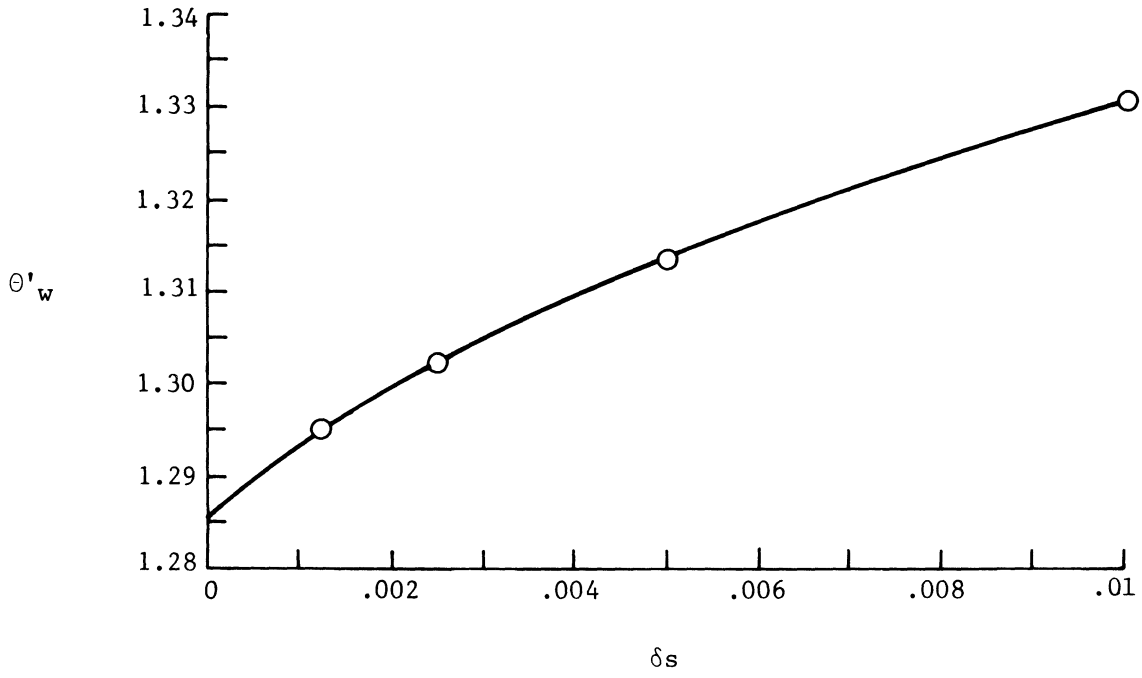

FIGURE IV-1.- Effect of step size, δs, on Θ'_w for the case of a sphere $M_\infty = 10.0$ with $R_o = 0$, $\Theta_w = 0.6T_o/T_e$ at $s = 1.5$, $\delta\eta = 0.10$ and with 5 iterations at each step.

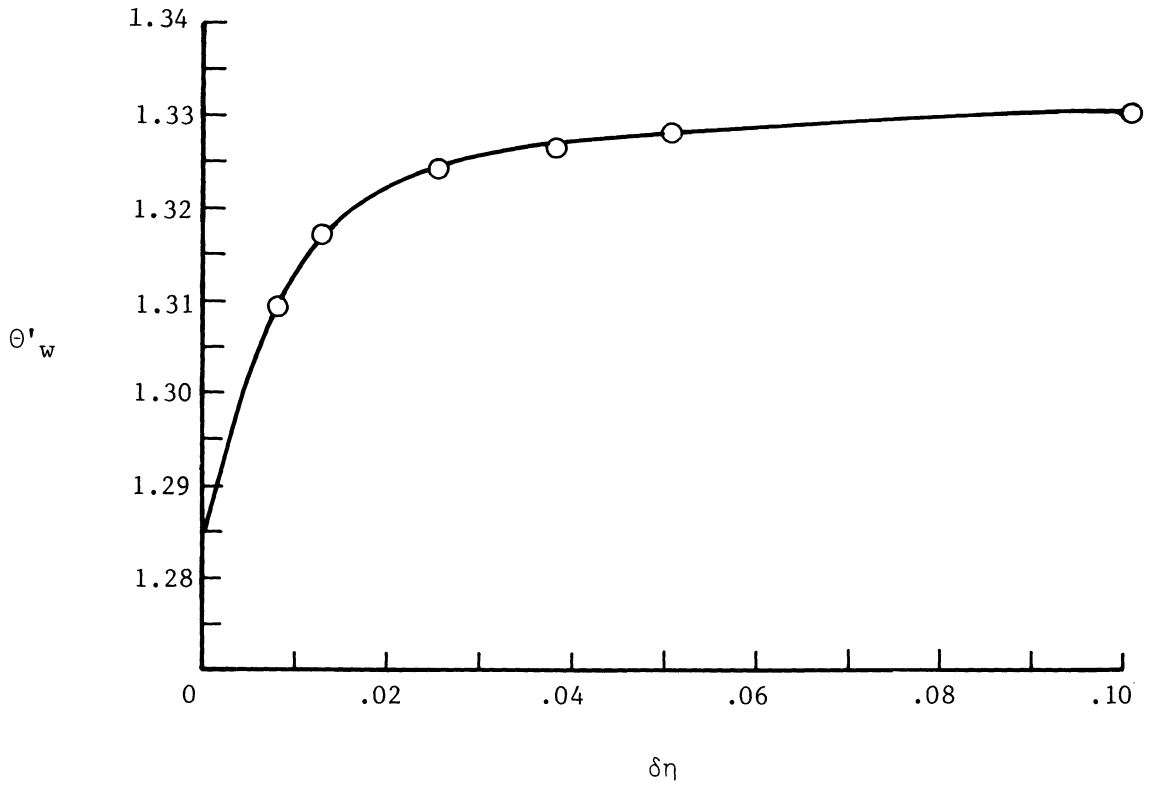

FIGURE IV-2.- Effect of step size $\delta\eta$ on Θ'_w for the case of a sphere at $M_\infty = 10.0$, with $R_o = 0$, $\Theta_w = 0.6T_o/T_e$ at $s = 1.5$, $\delta s = 0.10$ and with 5 iterations at each step.

function of both δs and $\delta\eta$ with the convergence criteria set at five iterations. From the results of the δs study it was found that a value of $\delta s \approx 0.0016$ would yield a value of Θ'_w at $s = 1.5$ which is within 1 percent of the extrapolated "exact" value of Θ'_w as δs approaches zero. A similar analysis of the effect of $\delta\eta$ shows $\delta\eta = 0.0035$ will yield Θ'_w within 1 percent of the exact value of Θ'_w as $\delta\eta$ approaches zero. If a solution within 5 percent of the "exact" values is acceptable, step sizes of $\delta s > 0.01$ and $\delta\eta > 0.10$ could be used. Obviously, using these larger step sizes results in considerable computer time savings.

3. Effects of Convergence Criteria on the Accuracy of the Solutions

The convergence criteria used in this analysis takes two forms. One method is to define a small quantity, ϵ, and require that the following conditions be satisfied. With the restriction that $\eta \neq 0$

$$\frac{\left|F_K(\eta) - F_{K-1}(\eta)\right|}{F_{K-1}(\eta)} \leq \epsilon, \qquad \text{(IV-1)}$$

and

$$\left|w_K(\eta) - w_{K-1}(\eta)\right| \leq \epsilon, \qquad \text{(IV-2)}$$

and

$$\frac{\left|\Theta_K(\eta) - \Theta_{K-1}(\eta)\right|}{\Theta_{K-1}(\eta)} \leq \epsilon, \qquad \text{(IV-3)}$$

where K indicates the number of iterations, and equations (IV-1), (2), and (3) must be simultaneously satisfied. With this method the solution continues to iterate until convergence is achieved. A second approach is to require a specific number of iterations, and assume convergence has been achieved.

For the case of a disc spinning at high rates with respect to the free-stream velocity, the effect of convergence criteria can be significant. However, the manner in which ϵ effects the solutions depends in part on step size in the normal direction ($\delta\eta$). The effects of ϵ on the derivatives at the wall are shown in table IV-3. With $\delta\eta = 0.025$ both F'_w and w'_w converge toward the values given by Hannah as ϵ is decreased. With $\delta\eta = 0.10$ F'_w converges toward Hannah's value but from the other direction while w'_w is diverging from Hannah's value.

Based upon these results it would seem necessary to restrict ϵ to values less than 0.01 with the additional condition that the boundary layer be traversed in approximately 100 steps whenever the dependent variables vary rapidly through the boundary layer.

The relation between the number of iterations at each s step and F'_w and Θ'_w for compressible flow over a sphere at $M_\infty = 10$ are shown on table IV-4. Included on this table is a value of F'_w from Davis[34] for one iteration. These values are taken at $s = 1.5$ on the sphere with step sizes of 0.10 or 0.01 for $\delta\eta$ and δs, respectively. It should be noted that the case $\delta s = 0.01$, $\delta\eta = 0.10$, and with five iterations is seemingly repeated in table IV-2. However, neither

TABLE IV-3.- EFFECT OF ϵ ON SOLUTIONS FOR A SPINNING DISC, $R_o = 400$

$\delta\eta = 0.025$			$\delta\eta = 0.10$	
ϵ	F'_w	w'_w	F'_w	w'_w
0.1	34.1321	-1.9880	30.3711	-1.9882
0.01	32.5386	-1.9840	31.5801	-2.0193
0.001	32.4208	-1.9835	31.7042	-2.0211
Hannah	32.3157	-1.9492		

TABLE IV-4.- EFFECT OF ITERATIONS ON F'_w AND Θ'_w AT $s = 1.5$ FOR THE CASE OF A SPHERE IN COMPRESSIBLE FLOW AT $M_\infty = 10.0$ WITH $\Theta_w = 0.6\ T_o/T_e$ AND $\delta s = 0.01$, AND $\delta\eta = 0.10$

Iterations K	F'_w	Θ'_w
1	1.8020	0.6336
2	1.8878	0.8930
3	1.9435	1.0625
4	1.9833	1.1848
5	2.0134	1.2780
6	2.0370	1.3516
7	2.0560	1.4108
10	2.0963	1.5383
100	2.2344	1.9933
Davis[34]	1.7591	

F'_w and Θ'_w from table IV-2 agree with the result shown in table IV-4. This is due to the fact that the stream conditions for each case were different.

Figures IV-3, IV-4 show the effect of iterations on the quantities F'_w and Θ'_w versus s with the number of iterations specified to be 1, 10, and 100. As can be seen the convergence is very slow the further along the body the solution progresses, however, the solution is converging as the data shown on figure IV-5 indicate. This figure shows the change in Θ'_w at $s = 1.5$ as a function of the specified number of iterations, K.

The data shown on table IV-4 and on figures IV-3 and IV-4 raise some serious questions concerning the application of finite difference methods to the solution of boundary-layer equations. The most obvious question concerns convergence of the solutions. In the region of the sphere where the flow is "almost" similar the solutions converge very quickly and the results obtained with one iteration do not vary appreciably with those for 100 iterations. However, as the solution marches along the body surface, the flow departs more and more from a similarity-type flow and convergence of the solutions requires a greater number of iterations. However, the change in solution value per iteration is quite small and consequently, a typical value of convergence criteria might well be satisfied, thus presenting a very misleading picture.

An investigation of the effects of iterations on the solutions for other bodies and flow conditions indicated that convergence is fairly

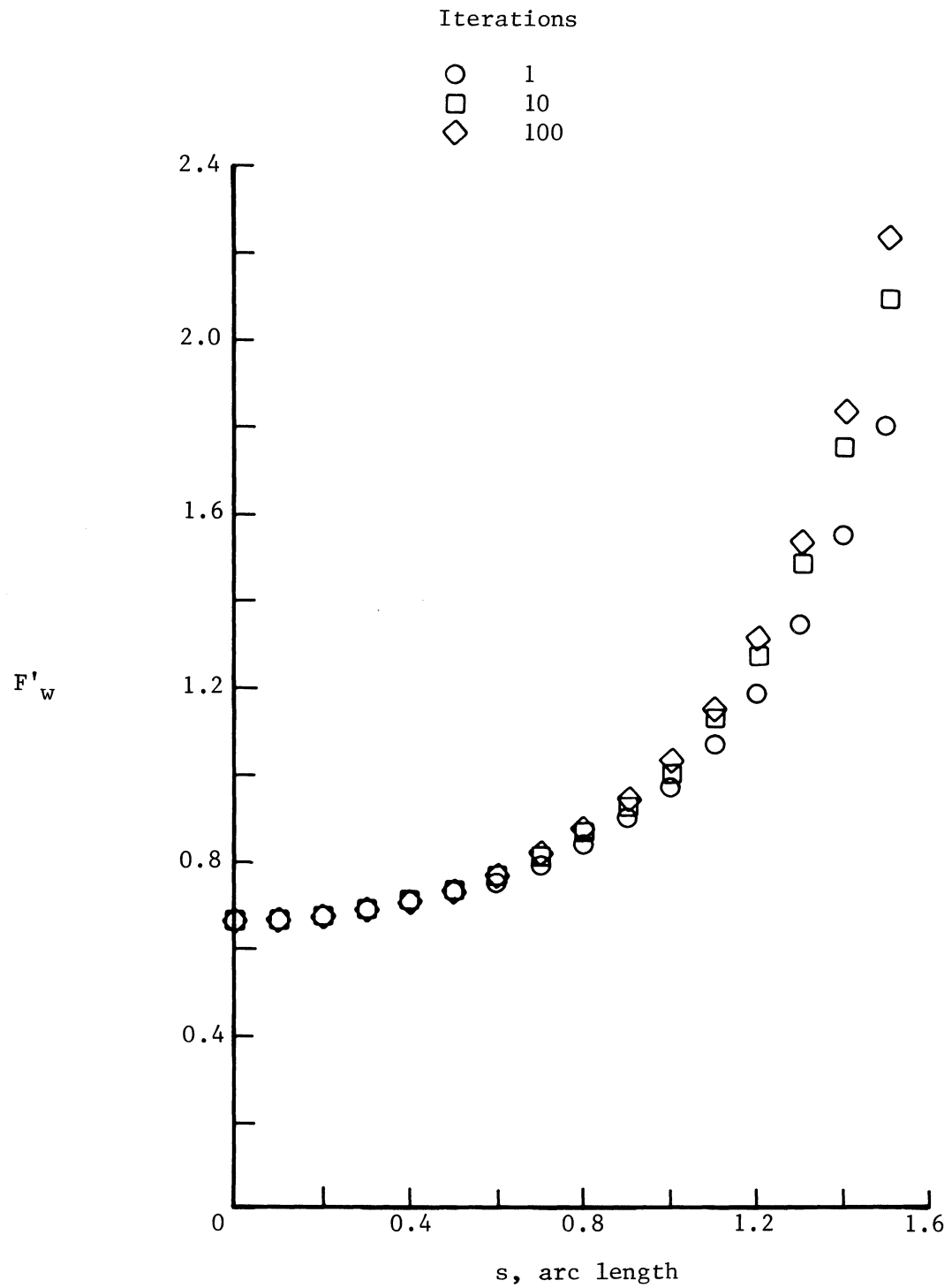

FIGURE IV-3.- Effect of iterations on F'_w - for the case of a sphere at $M_\infty = 10.0$ with $R_o = 0$, $\Theta_w = 0.6T_o/T_e$, $\delta s = 0.01$ $\delta\eta = 0.10$.

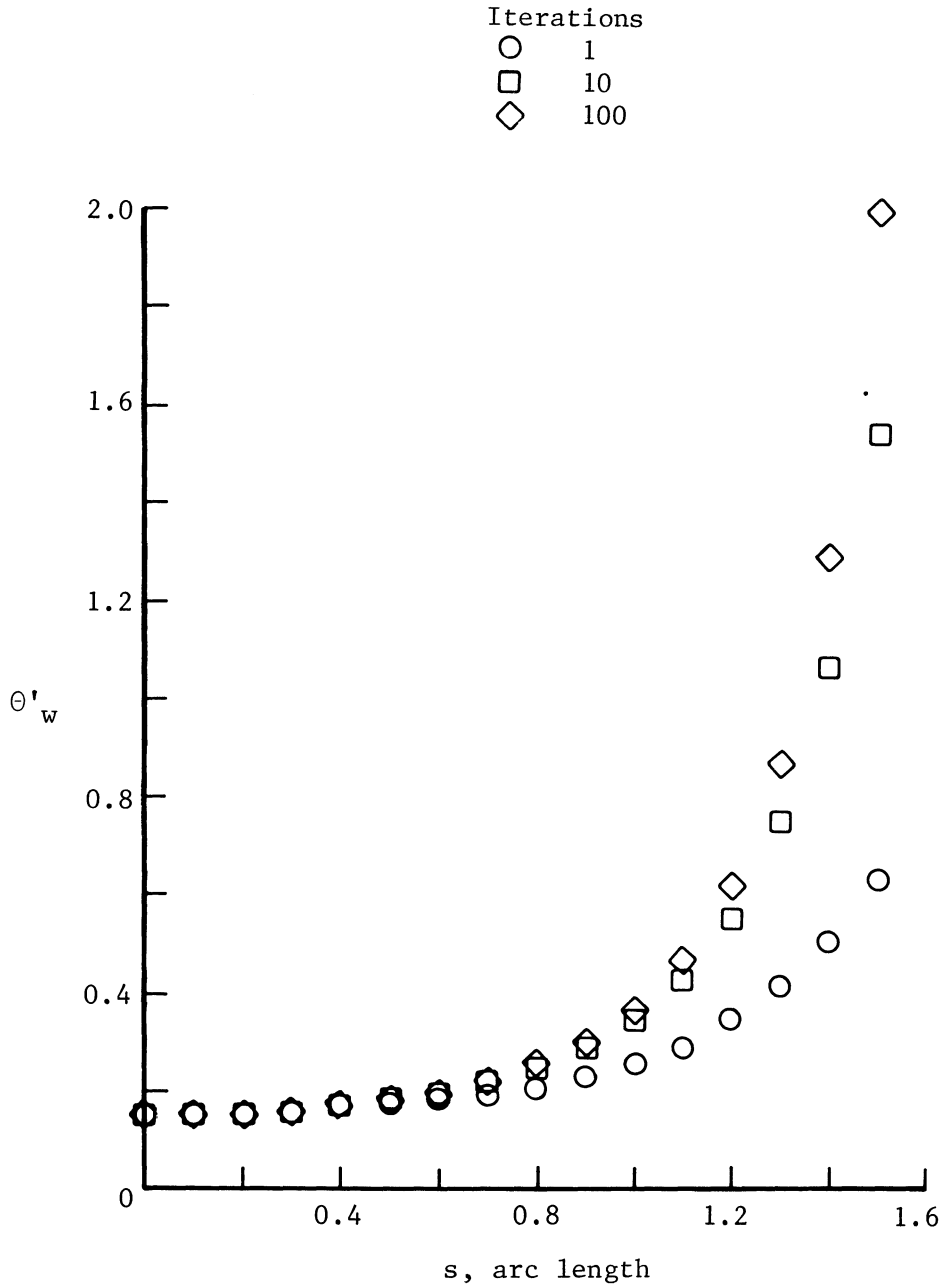

FIGURE IV-4.- Effect of iterations on Θ'_w - for the case of a sphere at $M_\infty = 10$, $R_o = 0$, $\Theta_w = 0.6T_o/T_e$ $\delta s = 0.01$, and $\delta\eta = 0.10$.

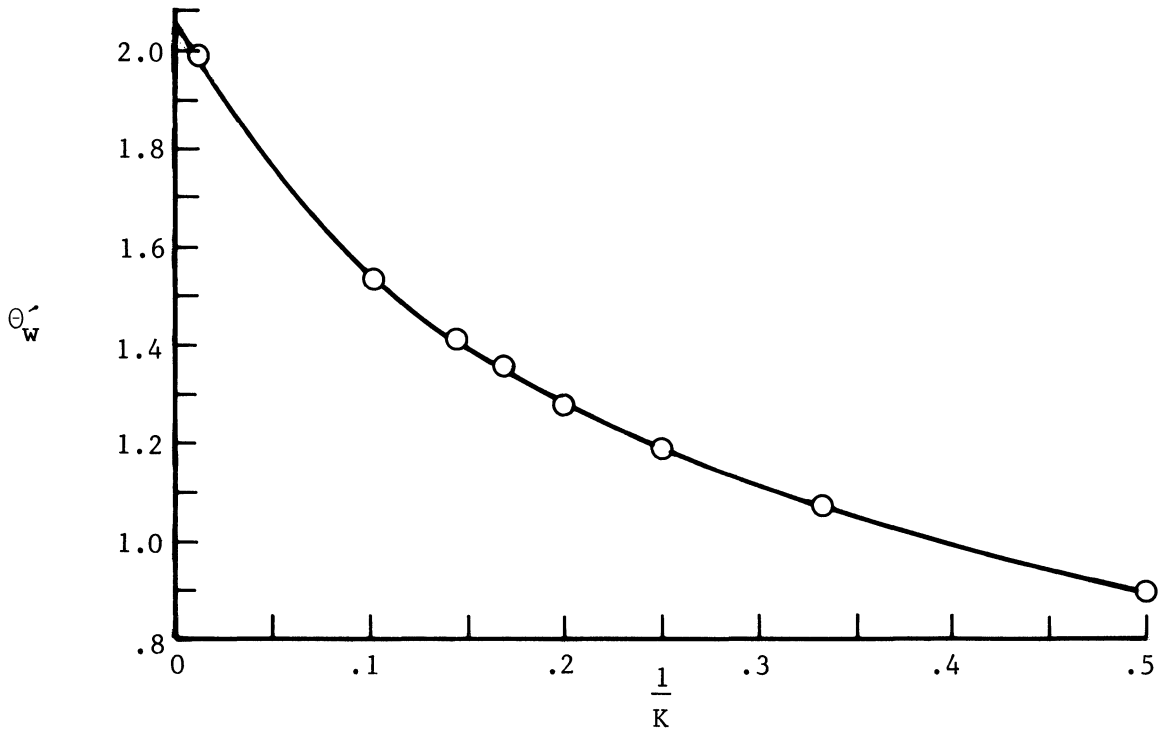

FIGURE IV-5.- Effect of number of iterations on θ'_w for the case of a sphere at $M_\infty = 10.0$, $s = 1.5$, $\delta\eta = 0.10$, $\delta s = 0.01$. K represents the number of iterations at each step in the s direction.

rapid with 5 to 10 iterations being required. This is probably due to the fact that for these cases the flow remains nearly similar as the solution marches along the body.

The most important conclusion one may form from these results is that whenever this method of solution is applied to boundary layer equations in regions where the flow departs appreciably from a similarity type flow, a sufficient number of iterations must be required to assure convergence.

4. Polynomials Used to Obtain Derivatives at the Wall

Although it is necessary to use a step size of 0.025 to obtain accurate results for F'_w and w'_w for the case of large R_o, the use of a third-order polynomial rather than a second-order polynomial to obtain derivatives at the wall improves accuracy and reduces computation time by allowing a larger step size to be used. For example, with $\epsilon = 0.001$ and $R_o = 400$ the percent difference between using second- and third-order polynomials to determine wall derivates is given in table IV-5.

TABLE IV-5.- EFFECT OF THE ORDER OF POLYNOMIALS USED TO EVALUATE WALL DERIVATIVES IN THE NORMAL DIRECTION. INCOMPRESSIBLE FLOW OVER A DISC WITH $R_o = 400$.

$\delta\eta$	$\left[\frac{F'_{w3} - F'_{w2}}{F'_{w3}}\right]$	$\left[\frac{W'_{w3} - W'_{w2}}{W'_{w3}}\right]$
0.025	0.0047	0.0025
0.05	0.0174	0.0069
0.10	0.580	0.112

In all instances the use of a 3rd-order polynomial brings the values of the wall derivatives closer to those obtained by Hannah.

5. Comparison With Previous Work

In order to verify the solutions obtained by the method outlined in the previous chapters, a comparison of the computed results with data previously obtained for various flow and geometry combinations was performed. In general, the quantities used for comparison purposes are the shear stress in the meridional and circumferential direction, and the heat flux at the body surface. Since the solution values are dependent upon step size and convergence criteria no effort was made to obtain exact correlation with previous work. Rather the results obtained herein were computed with nominal rather than optimum values of step size and convergence criteria. Since the previous work used in these comparisons ranges from exact solutions in the case of a spinning disc to solutions utilizing the Karman-Polhausen method in the case of the spinning sphere the agreement with the results computed herein will vary.

The velocity profiles for the case of an incompressible disc with no spin are compared with the results of Froessling as presented by Schlicting[33] to evaluate the stagnation point solutions. For this case the step size in the η direction was 0.10. The comparison is given in table IV-6.

TABLE IV-6.- COMPARISON OF VELOCITY PROFILES FOR INCOMPRESSIBLE STAGNATION POINT FLOW WITH EXACT SOLUTION

η	Froessling	Numerical method
0.2	0.1755	0.1756
0.4	0.3311	0.3312
1.6	0.4669	0.4670
0.8	0.5833	0.5834
1.0	0.6811	0.6812
1.2	0.7614	0.7616
1.6	0.8761	0.8762
2.0	0.9422	0.9424
2.4	0.9760	0.9762
2.8	0.9912	0.9913
3.2	0.9972	0.9972
3.6	0.9992	0.9992
4.0	0.9998	0.9998
4.4	0.9999	0.9999

Hannah[1] has presented results for the case of forced flow against an infinite rotating lamina. These represent exact solutions, consequently, the agreement with the results computed herein should be excellent.

In Hannah's formulation the condition of zero oncoming velocity could be handled thus giving solutions at $R_o = \infty$. The present formulation for the case of a spinning disc is valid for $R_o \gg 1.0$ but not for $R_o = \infty$. Consequently, the values of shear parameters are only given up to $R_o = 400$.

TABLE IV-7.- SHEAR PARAMETERS AS A FUNCTION OF SPIN RATE - INCOMPRESSIBLE FLOW OVER A SPINNING DISC

$\sqrt{R_o}$	R_o	$\frac{\sqrt{2}\, w'_w}{(1 + R_o)^{1/4}}$		$\frac{F'_w}{\sqrt{2}(1 + R_o)^{3/4}}$	
		Hannah	Computed	Hannah	Computed
0	0	-1.075	-1.079	0.656	0.656
0.5	0.25	-1.025	-1.030	0.583	0.583
1.0	1.0	-0.933	-0.939	0.468	0.467
2.0	4.0	-0.800	-0.803	0.343	0.341
∞	∞	-0.616	-0.626	0.255	0.254

Values of the shear parameters versus R_o are also shown on figures IV-6 and IV-7. The solid curve represents values from the computer program. The data points are from Hannah's report. In all cases $\eta = 0.0025$ and $\epsilon = 0.001$.

A comparison of the present method with the results of Illingsworth[5] for the case of a spinning cone in supersonic flow is shown in figures IV-7(a) and (b).

In Illingsworth's analysis data to terms of order s^4 for τ_s were presented, consequently, the results should not be expected to agree too well as s increases. For τ_ϕ terms to order s^2 only

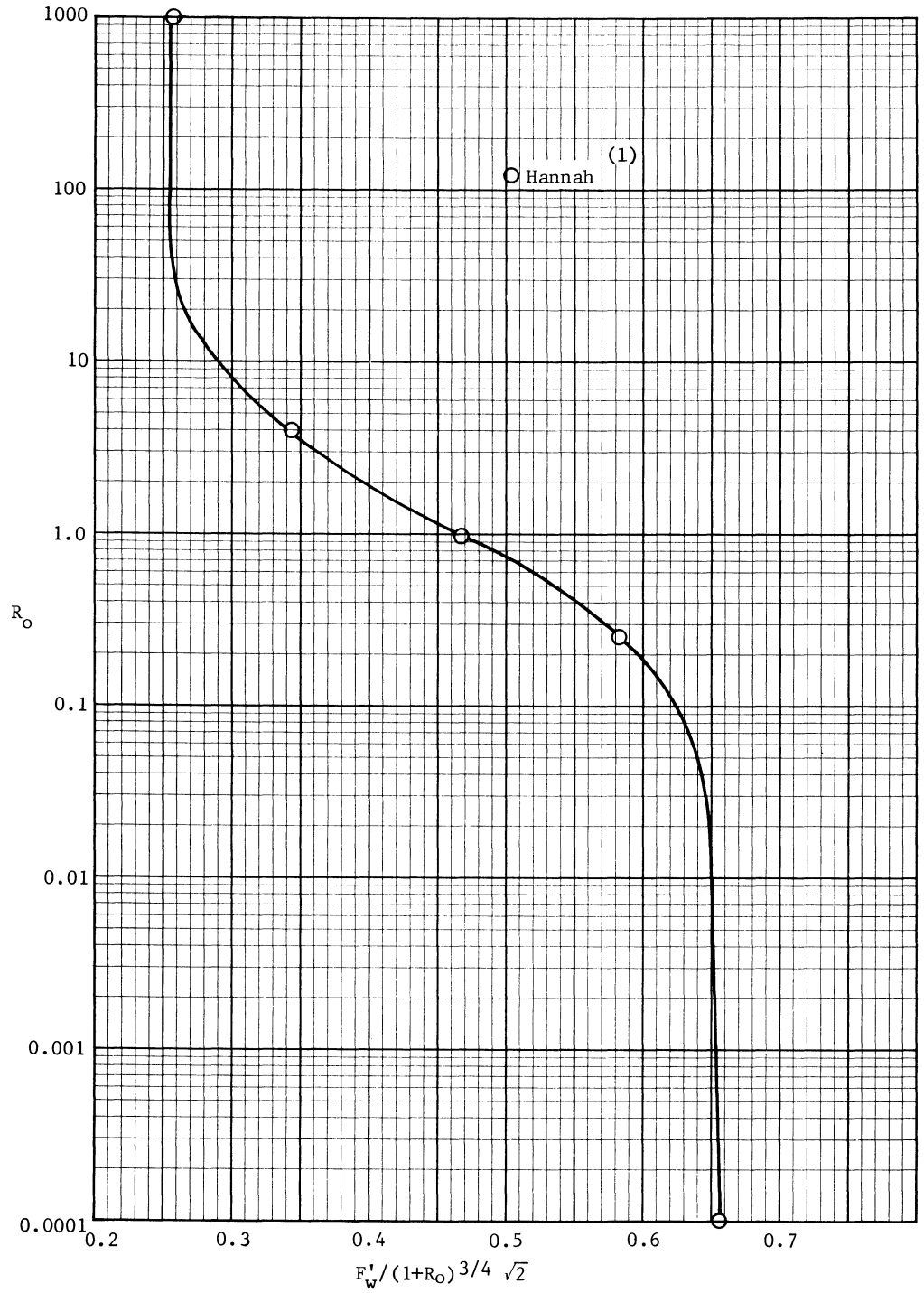

Figure IV-6(a).- Variation of the meridional shear parameter with spin for incompressible flow over a disc.

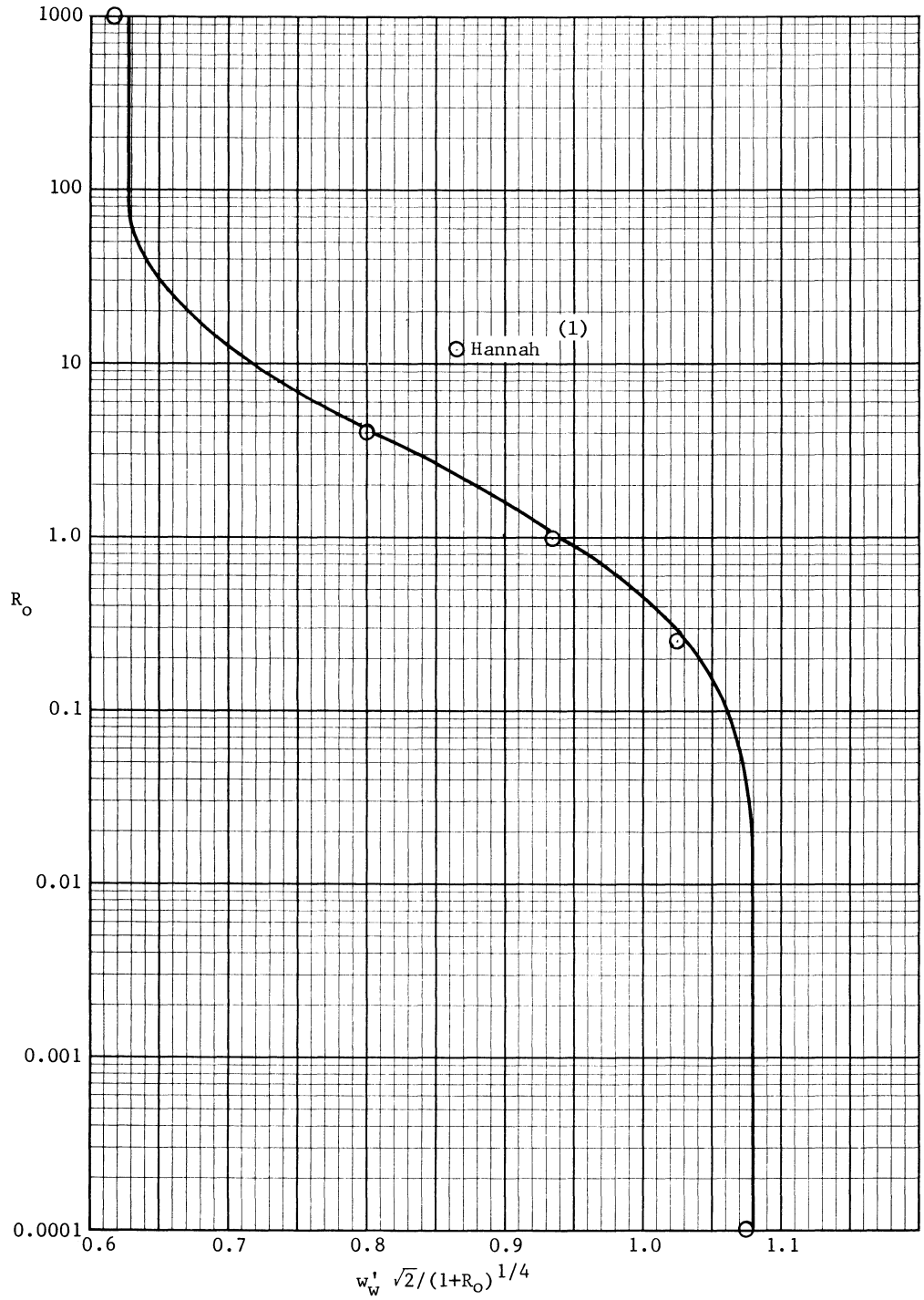

Figure IV-6(b).- Variation of the circumferential shear parameter versus spin for incompressible flow over a disc.

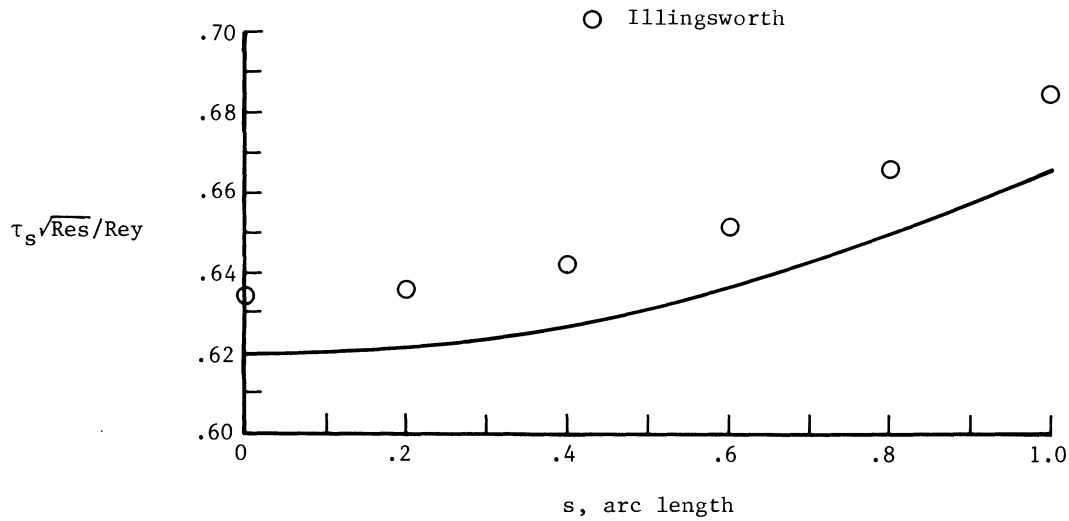

a) Meridonal shear stress, τ_s.

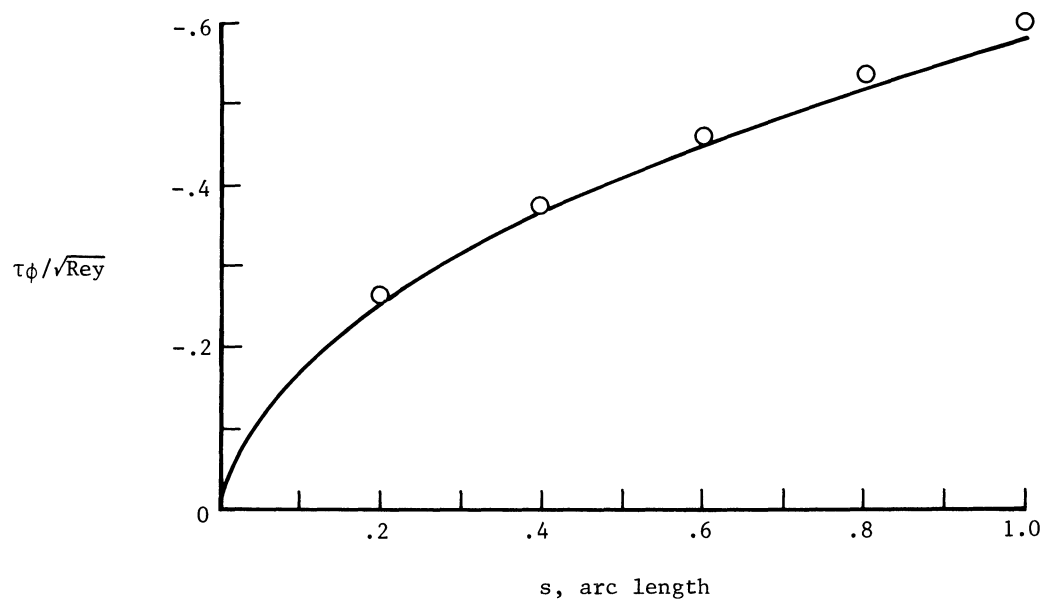

b) Circumferential shear stress, $\tau\phi$

FIGURE IV-7.- Comparison of shear stress on a 30° half angle cone at M_∞ = 2.0 and R = 0.25 with the results of Illingsworth. a) Meridonal shear stress, τ ; b) Circumferential shear stress, $\tau\phi$.

were presented. Also in his analysis $P_r = 1.0$, and the viscosity was assumed to vary linearly with temperature, consequently, $l = \rho\mu/\rho_e\mu_e = 1.0$ and the energy equation becomes completely uncoupled from the momentum equation.

Schlicting[6] has presented results for a spinning sphere in incompressible flow. These data are in the form of shear stress in the meridional and circumferential directions. Figures IV-8 and IV-9 show the variation of $\tau_s \sqrt{R_{es}}/Rey$ and $\tau_\phi/\sqrt{Rey}$ versus arc length along the sphere surface with spin rate varied. The data points are from Schlicting. In the case of meridional shear the two sets of data agree very well for $R_o = 0$ and 1.0 up to $s = 1.2$. However, as s increases beyond 1.2 the agreement between the two curves is not as good. Schlicting's method at first underestimates the shear stress and then overestimates it as the separation point is reached. The circumferential shearing stress does not agree as well as the meridional shearing stress. In fact, the value of τ_ϕ for $R_o = 1.0$ is less than the limiting value for $R_o = 0$ over most of the sphere. However, as the data shows τ_ϕ does not vary much between $R_o = 0$, and $R_o = 1.0$. Since Schlicting's method is limited to values of R_o less than about 1.2 no other comparisons could be made. Table IV-8 shows the variation of separation point with R_o. Schlicting's method consistently predicts that the separation point location will be further along the body.

The case of a sphere in a compressible flow with no spin was compared with the results of Davis. Although the method of solution is identical

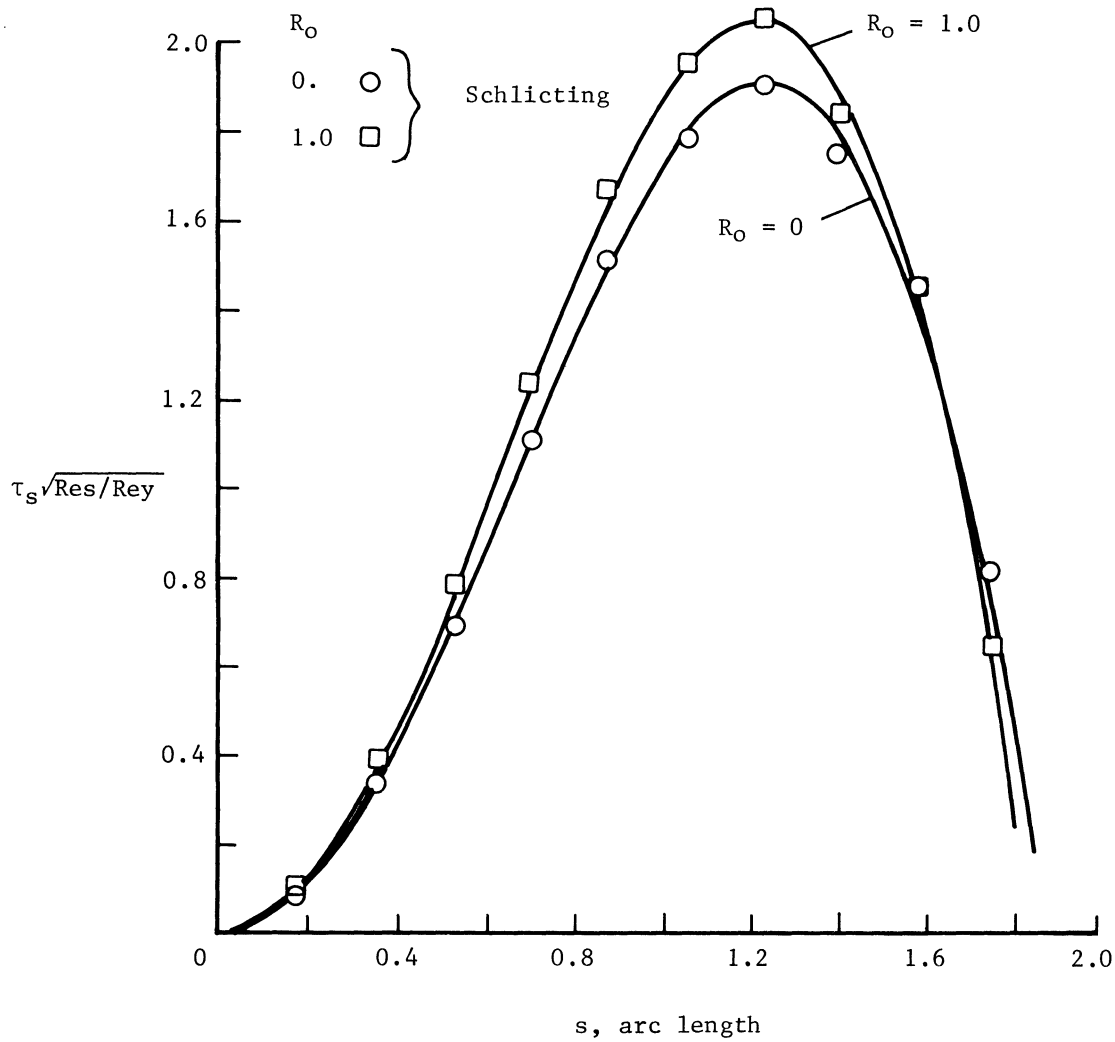

FIGURE IV-8.- Meridional shear stress versus arc length for incompressible flow over a sphere with R_o = 0., and 1.0.

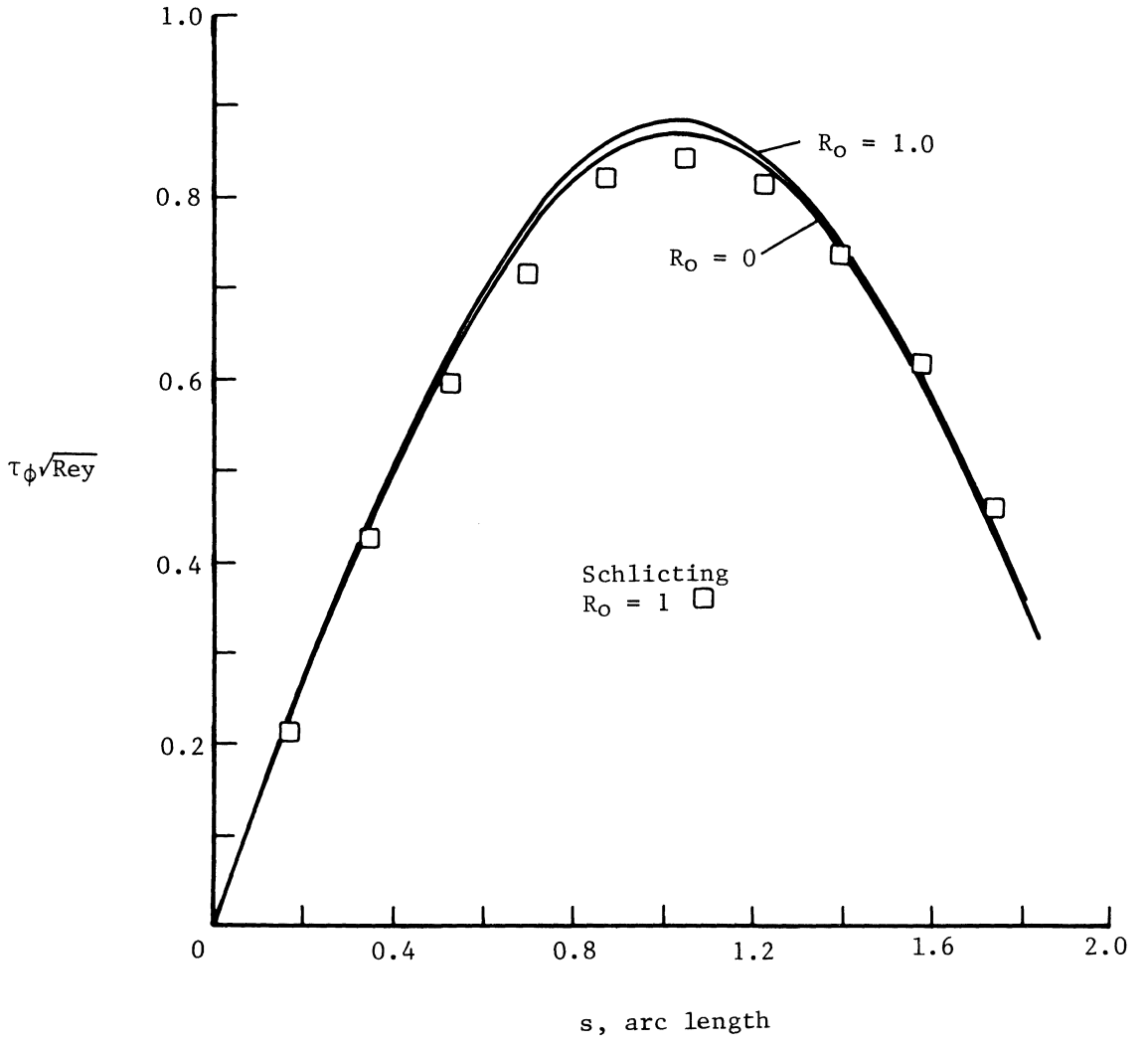

FIGURE IV-9.- Circumferential shear stress for incompressible flow over a sphere with R_o = 0 and 1.0.

TABLE IV-8.- SEPARATION POINT COMPARISON WITH SCHLICTING FOR INCOMPRESSIBLE FLOW OVER A SPHERE

s, rad	Degrees calculated	Degrees Schlicting	R_o
1.84-1.85	105.92-105.99	108.3	0
---	---	108	0.0625
1.83-1.80	104.85-105.42	107.2	0.25
1.82-1.83	104.27-104.55	106.2	0.5625
1.80-1.81	103.13-103.70	104.9	1.0
1.77-1.78	101.41-101.99	---	2.25
1.74-1.75	99.69-100.27	---	4.0

with Davis's, variations in the convergence criteria and step size cause the result to be in slight disagreement as the solution progresses along the body. Davis' convergence criteria is a requirement that F'_w not change by more than 0.001 whereas in this method $(P_K(\eta) - P_{K-1}(\eta))/P_{K-1}(\eta)$ must not be greater than 0.1, where K represents the number of iterations. In this present method this requirement is imposed upon all three dependent variables simultaneously. It was found that Davis' method required one iteration to converge, thus direct comparisons could be obtained by requiring this solution to make only one iteration. However, the step size discrepancy could not be easily accounted for; Davis specifies step size in the transformed coordinates $\delta\eta$ and $\delta\xi$ whereas in this method step size in the transformed coordinate $\delta\eta$ but in the untransformed coordinate δs, are specified thus $\delta\xi$ is a variable as the solution progresses along the body. This could account for the fact that the solutions are in

excellent agreement for small s but diverge as s grows larger. These comparisons are shown in figures IV-10 and IV-11.

The work of Koh and Price[28] most clearly parallels the method used herein. Consequently, the best agreement is anticipated. However, differences in the two analyses do exist. Koh and Price used a modified Crank Nicholson scheme whereas in this case a purely implicit scheme was used. Secondly, the step sizes chosen were both in the transformed variables whereas in this work the transformed step size in the meridional direction is constantly changing. Another factor affecting the comparison of these methods is the convergence criteria. The method of determining convergence is not given in their report, however, they do state that two or three iterations were required. In spite of these differences the agreement between the two analyses is very good. Figures IV-12 and IV-13 show typical comparisons of the nondimensional drag and moment versus spin rate.

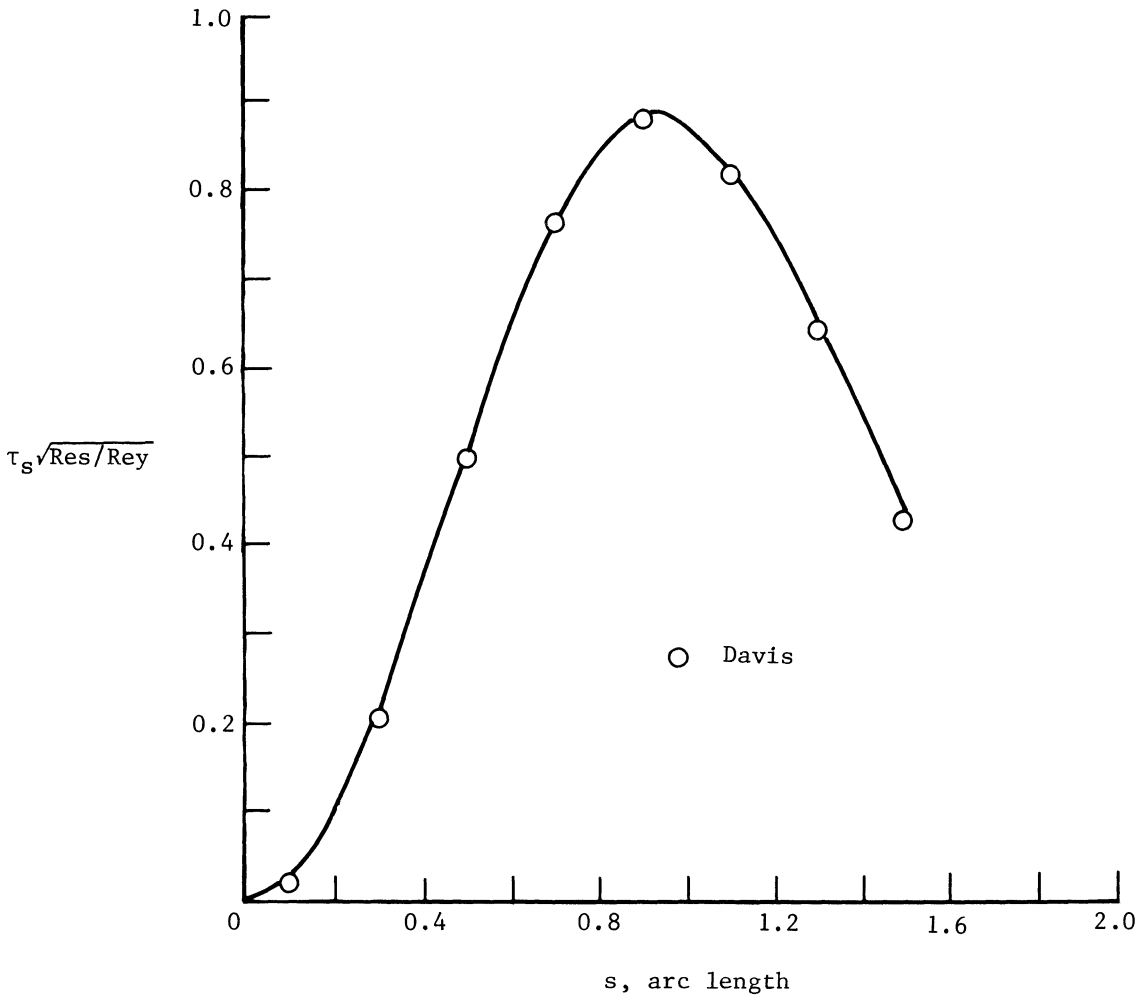

FIGURE IV-10.- Meridional shear stress for compressible flow over a sphere. $M_\infty = 10.$, $R_O = 0$, $\Theta_w = 0.6T_O/T_e$.

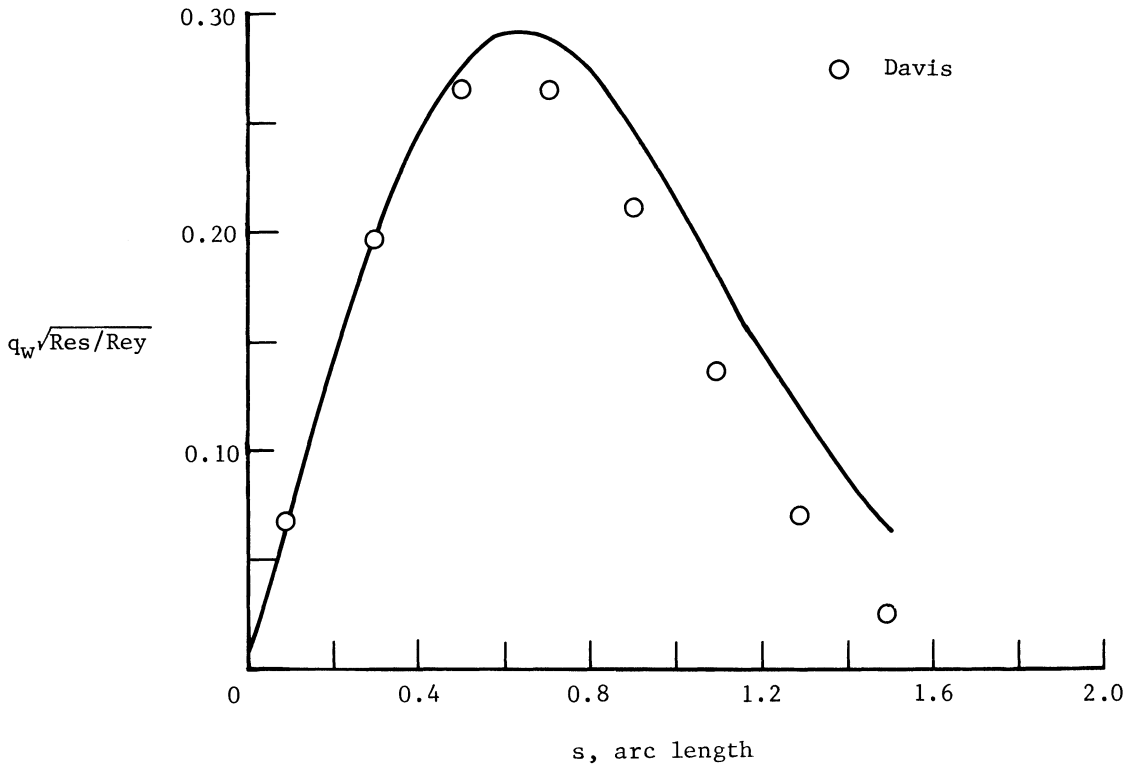

FIGURE IV-11.- Heat transfer coefficient for compressible flow over a sphere. $M_\infty = 10.$, $R_o = 0$, $\Theta_w = 0.6T_o/T_e$.

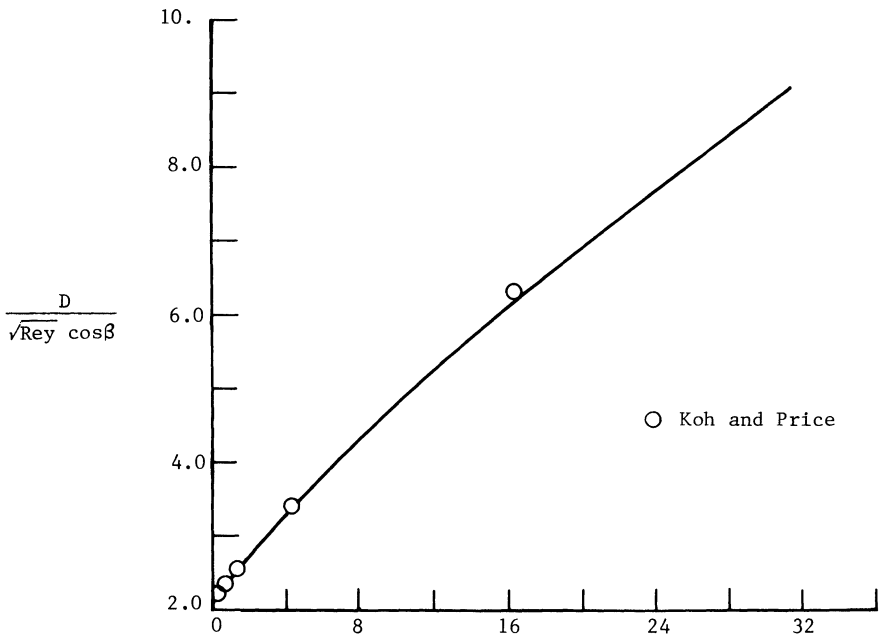

FIGURE IV-12.- Viscous drag on a 53.5° cone in incompressible flow versus spin rate.

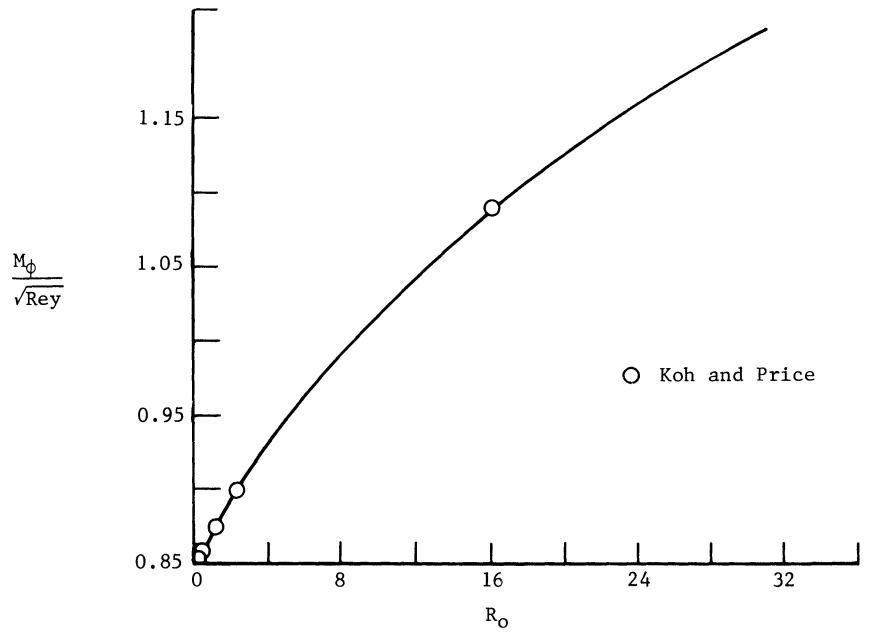

FIGURE IV-13.- Viscous moment on a 53.5° cone in incompressible flow versus spin rate.

CHAPTER V. RESULTS OF PARAMETER STUDY

Presentation and Discussion of Results

1. Introduction

The effects of spin on the boundary layer variables are presented in this chapter. In general, the shear stress in the meridional and circumferential directions are presented for each geometry, along with the displacement thickness. The heat transfer is also presented where applicable. Typical profiles of F, w, and Θ are also presented at a few values of s. The general format is to present these quantities as functions of arc length, s, and spin parameter R_o. The edge pressure p_e is also presented for those cases where it cannot otherwise be represented. The frictional drag and moment coefficients are also presented for all cases. In general, spin is shown to increase the meridional shear stress, and the circumferential shear stress. The variation of the displacement thickness with increasing spin rate depends on whether the flow is compressible or incompressible, δ_1 decreases with increasing spin rate for compressible flow and increases with increasing spin rate for incompressible flows. At high enough spin rates, overshoot occurs in the meridional velocity, and for compressible flow significant heating of the boundary layer accompanies spinning. This heating is caused by the vicous dissipation of the energy imparted to the boundary layer by the spinning body. The stream condition for each case is given in table V-1.

TABLE V-1.- STREAM CONDITIONS FOR EACH CASE PRESENTED

CASE NO.	1	2	3	4	5	6	7
U^*_∞ =	0.1×10^5,	0.98387×10^5,	0.1×10^5,	0.1×10^5,	0.1×10^5,	0.1×10^5,	0.1×10^5,
T^*_∞ =	0.4×10^5,	0.4×10^5,	0.4×10^5,	0.52×10^5,	0.4×10^5,	0.4×10^5,	0.4132×10^5,
ρ^*_∞ =	0.14×10^5,	0.2378×10^5,	0.14×10^5,	0.2378×10^5	0.2378×10^5,	0.14×10^5,	0.306×10^5,

For all cases γ = 1.4

R^* = 1728.56

S^* = 198.3

$\mu_\infty = .37\times10^{-6}$

CASE NO.	DESCRIPTION
1	Compressible flow over a cone
2	Compressible flow over a sphere
3	Compressible flow over a paraboloid
4	Incompressible flow over a cone
5	Incompressible flow over a sphere
6	Compressible flow over a hyperboloid
7	Compressible flow over a tangent ogive

Case 1. Compressible Flow Over a Cone

The results for the analysis of compressible flow over a cone are presented in figures V-1 to V-4. The meridional and circumferential shear stresses, and the displacement thickness are presented on figure V-1. The meridional shear stress, τ_s, increases with both spin rate and arc length due to the momentum imparted to the fluid which results in increased boundary layer meridional velocities. The circumferential shear stress, τ_ϕ, decreases with increasing R_o but the variation is not nearly as great. It should be recalled that T_ϕ is nondimensionalized using the spin rate, thus, τ^*_ϕ is actually increasing with spin rate. The displacement thickness, δ_1, increases with increasing R_o and s due to a decrease in density as temperatures in the boundary layer become higher. Figure V-2 shows variation of the meridional velocity function, F, versus R_o and η at s = 0., 0.5, and 1.0. Note as s or R_o become large velocity overshoot will occur in the boundary layer. Figure V-3 shows the variation of the circumferential velocity function, w, versus R_o and η at s = 0., 0.5 and 1.0. w decreases with increasing s or R_o. Once again w^* will be increasing with R_o or s since w is nondimensionalized using Ω^*. The effect of R_o and s on the temperature function Θ are shown on figure V-4. Increasing R_o or s cause Θ to increase drastically. In fact, at $R_o = 49$ and s = 1.0 temperatures in the boundary layer reach approximately 138000 ^oR. At these temperatures the assumption of a perfect

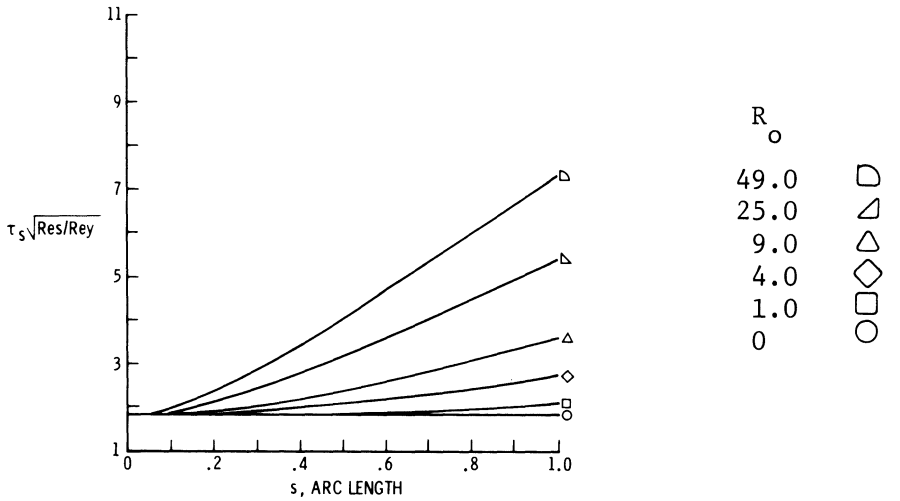

(a) MERIDONAL SHEAR STRESS, τ_s

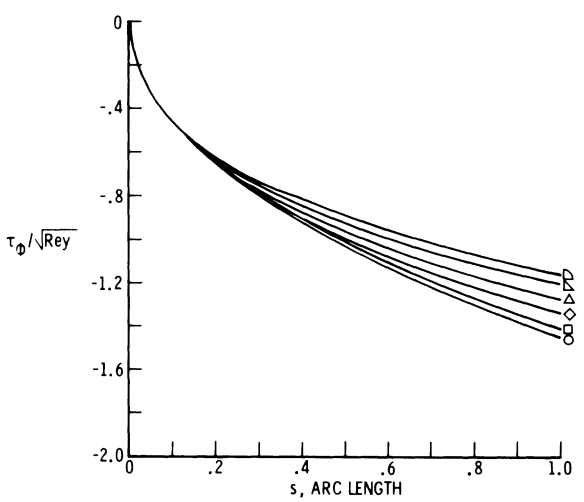

(b) CIRCUMFERENTIAL SHEAR STRESS, τ_ϕ

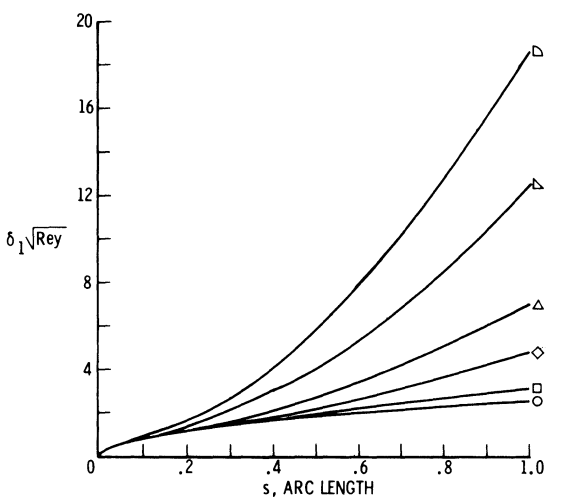

(c) DISPLACEMENT THICKNESS, δ_1

FIGURE V-1.- Compressible flow over a 30° half angle cone at M_∞ = 10. and $\hat{\theta_w}$ = 0; a) Meridional shear stress, τ_s; b) Circumferential shear stress, τ_ϕ; and c) Displacement thickness, δ_1, versus arc length, s, and spin parameter, R_o.

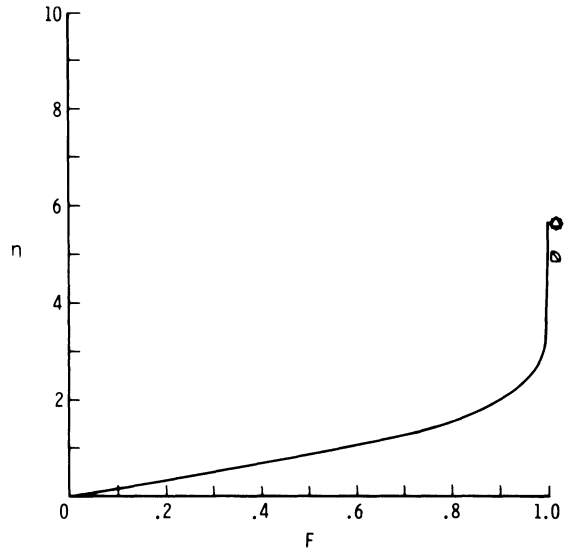

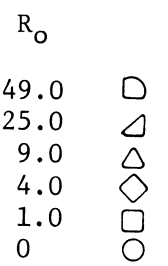

(a) s = 0.0

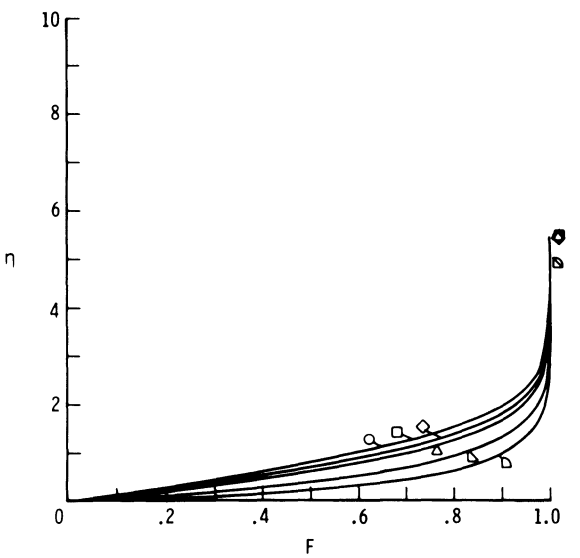

(b) s = 0.5

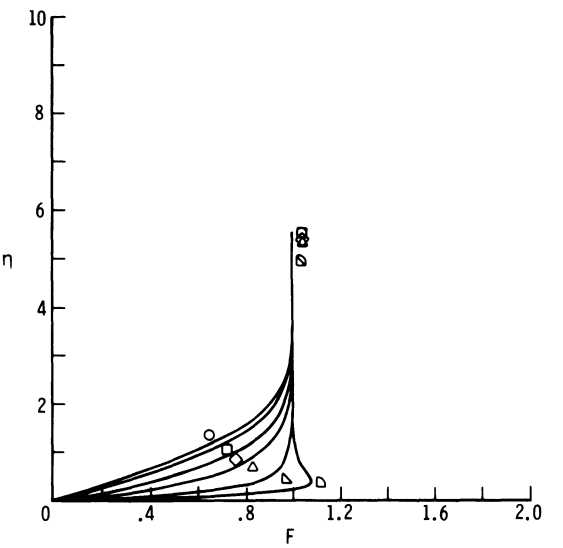

(c) s = 1.0

FIGURE V-2.- Compressible flow over a 30^{o} half angle cone at M_{∞} = 10. and $\Theta_{\hat{w}}$ = 0. Meridional velocity function, F, versus normal coordinate, η, and spin parameter, R_o, at three points on the cone; a) s = o.; b) s = 0.5; and c) s = 1.0.

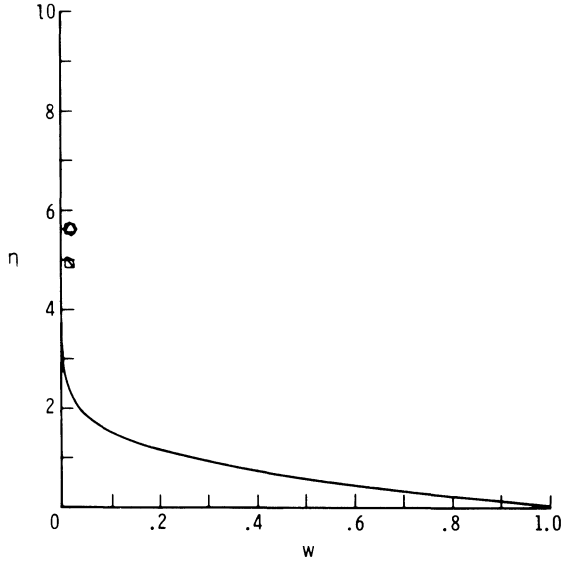

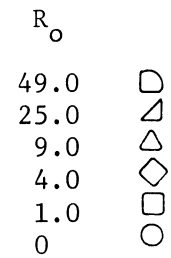

(a) s = 0.0

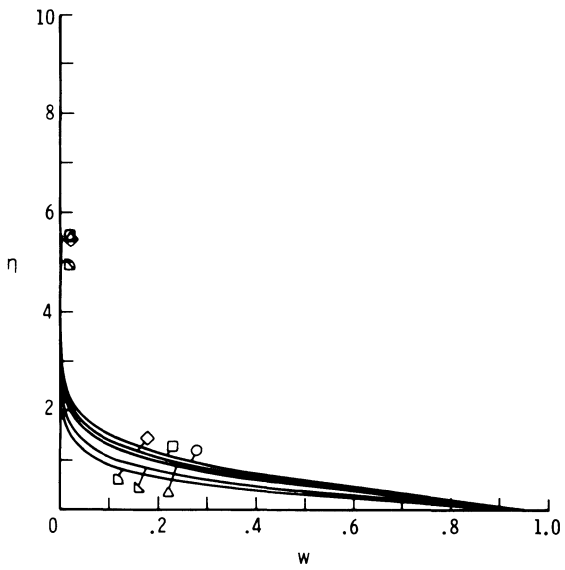

(b) s = 0.5

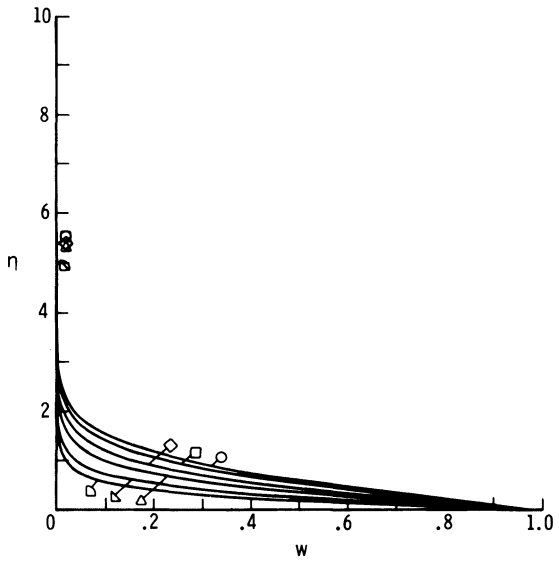

(c) s = 1.0

FIGURE V-3.- Compressible flow over a 30° half angle cone at M_∞ = 10. and $\Theta_w' = 0$. Circumferential velocity function, w, versus normal coordinate, η, and spin parameter, R_o, at three points on the cone; a) s = 0.; b) s = 0.5; c) s = 1.0.

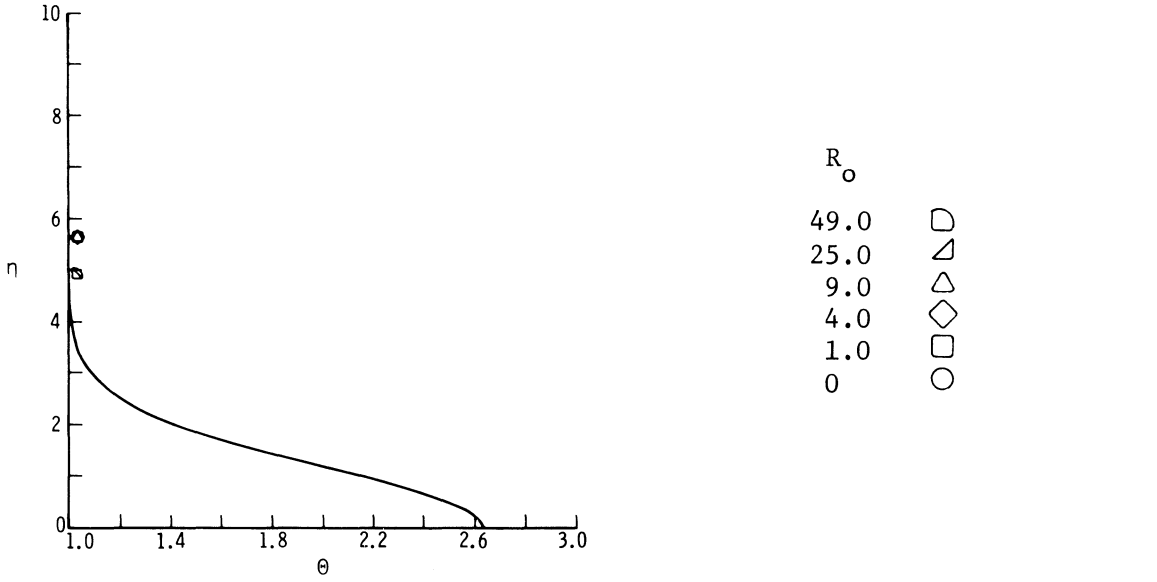

(a) s = 0.0

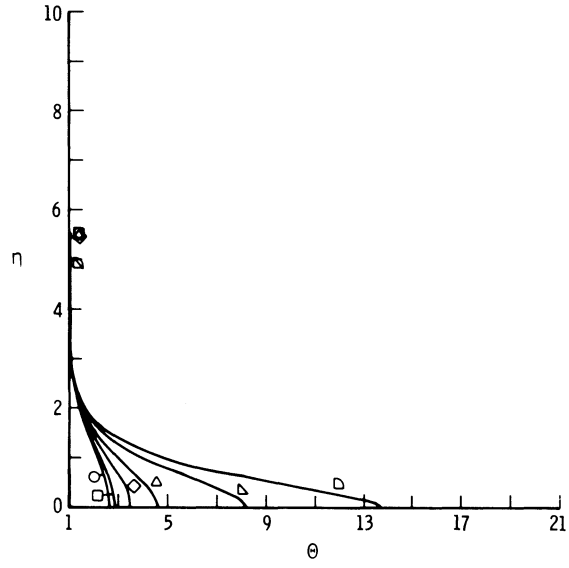

(b) s = 0.5

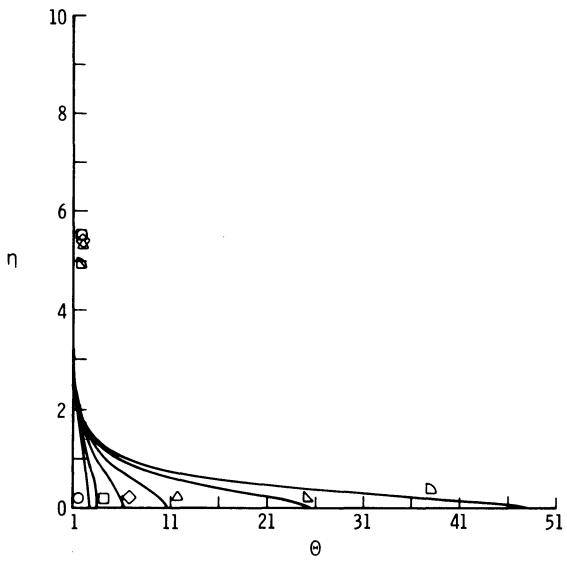

(c) s = 1.0

FIGURE V-4.- Compressible flow over a 30° half angle cone at M_∞ = 10. and Θ_w' = 0. Temperature function, Θ, versus normal coordinate, η, and spin parameter, R_o, at three points on the core; a) s = 0.; b) s = 0.5; c) s = 1.0.

gas is not valid and, in fact, the air has gone through the stages from a perfect gas flow to a nonequilibrium flow to an equilibrium flow with dissociation.

Case 2. Compressible Flow Over a Sphere

The case of a sphere in a compressible flow is shown on figures V-5 to V-8. The free stream Mach number for this case was 10., and a wall condition of $\Theta_w' = 0.$ is specified. The solutions are shown for a maximum value of $s = 1.50$. As would be expected τ_s increases with R_o as in the other cases, however, the peak value is approximately eight times the no spin value as compared to an increase of less than four times for the incompressible flow over a sphere. The variation in τ_ϕ with R_o occurs on the forward portion of the sphere between $s = 0$ and .8, for $s > .8$ τ_ϕ is essentially constant with s. The displacement thickness increases by a factor of about 19 at $s = 1.5$ for the maximum spin case. Note that near the stagnation point negative values of δ_1 occur due to velocity overshoot, however, as s increases the increase in temperature with a resulting decrease in density ratio causes δ_1 to become positive. The velocity profile in the meridional direction shows a maximum overshoot of about 4.25 at $s = 1.0$ and $R_o = 49$. The circumferential velocity w decreases with R_o at all three s locations shown. Note w^* increases with R_o. The most notable effect of spin in the compressible flow cases is the heating which takes place. In fact, as figure V-8(b) shows values of T_w^* reach approximately $440000\ ^oR$ at $s = 1.0$ and $R_o = 49$. Even higher temperatures are calculated at larger values of s.

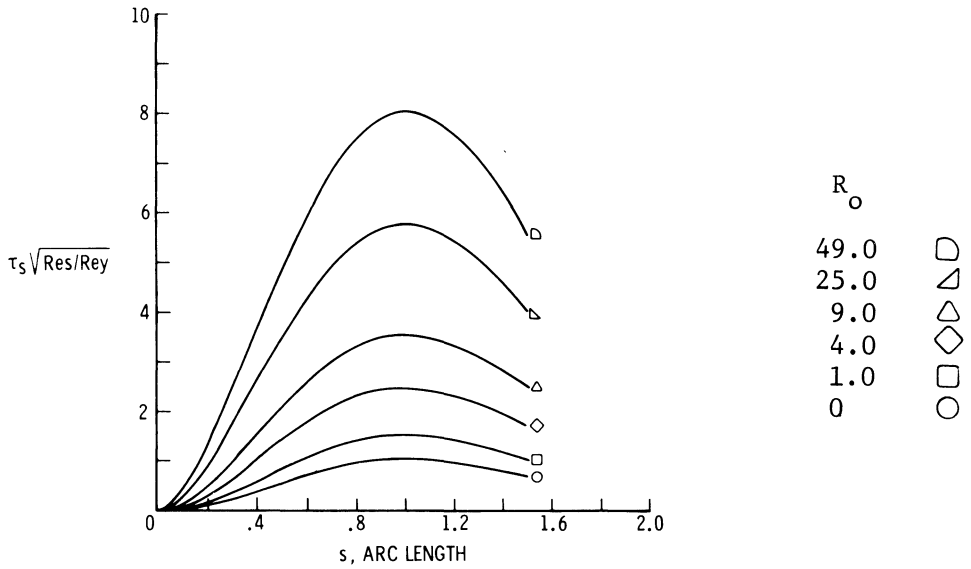

(a) MERIDONAL SHEAR STRESS, τ_s

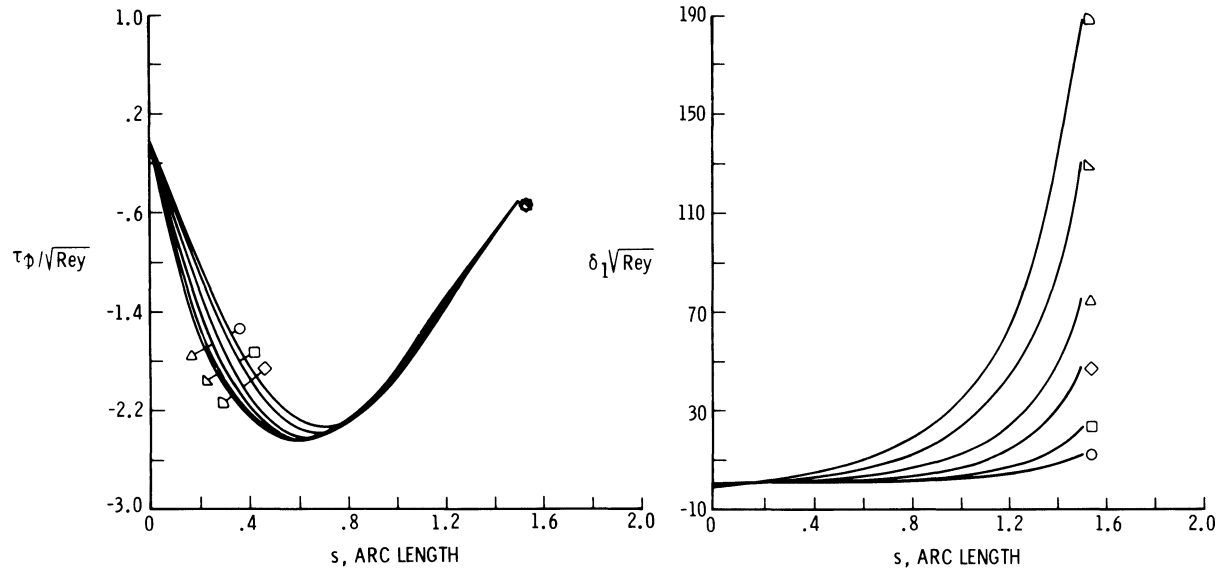

(b) CIRCUMFERENTIAL SHEAR STRESS, τ_ϕ (c) DISPLACEMENT THICKNESS, δ_1

FIGURE V-5.- Compressible flow over a sphere at M_∞ = 10. and Θ_w' = 0; a) Meridional shear stress, τ_s; b) Circumferential shear stress, τ_ϕ; and c) Displacement thickness, δ_1, versus arc length, s, and spin parameter, R_o.

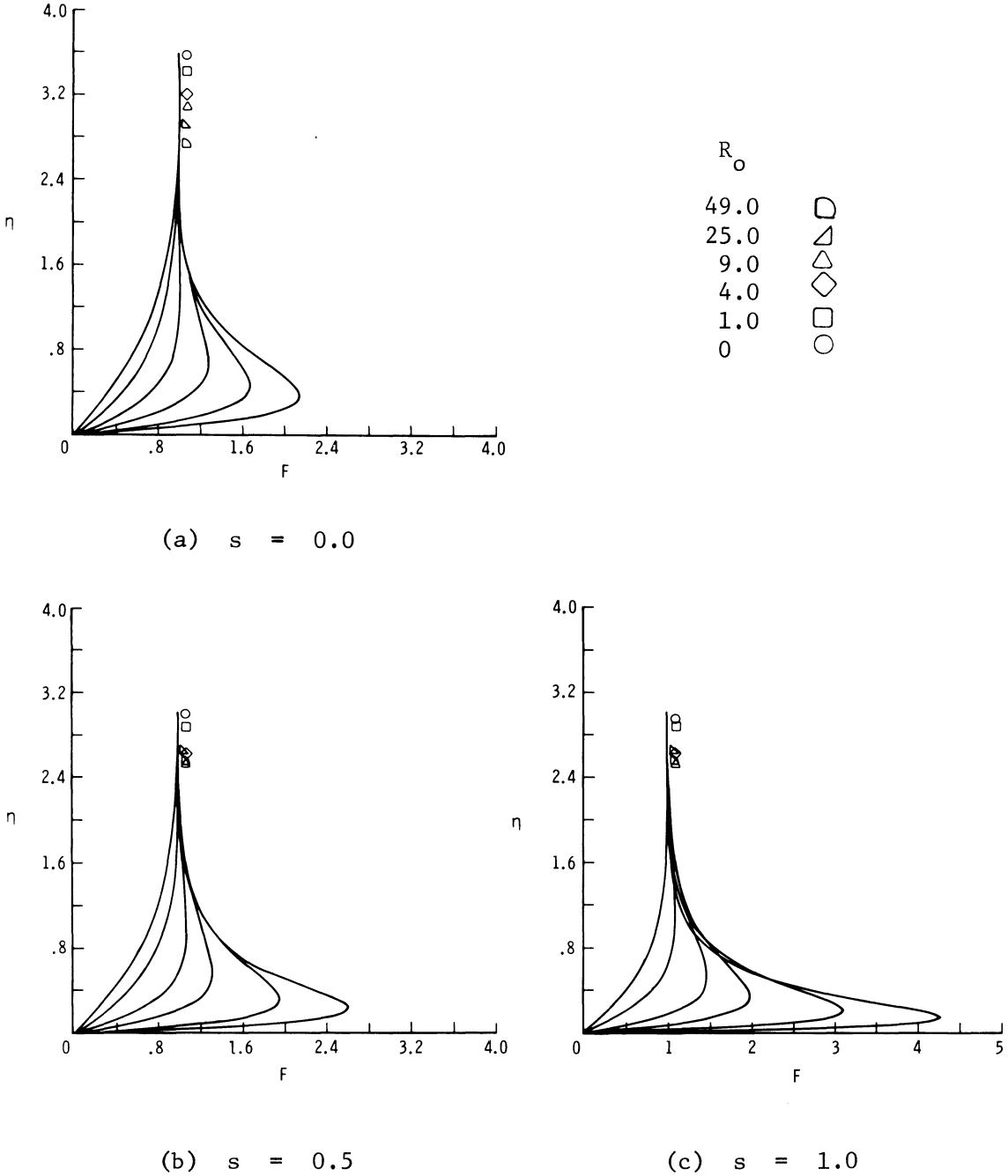

(a) s = 0.0

(b) s = 0.5

(c) s = 1.0

FIGURE V-6.- Compressible flow over a sphere at M_∞ = 10. and θ_w' = 0. Meridional velocity function, F, versus normal coordinate, η, and spin parameter, R_o, at three points on the sphere; a) s = 0.; b) s = 0.5; and c) s = 1.0.

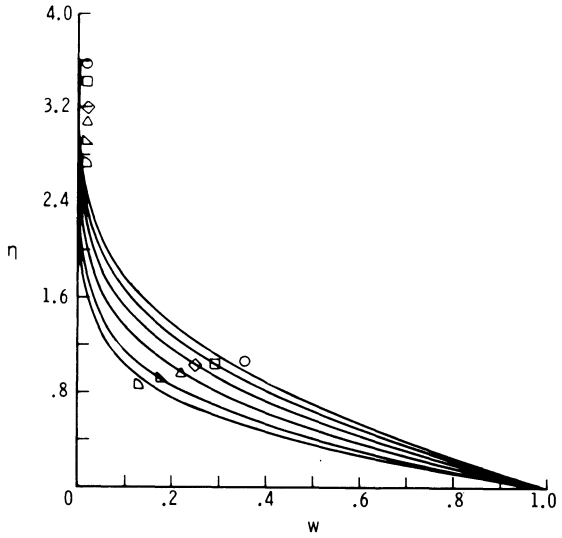

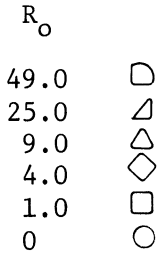

(a) s = 0.0

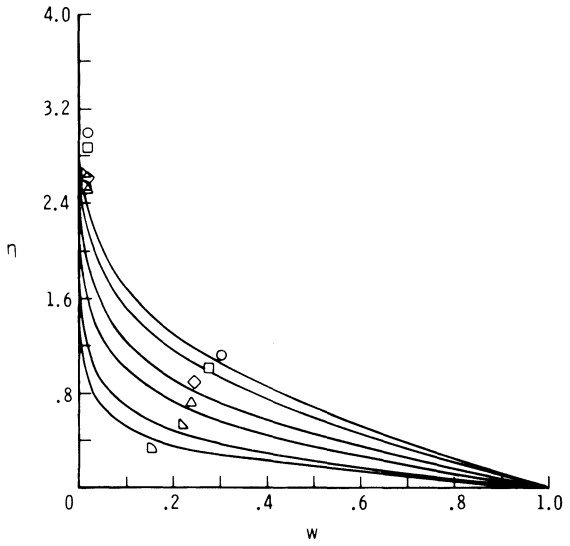

(b) s = 0.5

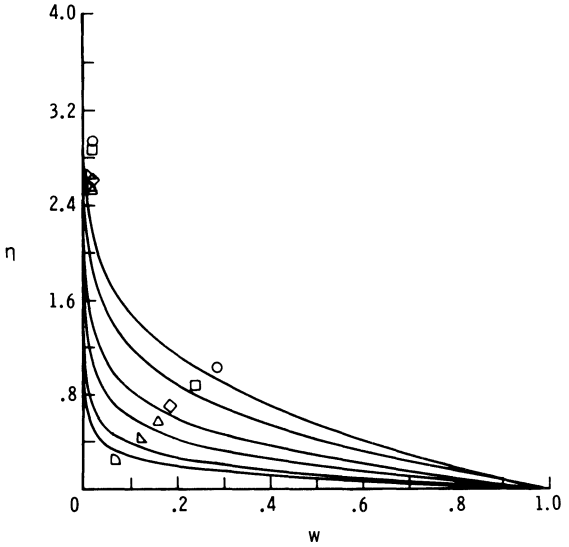

(c) s = 1.0

FIGURE V-7.- Compressible flow over a sphere at M_∞ = 10. and θ_w' = 0. Circumferential velocity function, w, versus normal coordinate, η, and spin parameter, R_o, at three points on the sphere; a) s = 0.; b) s = 0.5; c) s = 1.0.

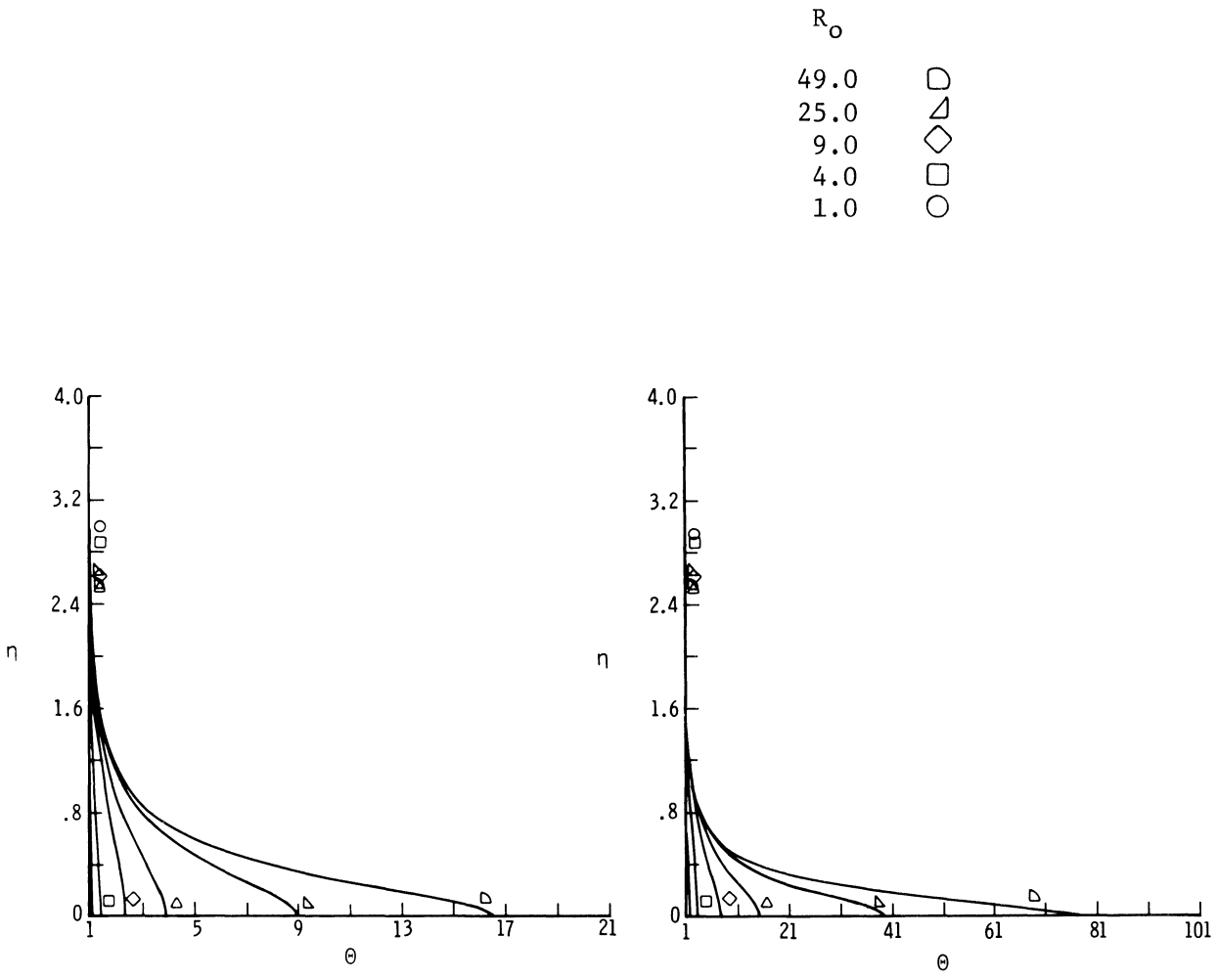

FIGURE V-8.- Compressible flow over a sphere at M_∞ = 10. and Θ_w' = 0. Temperature function, Θ, versus normal coordinate, η, and spin parameter, R_o, at two points on the sphere; a) s = 0.5; b) s = 1.0.

Case 3. Compressible Flow Over a Paraboloid

The edge pressure, p_e, on a paraboloid at $M_\infty = 10$ is shown on figure V-9. The radius of curvature of the paraboloid at the stagnation point is 1.0. τ_s, τ_ϕ, and δ_1 for this case are shown on figure V-10. The effect of spin on τ_s, τ_ϕ, and δ_1 is similar to the results of case 2. Once again τ_ϕ is not greatly affected by spin rate. The meridional velocity function, F, is shown versus, η, at $s = 0., 2.0$ and 4.0 on figure V-11. The circumferential velocity function, w, is shown on figure V-12 and the temperature function, Θ is shown on figure V-13 at $s = 2.0$ and 4.0.

Case 4. Incompressible Flow Over a Cone

A cone semi-vertex angle of 30° was selected for this case yielding $j \approx .11$ in the expression for u_e. Values of R_o of 0, 1, 4, 16, 25 and 49 were used in this study. Free-stream conditions were such that a Reynolds number of 6.427×10^5 resulted. The cone semi-vertex angle resulted in a value of β of about 0.0709. These results are shown on figures V-14 to V-16.

As previously obtained the value of F'_w for the case of $R_o = 0$ is constant, as could be expected since similar solutions exist for this case. However, for values of $R_o \neq 0$ similar solutions do not exist and F'_w becomes a function of s. The effect of spin on τ_s results in a considerable increase in shear stress as s or R_o increase. τ_ϕ is not affected to as great a degree.

The displacement thickness behaves in a predictable manner. The contribution of the centrifugal force caused by the spinning body causes

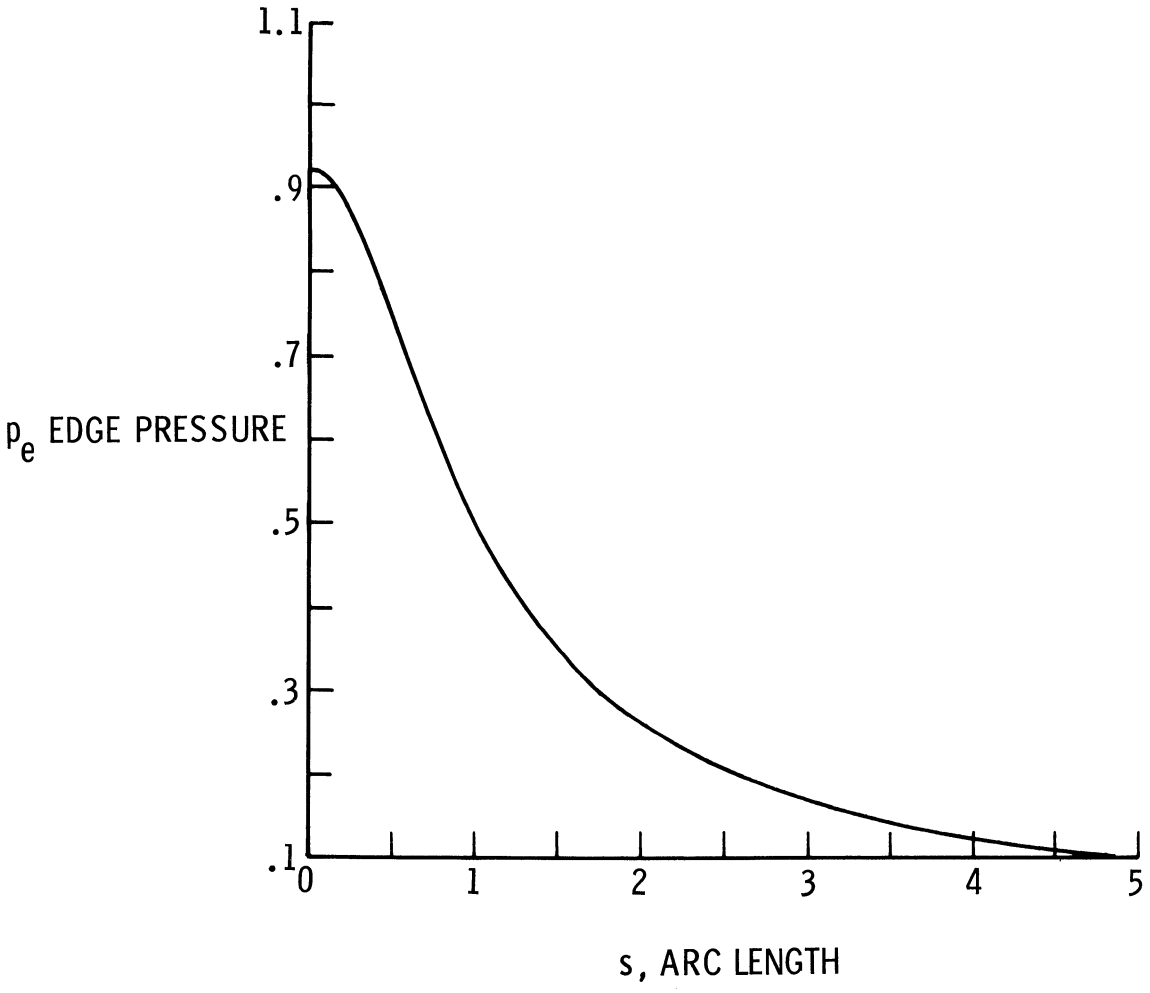

FIGURE V-9.- Compressible flow over a paraboloid with radius of curvature at the stagnation point = 1.0, at M_∞ = 10. and $\Theta_w' = 0$. Edge pressure, p_e, versus arc length, s.

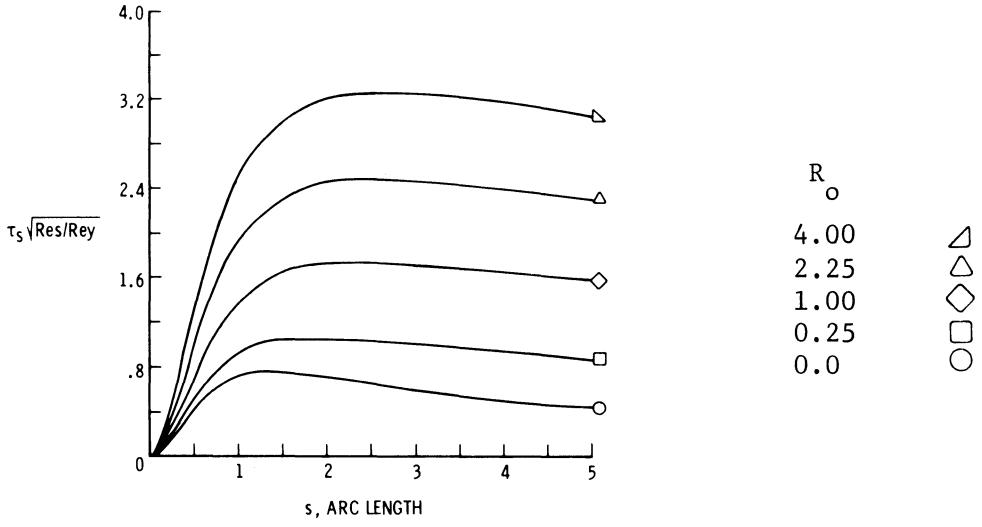

(a) MERIDONAL SHEAR STRESS, τ_s

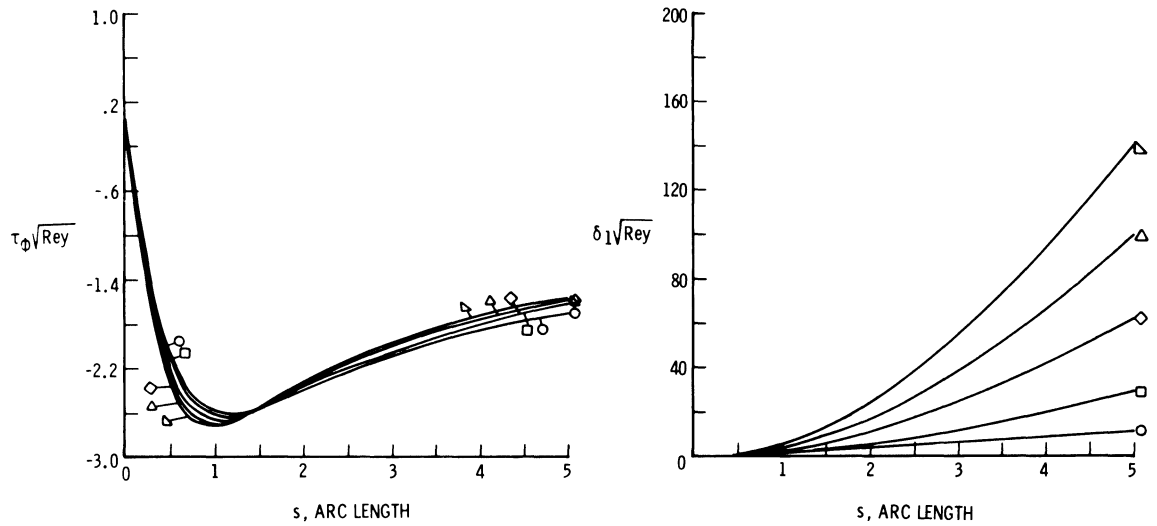

(b) CIRCUMFERENTIAL SHEAR STRESS, τ_ϕ (c) DISPLACEMENT THICKNESS, δ_1

FIGURE V-10.- Compressible flow over a paraboloid with radius of curvature at the stagnation point = 1.0, at M_∞ = 10. and $\Theta_w' = 0.$; a) Meridional shear stress, τ_s; b) Circumferential shear stress, τ_ϕ; and c) Displacement thickness, δ_1, versus arc length, s, and spin parameter, R_o.

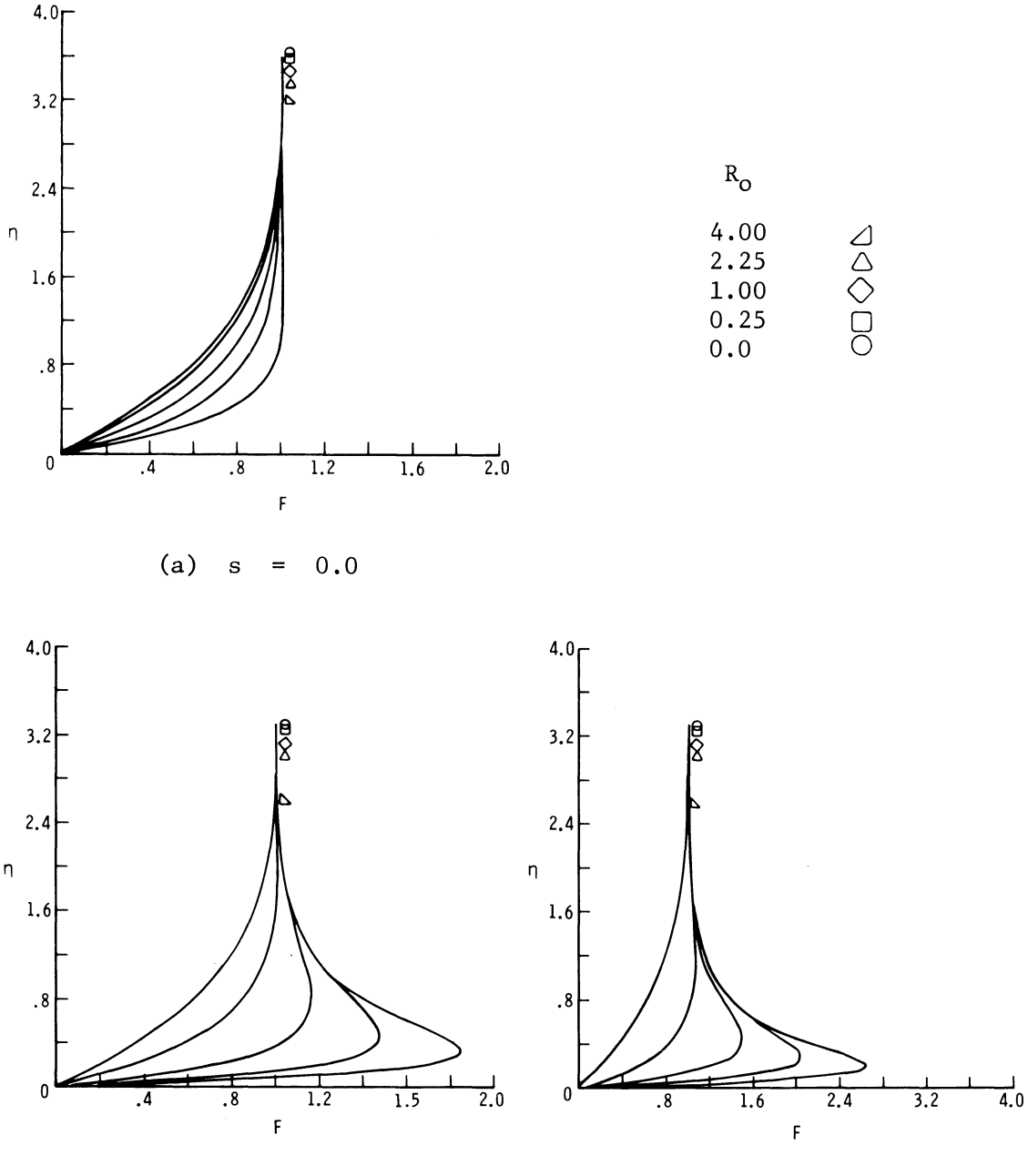

FIGURE V-11.- Compressible flow over a paraboloid with radius of curvature at the stagnation point = 1.0, at M_∞ = 10. and Θ_w = 0. Meridional velocity function, F, versus normal coordinate, η, and spin parameter, R_o, at three points on the paraboloid; a) s = 0.; b) s = 2.0; and c) s = 4.0.

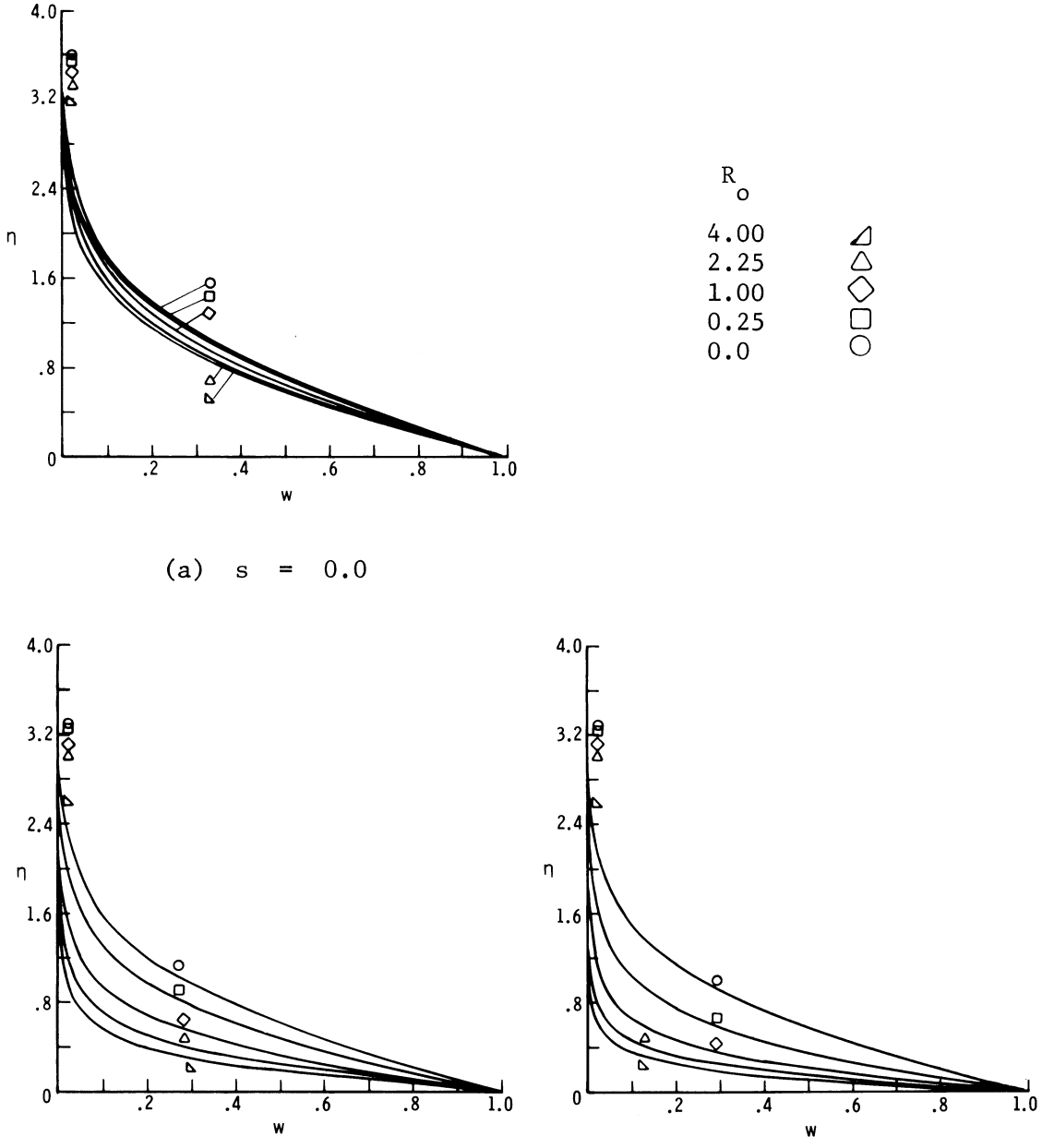

(a) s = 0.0

(b) s = 2.0

(c) s = 4.0

FIGURE V-12.- Compressible flow over a paraboloid with radius of curvature at the stagnation point = 1.0, at M_∞ = 10. and $\theta_w' = 0$. Circumferential velocity function, w, versus normal coordinate, η, and spin parameter, R_o, at three points on the paraboloid; a) s = 0.; b) s = 2.0; c) s = 4.0.

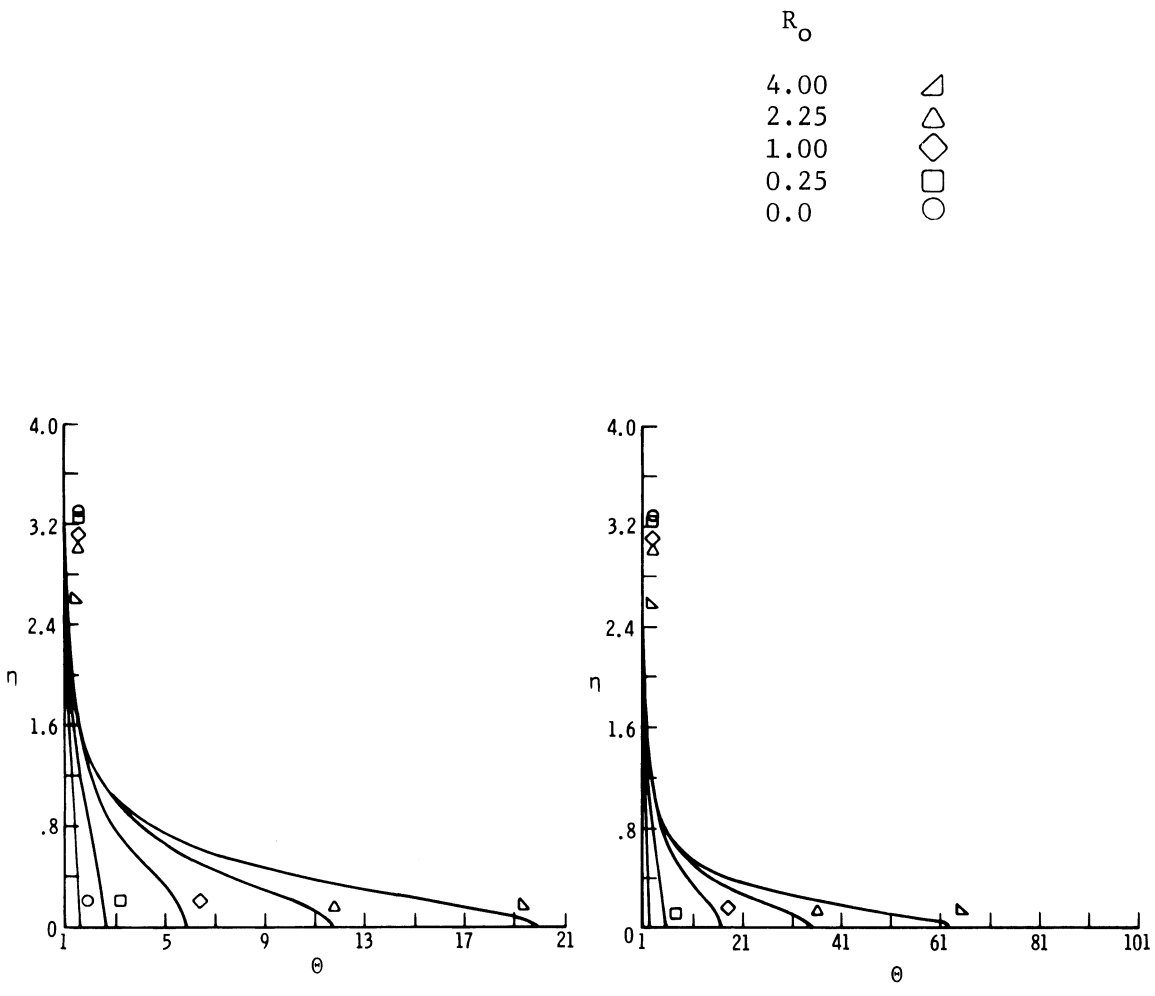

(a) s = 2.0 (b) s = 4.0

FIGURE V-13.- Compressible flow over a paraboloid with radius of curvature at the stagnation point = 1.0, at M_∞ = 10. and $\Theta_w' = 0$. Temperature function, Θ, versus normal coordinate, η, and spin parameter, R_o, at two points on the paraboloid; a) s = 2.0; b) s = 4.0.

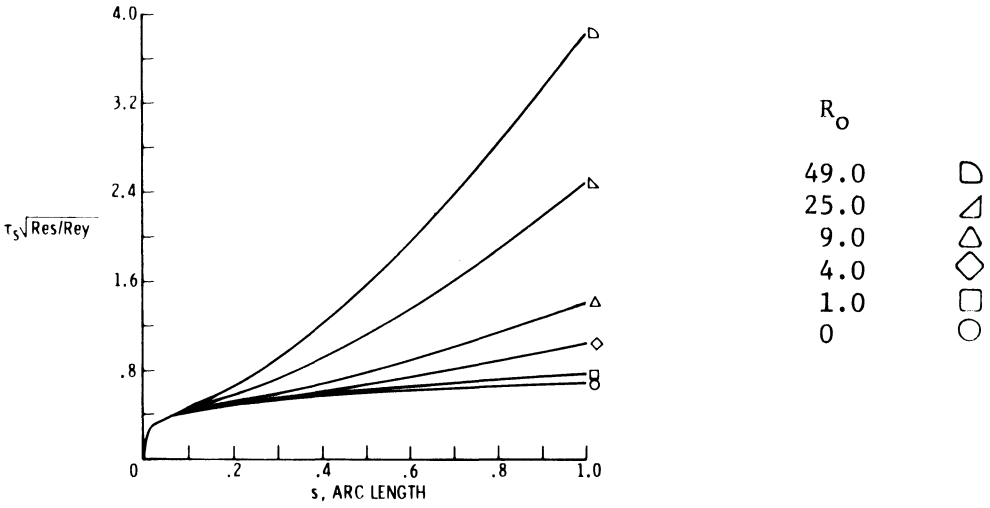

(a) MERIDONAL SHEAR STRESS, τ_s

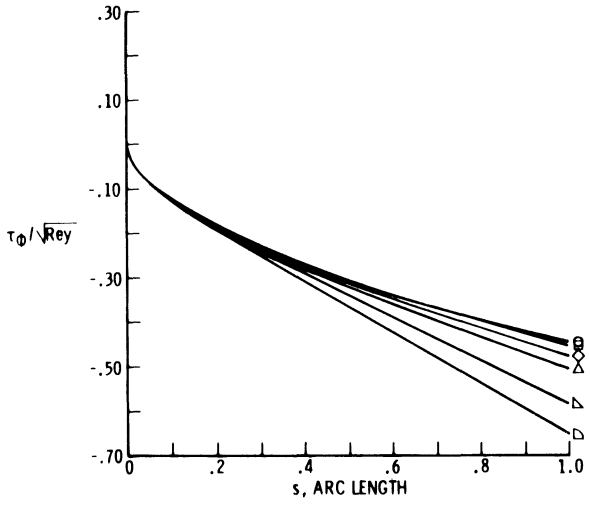

(b) CIRCUMFERENTIAL SHEAR STRESS, τ_ϕ

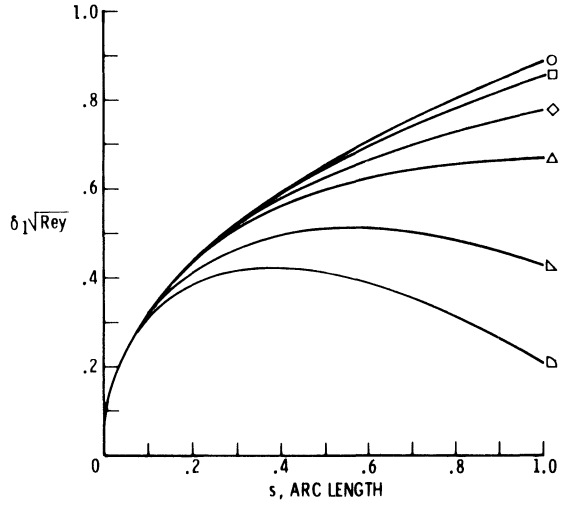

(c) DISPLACEMENT THICKNESS, δ_1

FIGURE V-14.- Incompressible flow over a 30° half angle cone. a) Meridional shear stress, τ_s; b) Circumferential shear stress, τ_ϕ; and c) Displacement thickness, δ_1, versus arc length, s, and spin parameter, R_o.

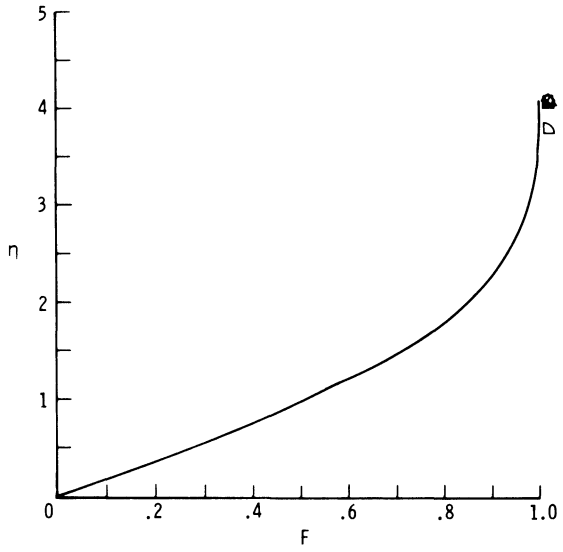

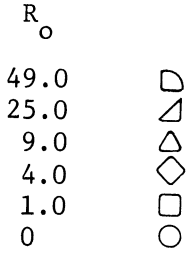

(a) s = 0.0

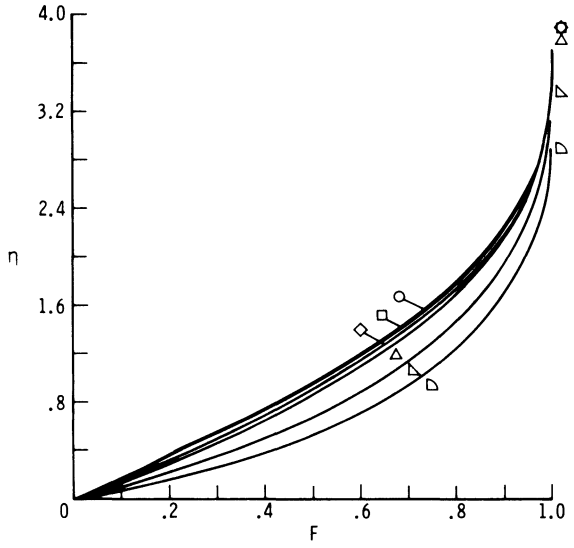

(b) s = 0.5

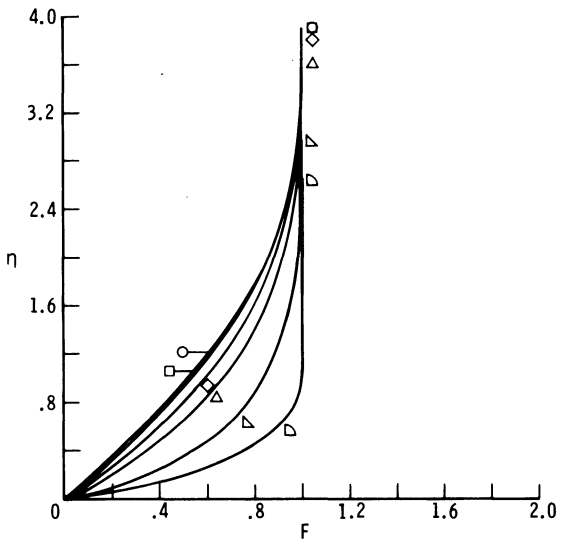

(c) s = 1.0

FIGURE V-15.- Incompressible flow over a 30° half angle cone. Meridional velocity function, F, versus normal coordinate, η, and spin parameter, R_o, at three points on the cone; a) s = 0.; b) s = 0.5; and c) s = 1.0.

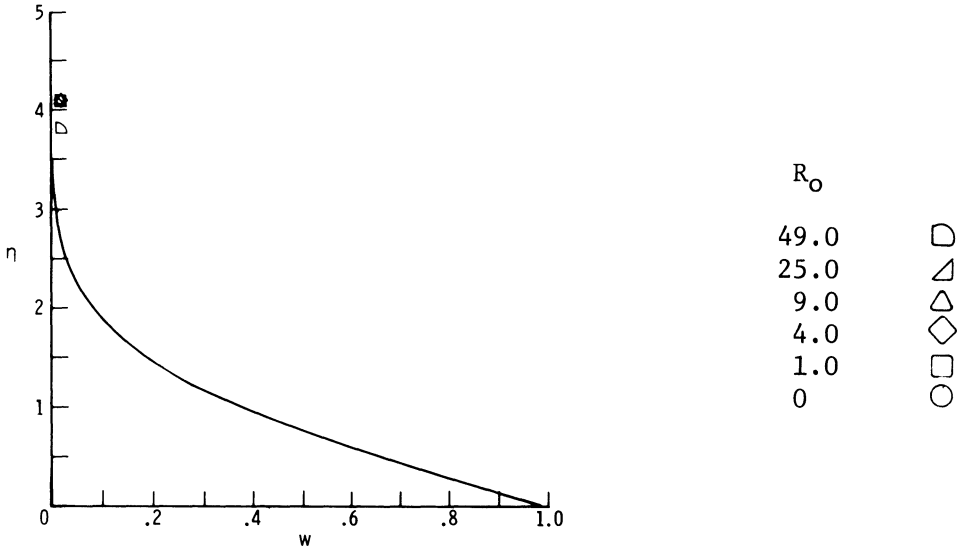

(a) s = 0.0

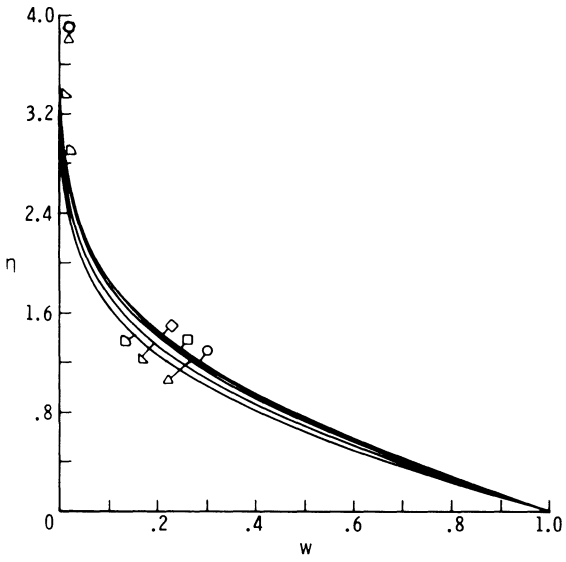

(b) s = 0.5

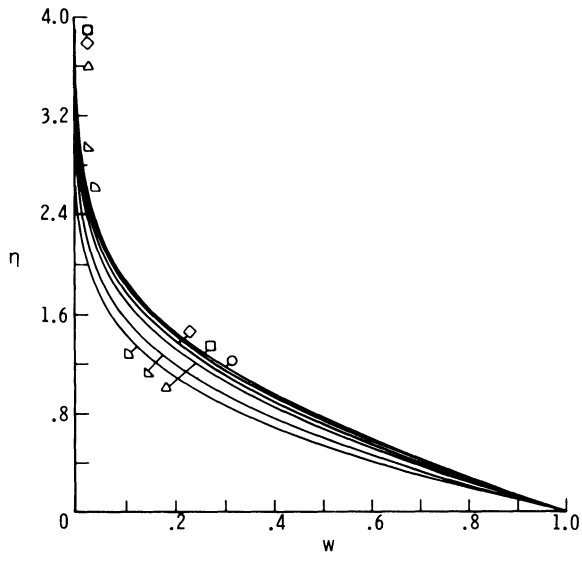

(c) s = 1.0

FIGURE V-16.- Incompressible flow over a 30° half angle cone. Circumferential velocity function, w, versus normal coordinate, η, and spin parameter, R_o, at three points on the cone; a) s = 0.; b) s = 0.5; c) s = 1.0.

the meridional velocities to be higher than the no-spin case thereby decreasing δ_1. In fact, for large enough values of either R_o or s, values of $F > 1.0$ would occur in the boundary layer thereby resulting in negative values of δ_1.

Typical velocity profiles at three s locations are shown for various values of R_o. Also indicated on these figures is the value of η_e as a function of R_o and s. The symbol location along the ordinate gives the value of η_e for the corresponding value of R_o. As in the case of incompressible flow about a sphere $\Theta \approx 1.0$ for all values of spin. The cone in question has a slant height of 1.0.

Case 5. Incompressible Flow Over a Sphere

Data for the case of a spinning sphere in incompressible flow is shown in Figure V-17 to V-19. Spin parameter values of 0, 1, 4, 9, 25, and 49 were used. Since the potential flow solution was used to determine the edge conditions flow separation occurs for these cases. The location of the point of flow separation moves forward as R_o increases. For $R_o = 0$ the separation point occurs between $s = 1.80$ and $s = 1.81$ whereas for $R_o = 49$ the separation point occurs between $s = 1.60$ and $s = 1.61$. The effect of R_o on the separation point is shown in table V-2.

The quantity $\tau_s\sqrt{\frac{R_{es}}{Rey}}$ increases with R for $S < 1.6$ but as the separation point is approached it decreases with increasing R_o. The quantity $\tau_\phi \Big/ \sqrt{Rey}$ increases steadily with increasing R_o for all values of s. The displacement thickness δ_1 increases with

TABLE V-2.- VALUE OF Bl AT WHICH SEPARATION OCCURS FOR VARIOUS VALUES OF R_o - INCOMPRESSIBLE FLOW OVER A SPHERE

R_o	Bl	s_{sep}
0	-0.44962 to -0.47826	1.80 - 1.81
1.0	-0.34463 -0.36952	1.76 - 1.77
4.0	-0.23212 -0.25313	1.71 - 1.72
9.0	-0.13677 -0.15463	1.66 - 1.67
25.0	-0.07075 -0.08649	1.62 - 1.63
49.0	-0.04071 -0.05550	1.60 - 1.65

increasing s but in all instances the effect of spin is to decrease δ_1. In fact, $\delta_1 < 0$ occur for $s < 1.0$ and $R_o > 25$. For small values of R_o, δ_1 increases with R_o as separation is approached.

The velocity profiles show that increasing R_o causes values of F greater than 1.0 in the boundary layer, however, the maximum overshoot is only about 13 percent as compared to the much greater values obtained for other cases. The circumferential velocity profiles show smaller values of w at given values of η as R_o increases. This is due to the fact that w has been nondimensionalized using the value of spin rate Ω^*. The actual value of w^* increases with R_o.

The effect of spin on the temperature in the boundary layer is negligible. The boundary condition at the wall, $\Theta'_w = 0$ results in values of $\Theta \approx 1.0$ through the boundary layer for all spin values.

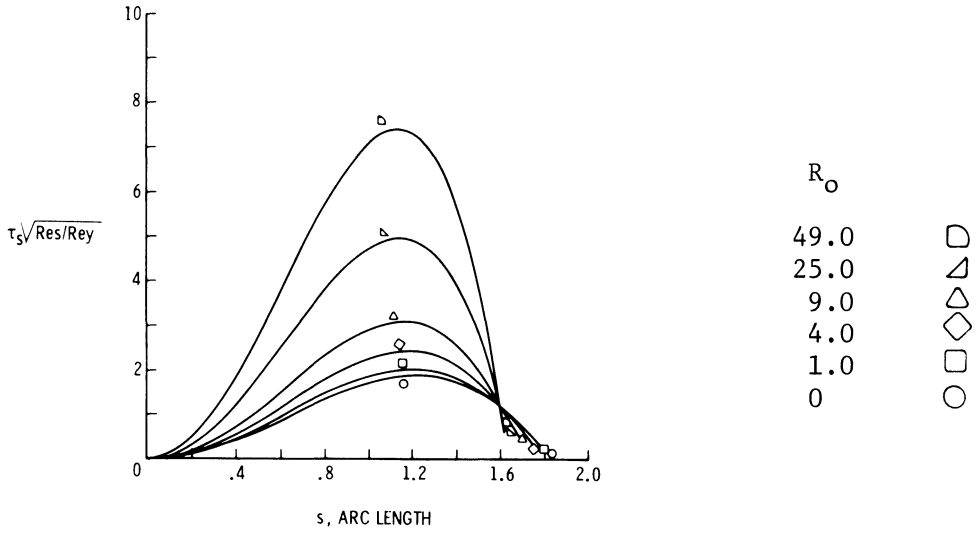

(a) MERIDONAL SHEAR STRESS, τ_s

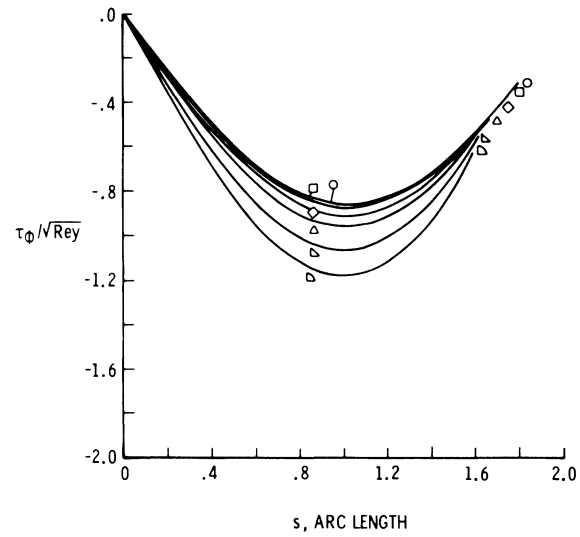

(b) CIRCUMFERENTIAL SHEAR STRESS, τ_ϕ

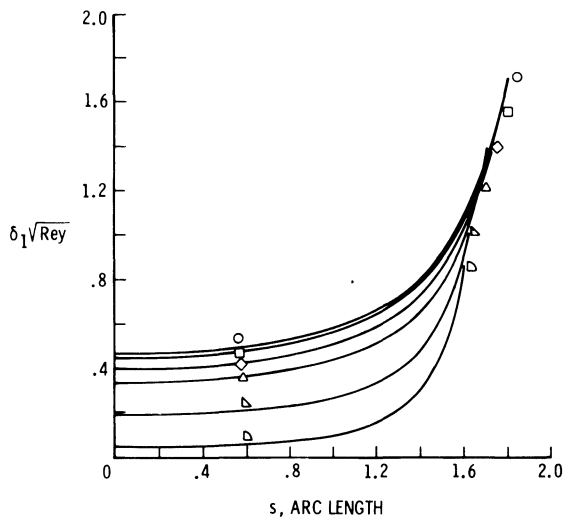

(c) DISPLACEMENT THICKNESS, δ_1

FIGURE V-17.- Incompressible flow over a sphere; a) Meridional shear stress, τ_s; b) Circumferential shear stress, τ_ϕ; and c) Displacement thickness, δ_1, versus arc length, s, and spin parameter, R_o.

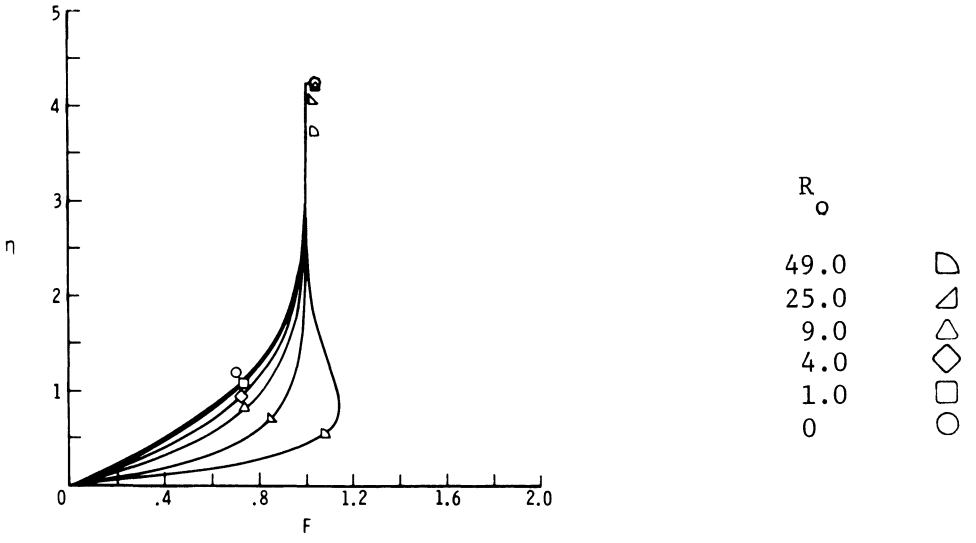

(a) s = 0.0

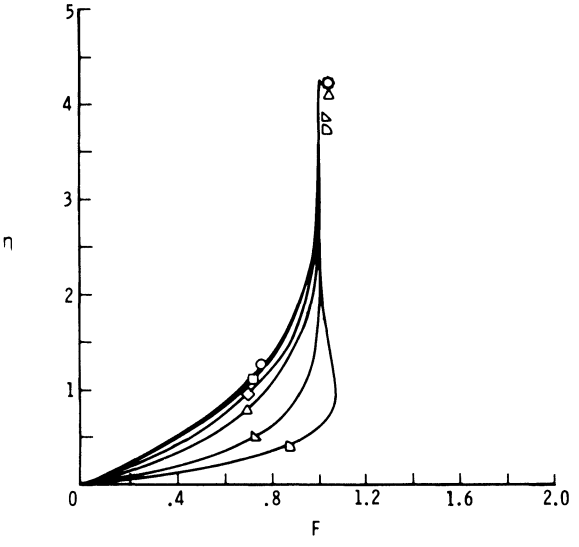

(b) s = 1.0

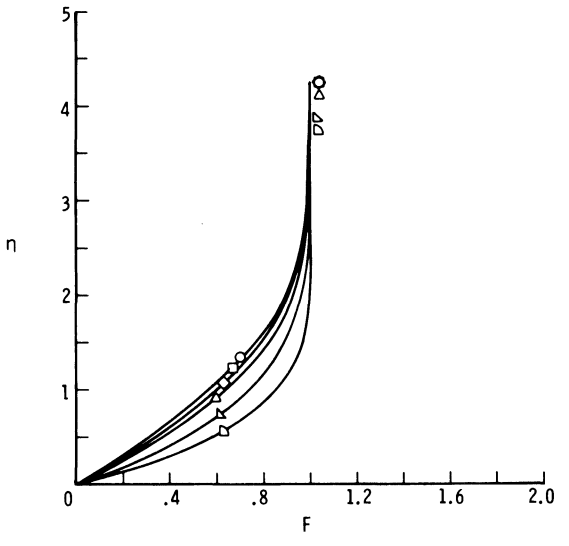

(c) s = 1.5

FIGURE V-18.- Incompressible flow over a sphere. Meridional velocity function, F, versus normal coordinate, η, and spin parameter, R_o, at three points on the sphere; a) s = 0.; b) s = 1.0; and c) s = 1.5.

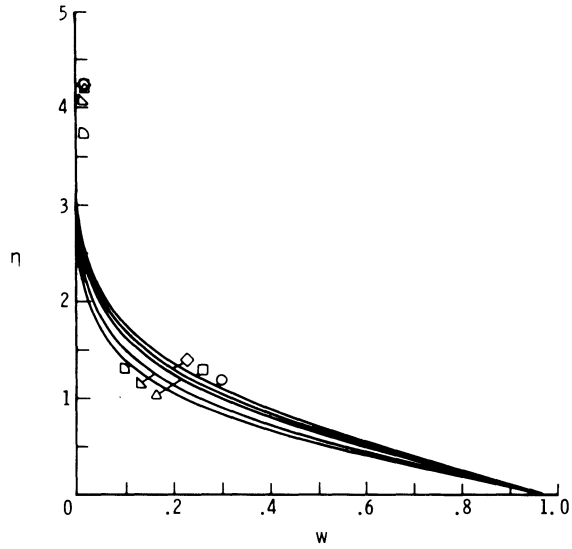

R_o

49.0
25.0
9.0
4.0
1.0
0

(a) s = 0.0

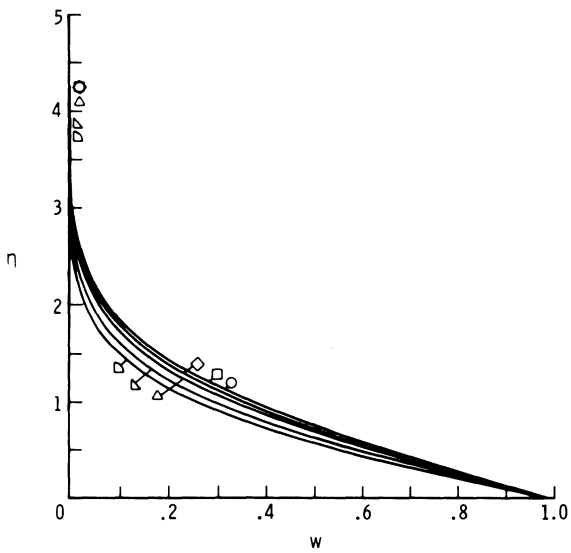

(b) s = 1.0

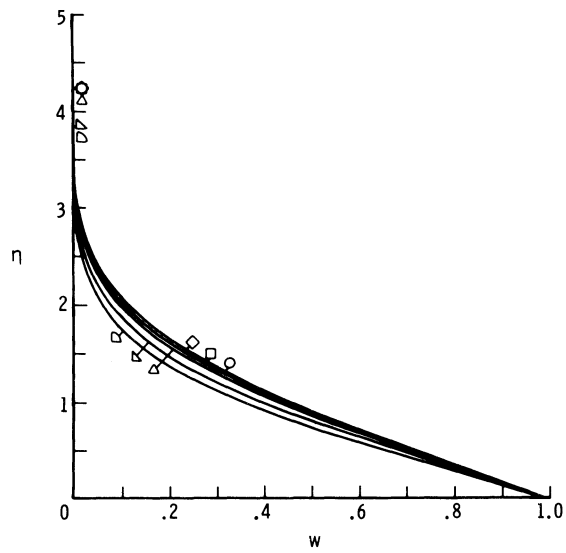

(c) s = 1.5

FIGURE V-19.- Incompressible flow over a sphere. Circumferential velocity function, w, versus normal coordinate, η, and spin parameter, R_o, at three points on the sphere; a) s = 0.; b) s = 1.0; c) s = 1.5.

Case 6. Compressible Flow Over a Hyperboloid

Figures V-21 to V-24 show the results for the case of a $M_\infty = 10$ flow over a hyperboloid with radius of curvature at the stagnation point equal to 1.0 and slope of the asymptotes equal to 22.5°. Values for R_o up to 4.0 are presented. The edge pressure is shown on figure V-20 τ_s behaves as expected, however, τ_ϕ does not vary appreciably for the spin values shown. δ_1 behaves in a manner similar to the other compressible flow cases. Maximum overshoot of the meridional velocity is about 1.87 at $s = 2.0$ and $R_o = 4.0$. Even at the relatively low values of R_o the temperature at the surface reaches values of about 18 times the edge value at $s = 2.0$ and $R_o = 4.0$.

Case 7. Compressible Flow Over a Tangent Ogive

The results for the case of a tangent ogive with a fineness ratio of 3.563 and a radius of curvature of 100 in a Mach 10.0 flow are shown on figures V-26 to V-29. The edge pressure for this case is shown on figure V-25. Values of R_o up to 4.0 were used and the solutions were obtained for values of $s \approx 47$. The tangency point occurs at a value of $s \approx 53.863$. τ_s behaves predictably, however, τ_ϕ behaves differently than any previous case. R_o has the effect of shifting the location of the maximum value of τ_ϕ and also between $s = 5$ and 40 the variation of τ_ϕ with R_o at a given value of s is not monotonic. The quantity $\tau_\phi \Omega^*$, however, does behave monotonically with respect to R_o for all s. δ_1, behaves as in the other compressible flow cases, however, due to the combined effects of a favorable pressure gradient on the tangent ogive body and spin, the values become much larger

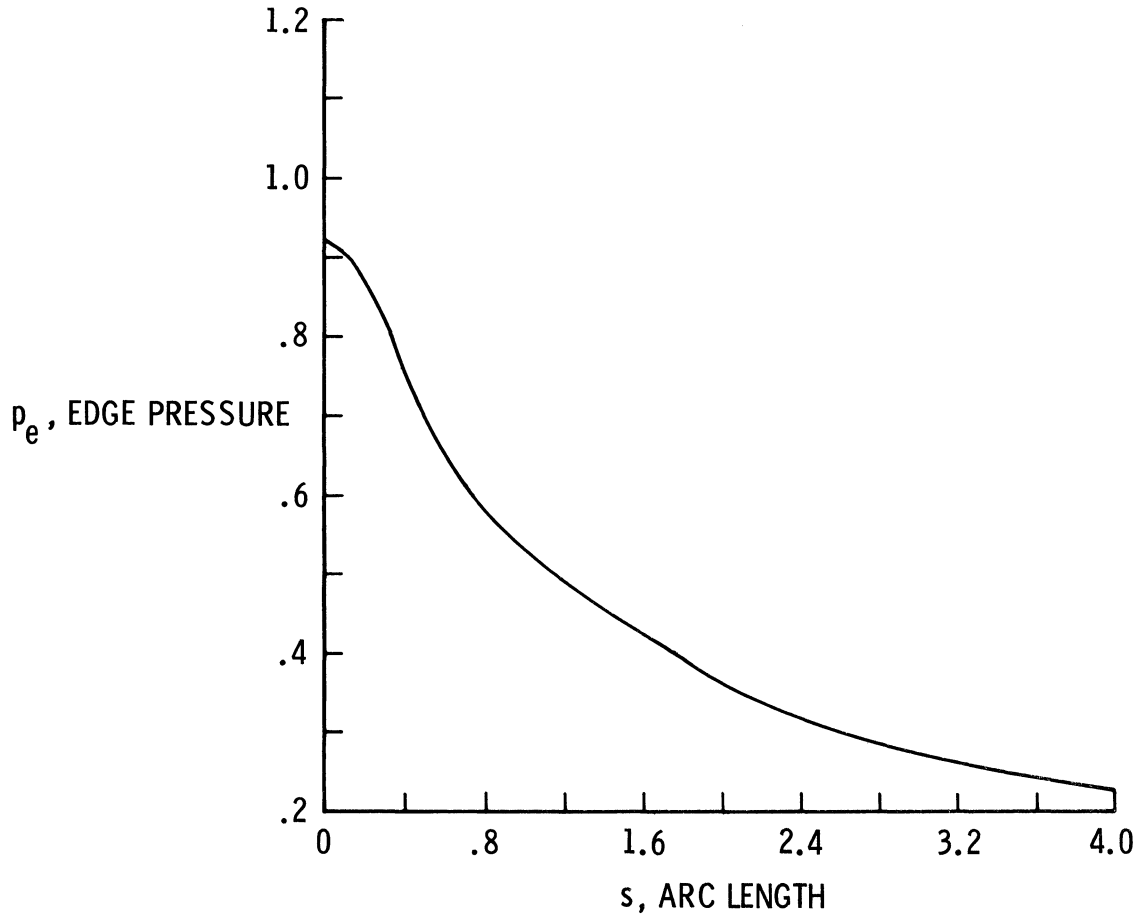

FIGURE V-20.- Compressible flow over a hyperboloid with 22.5° asymptotes, and radius of curvature at the stagnation point = 1.0. Edge pressure, p_e, versus arc length, s.

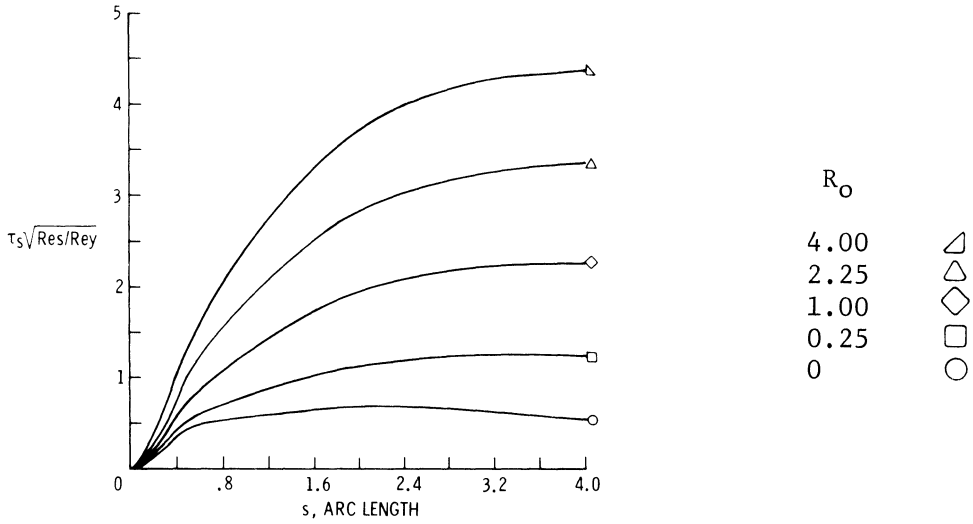

(a) MERIDONAL SHEAR STRESS, τ_s

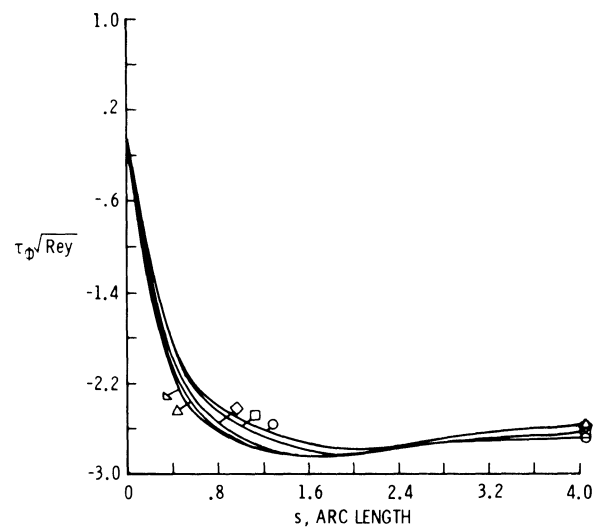

(b) CIRCUMFERENTIAL SHEAR STRESS, τ_ϕ

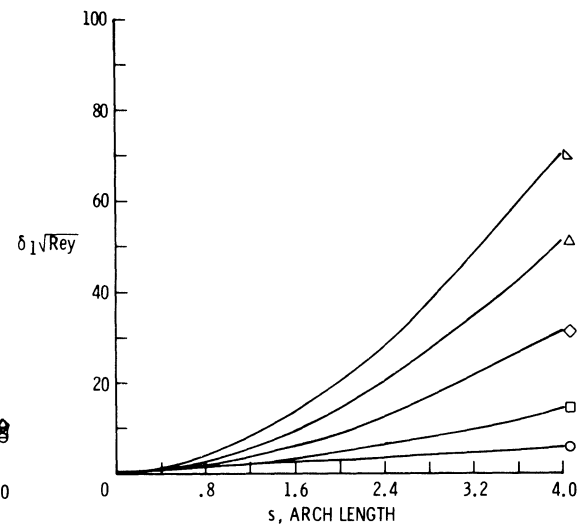

(c) DISPLACEMENT THICKNESS, δ_1

FIGURE V-21.- Compressible flow over a hyperboloid with 22.5° asymptotes, and radius of curvature at the stagnation point = 1.0, at M_∞ = 10. and θ_w' = 0; a) Meridional shear stress, τ_s; b) Circumferential shear stress, τ_ϕ; and c) Displacement thickness, δ_1, versus arc length, s, and spin parameter, R_o.

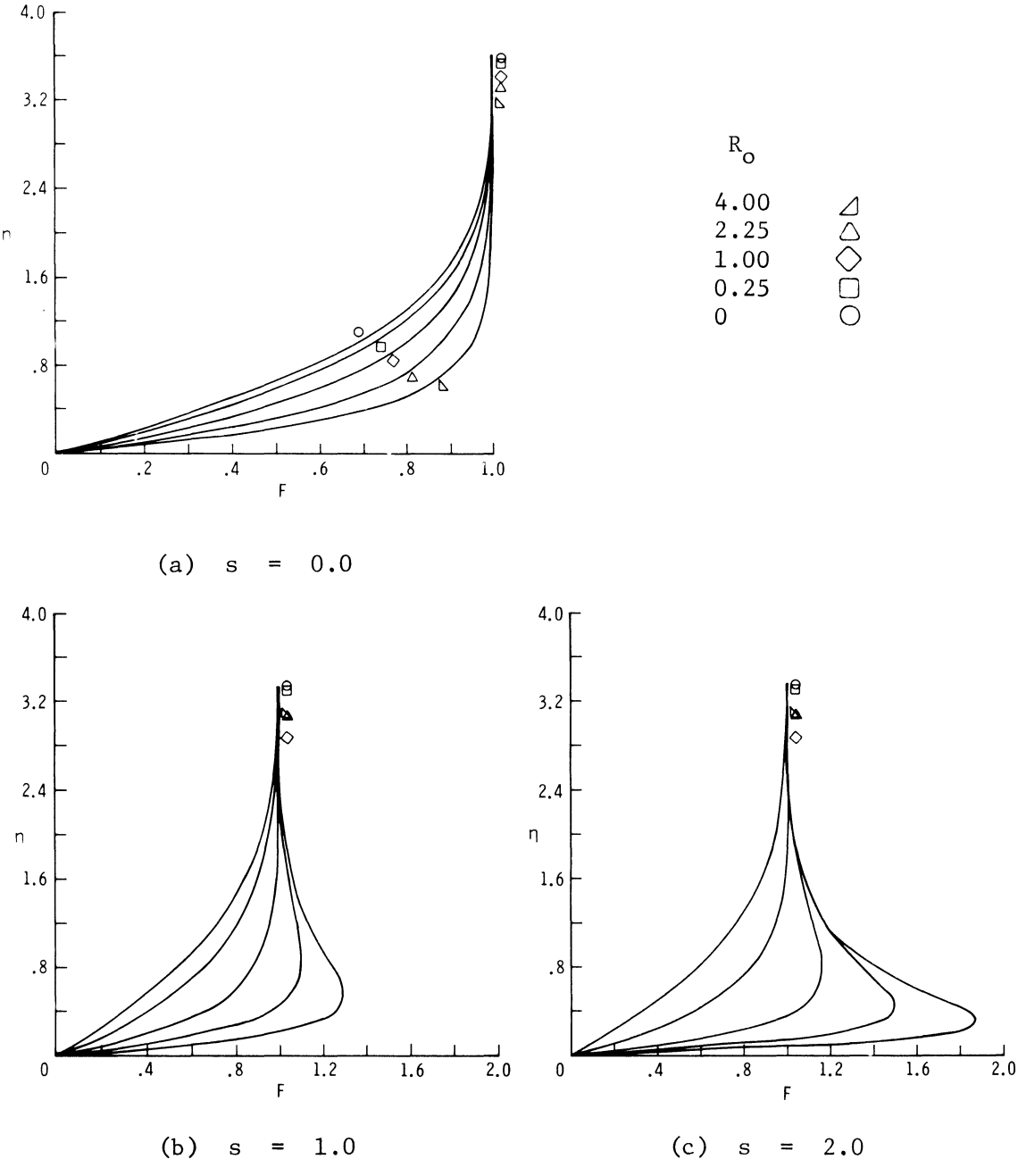

FIGURE V-22.- Compressible flow over a hyperboloid with 22.5° asymptotes and radius of curvature at the stagnation point = 1.0, at M_∞ = 10. and θ_w' = 0. Meridional velocity function, F, versus normal coordinate, η, and spin parameter, R_o, at three points on the hyperboloid; a) s = 0.; b) s = 1.0; and c) s = 2.0.

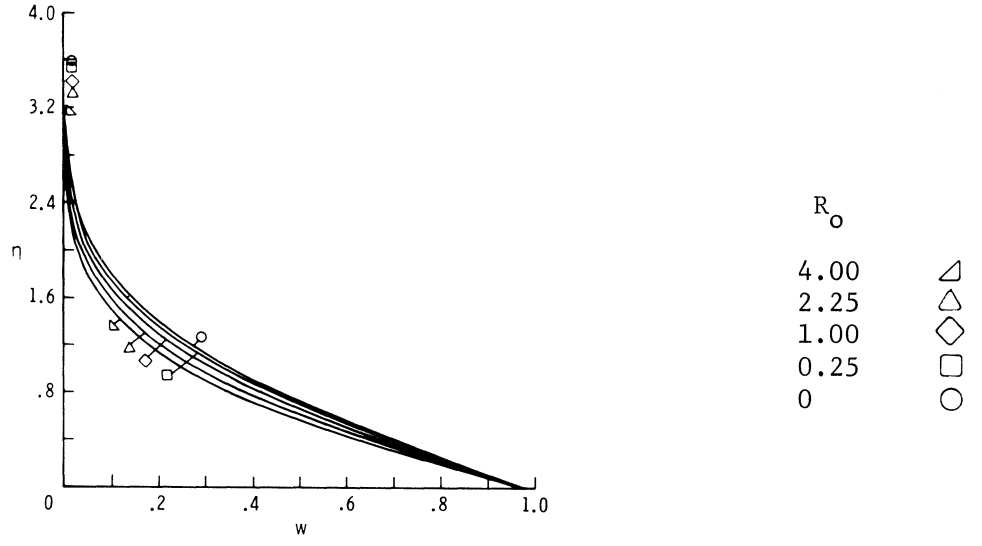

(a) s = 0.0

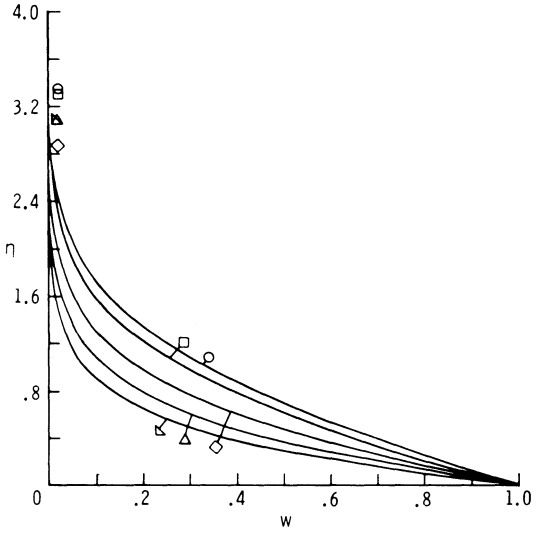

(b) s = 1.0

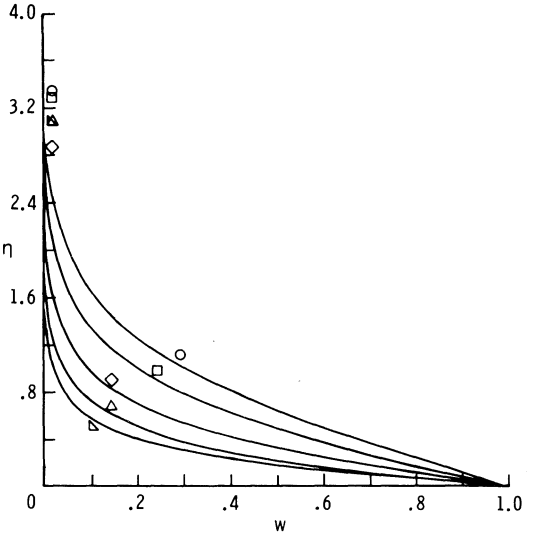

(c) s = 2.0

FIGURE V-23.- Compressible flow over a hyperboloid with 22.5° asymptotes and radius of curvature at the stagnation point = 1.0, at M_∞ = 10. and Θ_w' = 0. Circumferential velocity function, w, versus normal coordinate, η, and spin parameter, R_o, at three points on the hyperboloid; a) s = 0.; b) s = 1.0; c) s = 2.0.

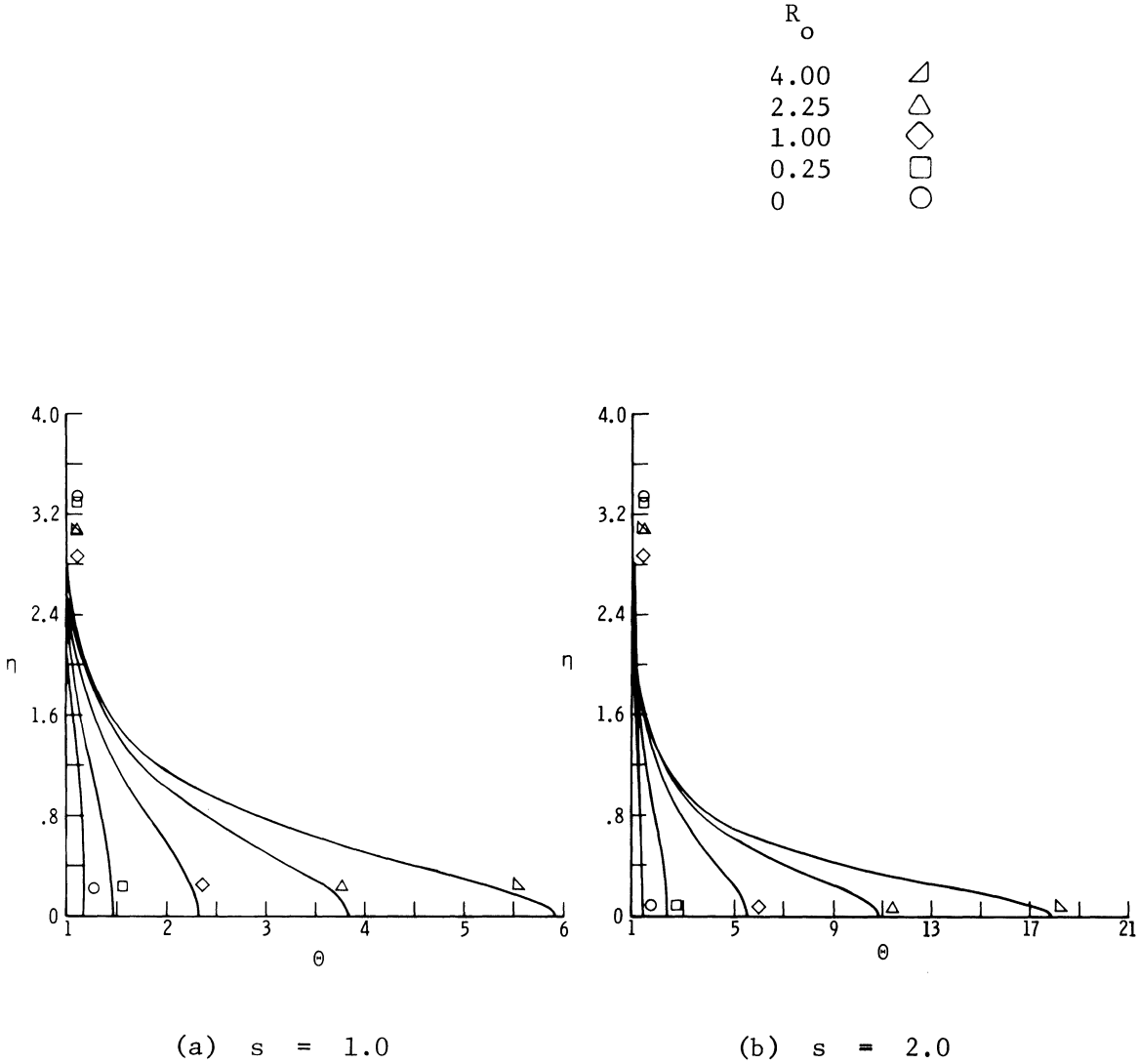

(a) s = 1.0 (b) s = 2.0

FIGURE V-24.- Compressible flow over a hyperboloid with 22.5° asymptotes and radius of curvature at the stagnation point = 1.0, at M_∞ = 10. and $\Theta_w' = 0$. Temperature function, Θ, versus normal coordinate, η, and spin parameter, R_o, at two points on the hyperboloid; a) s = 1.0; b) s = 2.0.

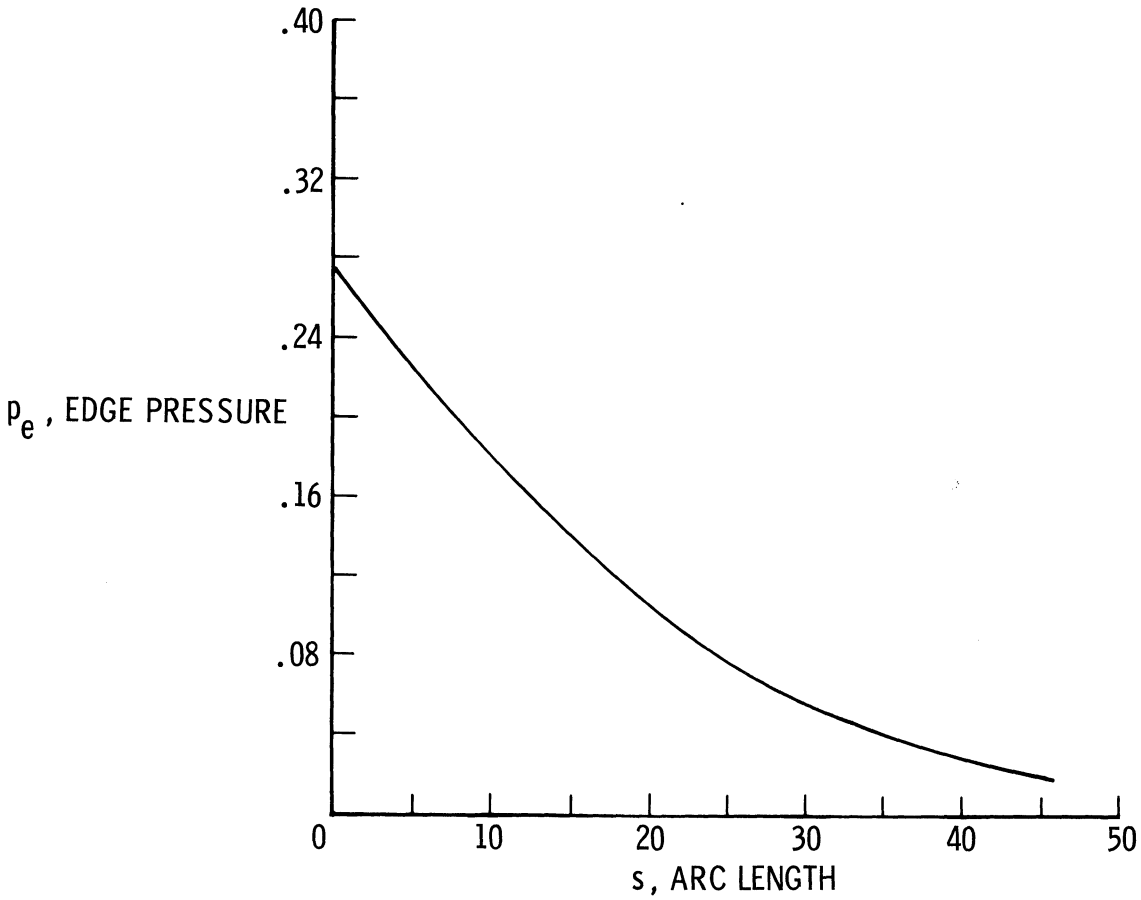

FIGURE V-25.- Compressible flow over a tangent ogive with fineness ratio of 3.563 and a radius of curvature of 100. Edge pressure, p_e, versus arc length, s.

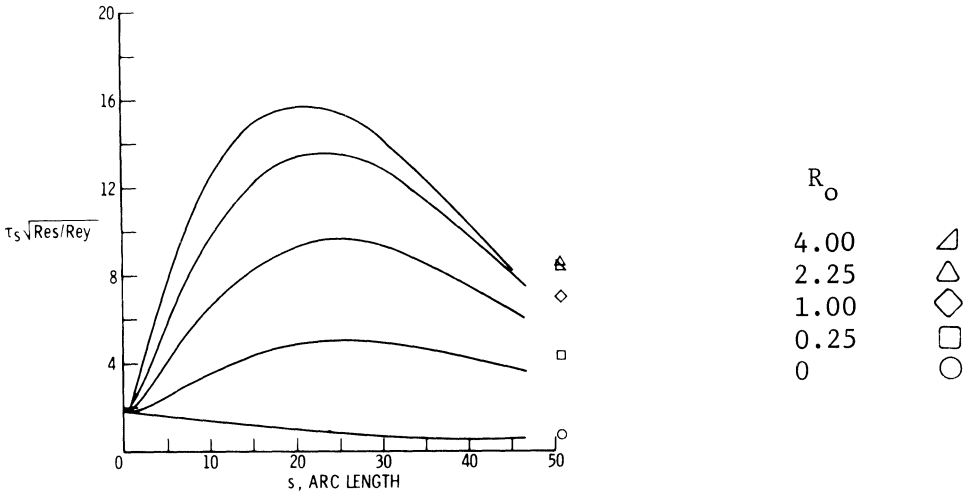

(a) MERIDONAL SHEAR STRESS, τ_s

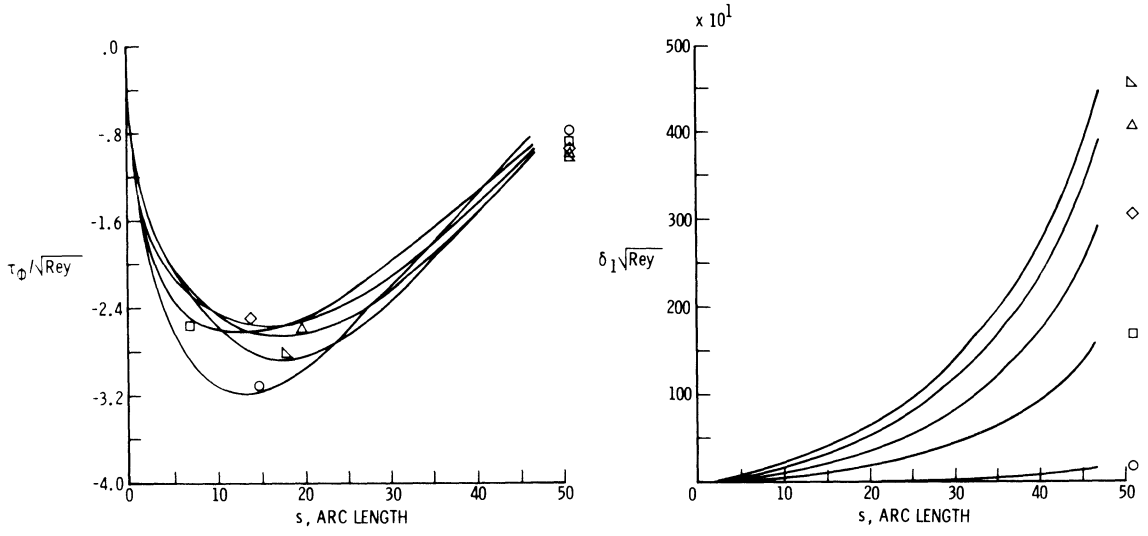

(b) CIRCUMFERENTIAL SHEAR STRESS, τ_ϕ (c) DISPLACEMENT THICKNESS, δ_1

FIGURE V-26.- Compressible flow over a tangent ogive with fineness ratio of 3.563 and a radius of curvature of 100, at M_∞ = 10. and Θ_w' = 0; a) Meridional shear stress, τ_s; b) Circumferential shear stress, τ_ϕ; and c) Displacement thickness, δ_1, versus arc length, s, and spin parameter, R_o.

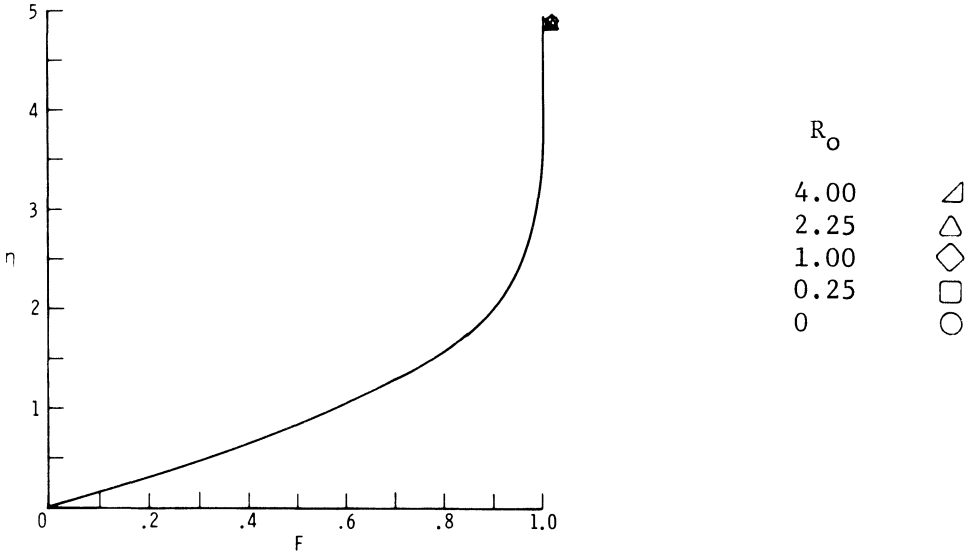

(a) s = 0.0

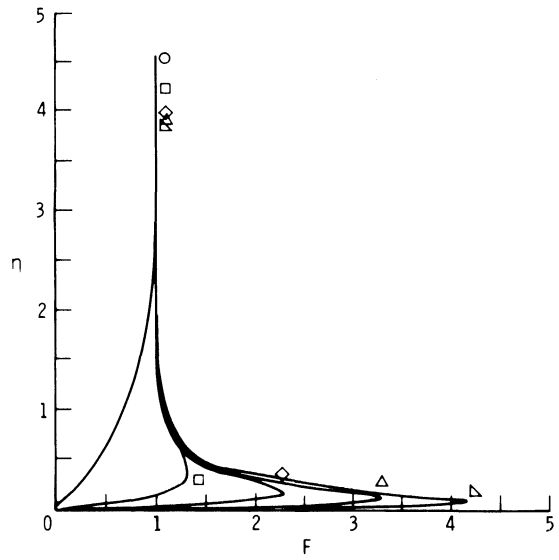

(b) s = 15.0

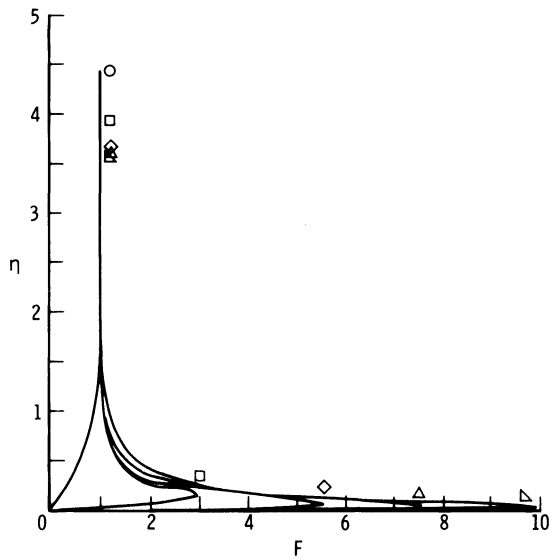

(c) s = 30.0

FIGURE V-27.- Compressible flow over a tangent ogive with fineness ratio of 3.563 and a radius of curvature of 100, at M_∞ = 10. and Θ_w' = 0. Meridional velocity function, F, versus normal coordinate, η, and spin parameter, R_o, at three points on the ogive; a) s = 0.; b) s = 15.; and c) s = 30.

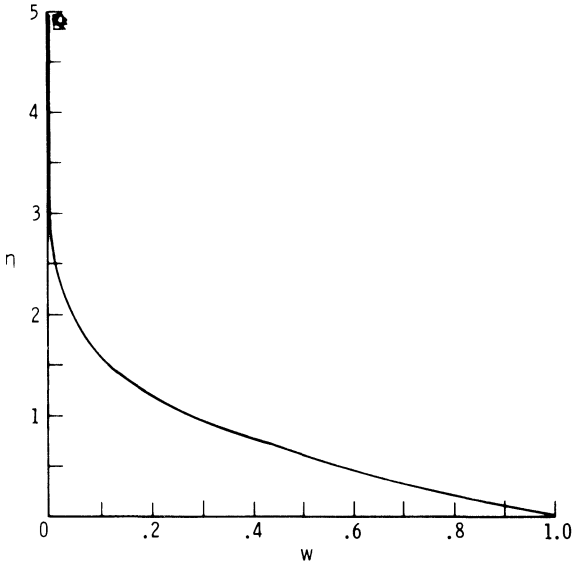

R_o

4.00
2.25
1.00
0.25
0.0

(a) s = 0.0

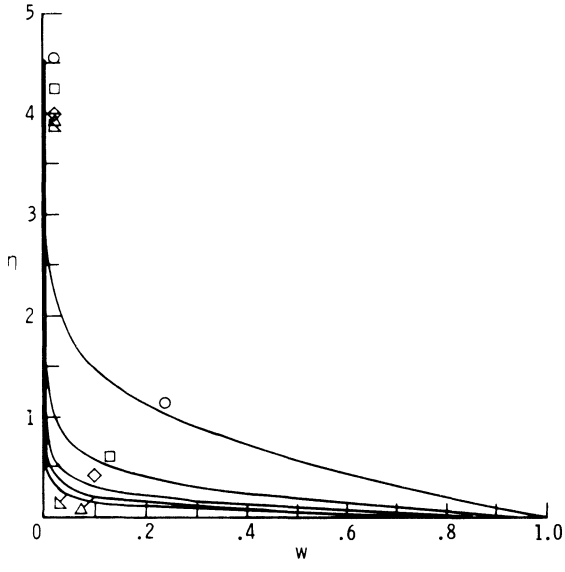

(b) s = 15.0

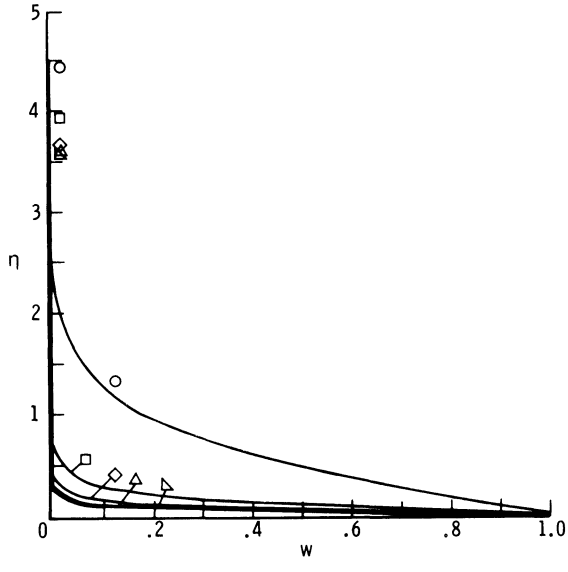

(c) s = 30.0

FIGURE V-28.- Compressible flow over a tangent ogive with fineness ratio of 3.563 and a radius of curvature of 100, at M_∞ = 10. and Θ_w' = 0. Circumferential velocity function, w, versus normal coordinate, η, and spin parameter, R_o, at three points on the ogive; a) s = 0.; b) s = 15.; c) s = 30.

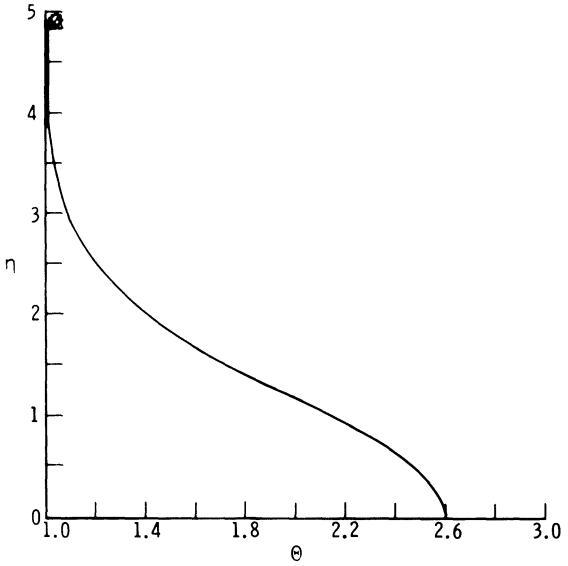

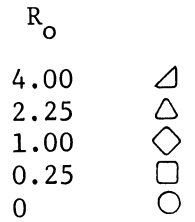

(a) s = 0.0

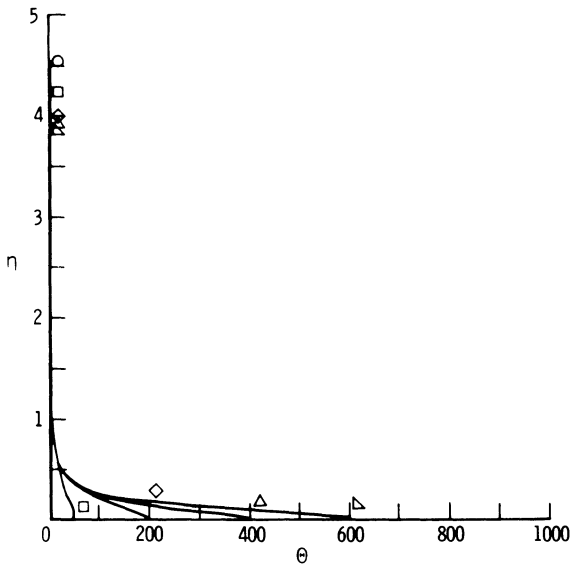

(b) s = 15.0

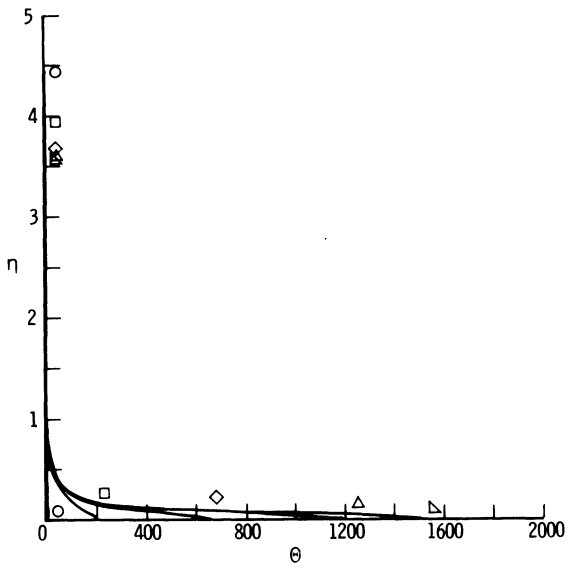

(c) s = 30.0

FIGURE V-29.- Compressible flow over a tangent ogive with fineness ratio of 3.563 and a radius of curvature of 100, at M_∞ = 10. and Θ_w' = 0. Temperature function, Θ, versus normal coordinate, η, and spin parameter, R_o, at three points on the ogive; a) s = 0.; b) s = 15.; c) s = 30.

than for previous cases. At $S = 45$ ft and $R_o = 4.0$, $\delta_1^* = .5$ ft, the maximum meridional velocity overshoot is about 10, and the maximum wall temperature is about 1600 T_e at $S = 30$ and $R_o = 4.0$. Again, these high temperatures violate the basic assumptions of this formulation.

In addition to shear stresses and displacement thickness, the shear stresses have been integrated over the surface of the various bodies and the results are presented in the form of a frictional drag coefficient, C_{D_f}, and a frictional moment, C_{m_ϕ}, versus spin rate, R_o, on figures V-30 and V-31. Following the trends observed in the behavior of τ_s with increasing R_o, C_{D_f} also increases appreciably with R_o. However, the variation of C_{D_f} with $\sqrt{R_o}$ seems to be almost linear as R_o increases. The case numbers listed on the figures are identified on table V-1. The variation of C_{m_ϕ} with $\sqrt{R_o}$ is shown on figure V-31. These results indicate that C_{m_ϕ} is almost constant with $\sqrt{R_o}$ for all configurations except the case of compressible flow over a parabola.

The effects of wall temperature were determined for the case of a 30^o cone at $M_\infty = 10$. The wall temperature was varied from $\Theta_w = .1$, 1.0 and 5.0 at value of $R_o = 0$, 25. In general, the effect of spin was to decrease the effect of wall temperature on the boundary layer variables. This is due to the fact that at $R_o = 0$ the temperature profiles which result from each of the values of Θ_w are quite *different whereas for $R_o = 25$ the temperature profiles are quite* similar. The only differences being the magnitude of Θ near the wall.

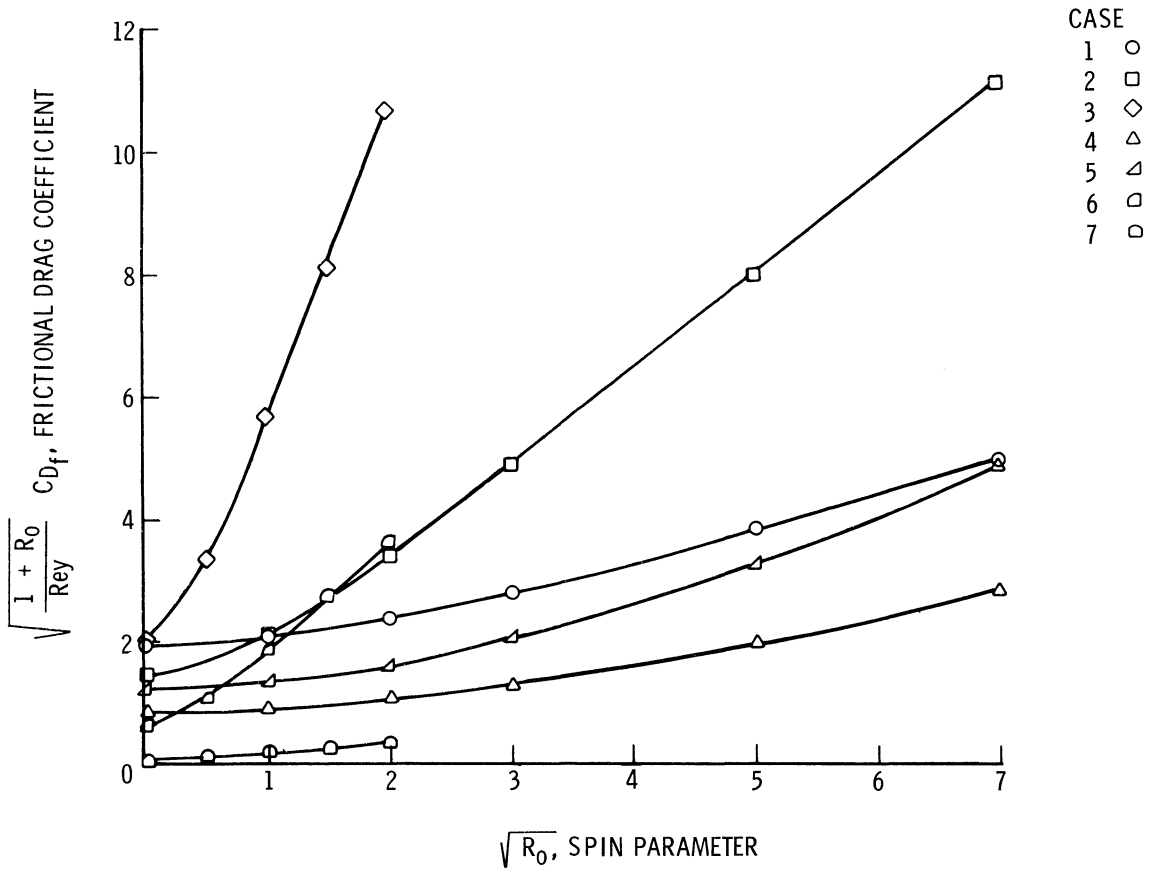

Figure V-30.- Frictional drag coefficient, C_{D_f}, versus spin parameter, R_o.

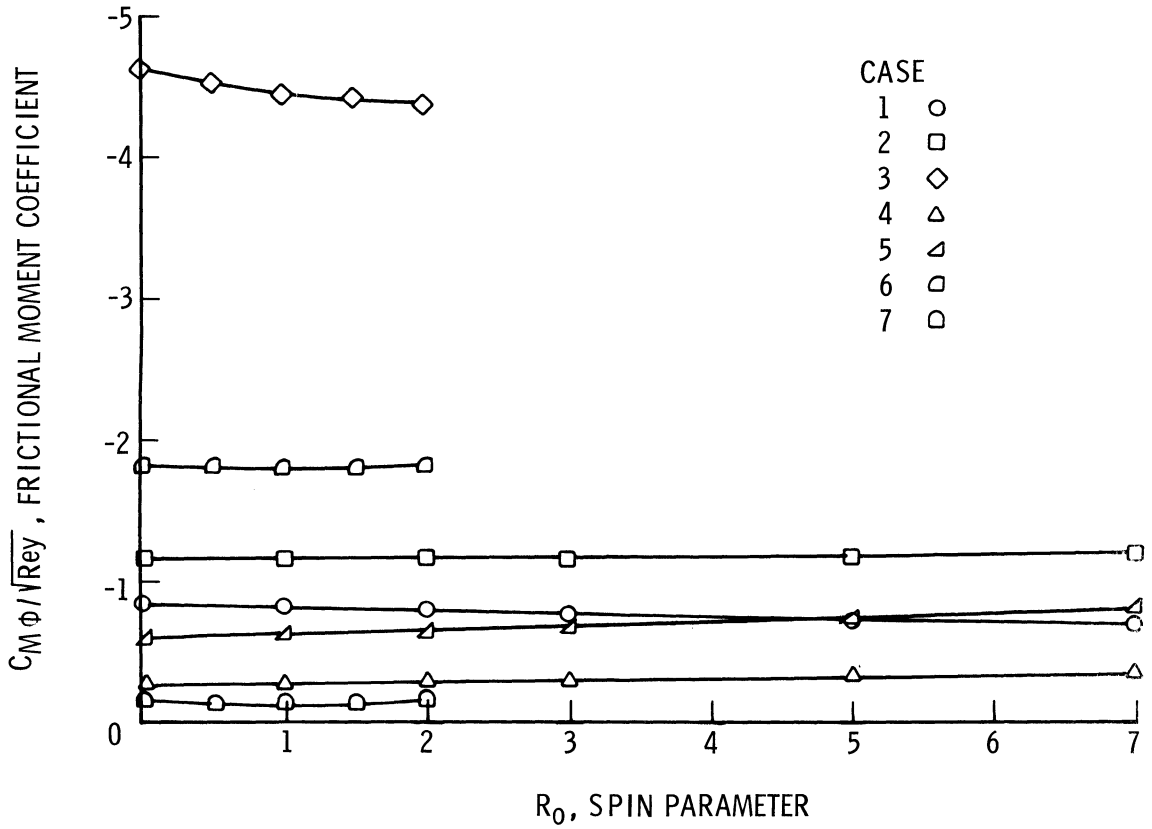

Figure V-31.- Frictional moment coefficient, C_{M_ϕ}, versus spin parameter, R_o.

The effect of increasing Θ_w on meridional and circumferential shear stress was to decrease these values resulting in a decrease in C_{D_f} and C_{m_ϕ}. δ_1 increases with increasing Θ_w due to the decrease in density in the boundary layer. Values of C_{D_f} and C_{m_ϕ} versus Θ_w and R_o are given in table V-3.

TABLE V-3.- VARIATION OF C_{D_f} and C_{m_ϕ} With Θ_w and R_o FOR A 30° CONE WITH $M_\infty = 10.0$

Θ_w	$\sqrt{1 + R_o} C_{D_f} / \sqrt{Re_y}$		$C_{M_\phi} / \sqrt{Re_y}$	
	$R_o = 0$	$R_o = 5$	$R_o = 0$	$R_o = 5$
.1	2.415	7.04	-1.081	-1.079
1.0	2.16	6.02	- .944	-1.02
5.0	1.745	4.66	- .706	- .870
*	1.927	6.016	- .830	- .711

*$\Theta_w' = 0$

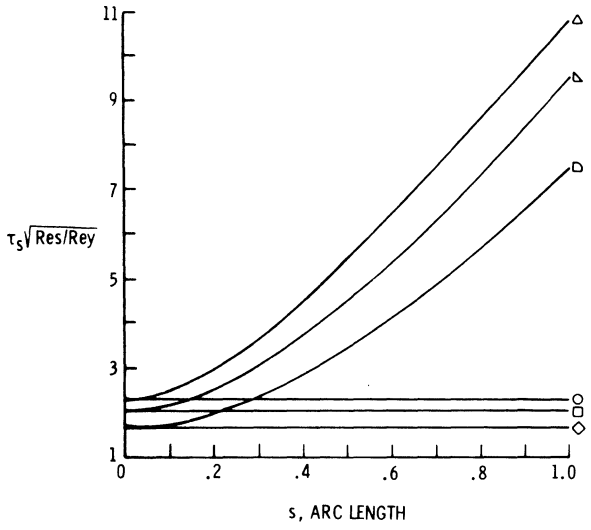

R_o	θ_w
25	5.0
25	1.0
25	0.1
0	5.0
0	1.0
0	0.1

(a) MERIDONAL SHEAR STRESS, τ_s

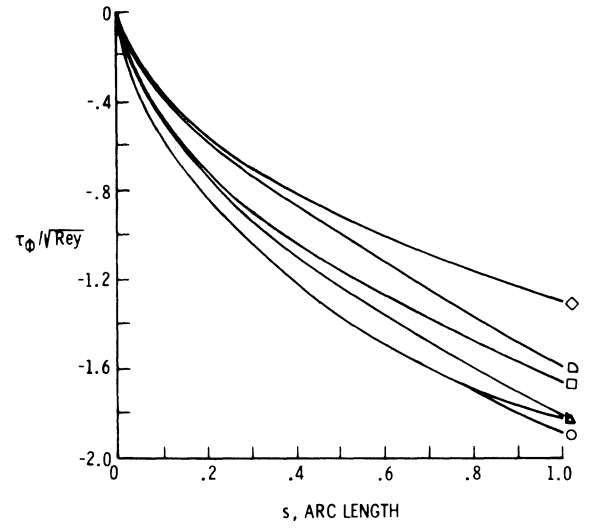

(b) CIRCUMFERENTIAL SHEAR STRESS, τ_ϕ

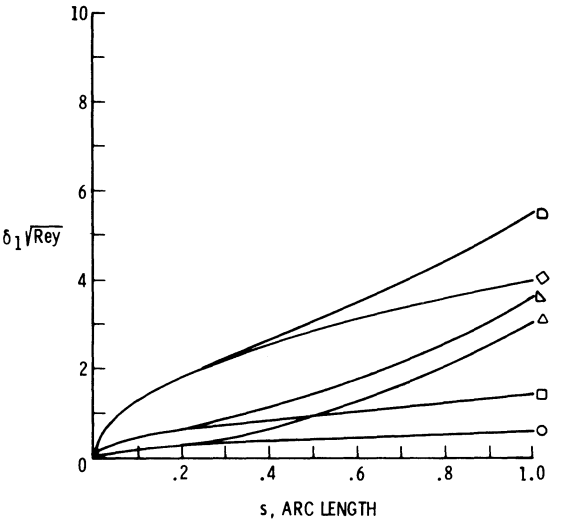

(c) DISPLACEMENT THICKNESS, δ_1

FIGURE V-32.- Compressible flow over a 30° half angle cone at M_∞ = 10. and with θ_w = 0.1, 1.0, 5.0; a)Meridional shear stress, τ_s, b) Circumferential shear stress, τ_ϕ; and c) Displacement thickness, δ_1, versus arc length, s, and spin parameter, R_o.

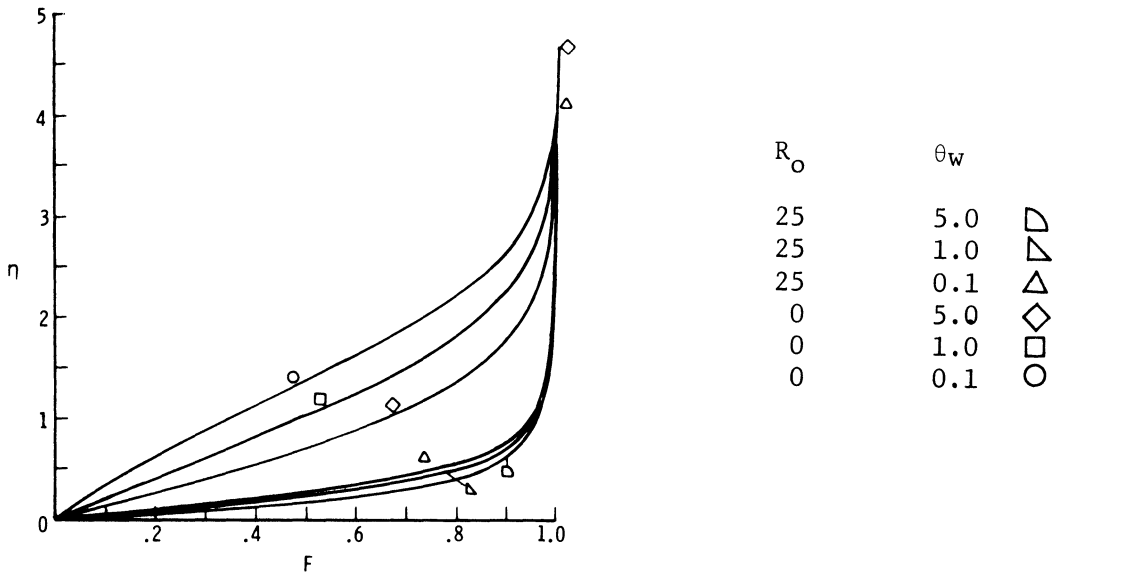

(a) MERIDONAL VELOCITY FUNCTION, τ_s

s = 1.0

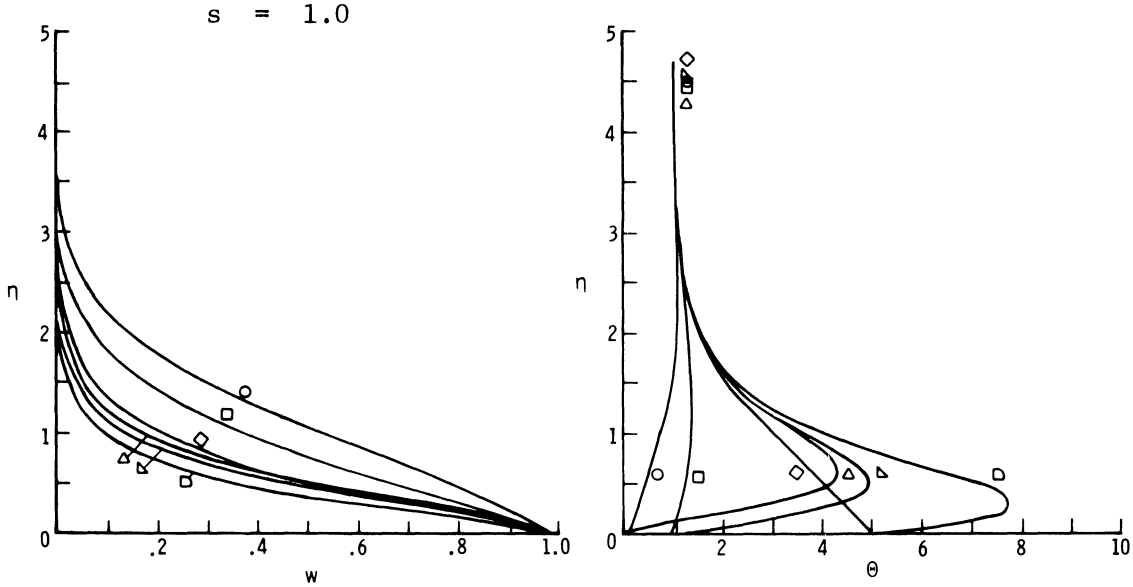

(b) CIRCUMFERENTIAL VELOCITY FUNCTION, τ_ϕ (c) TEMPERATURE FUNCTION, Θ

s = 1.0 s = 1.0

Figure V-33.- Compressible flow over a 30° half angle cone at M_∞ = 10. and with θ_w = 0.1, 1.0, 5.0. a) Meridional velocity function, F; b) circumferential velocity function, w; c) and temperature function, Θ, versus normal coordinate, η, and spin parameter, R_o, at s = 1.0.

CONCLUDING REMARKS

The results of this study indicate that an implicit finite difference method can be used to obtain an accurate solution to the equations describing the laminar compressible or incompressible boundary layer on a spinning body of revolution. The accuracy of the solution will depend to a great deal on the gradients which the boundary layer variables exhibit. In general, when larger gradients occur, that is, when the flow departs from a similarity type flow convergence becomes very slow and a sufficient number of iterations must be specified at each s location to insure the accuracy of the solutions.

Although some of the spin rates used in this analysis exceed values which would realistically be expected to be encounted, the results, nevertheless, are useful in that the trends of the boundary layer variables with spin rate have been determined. One must, of course, beware of extrapolating such data to cases in which the basic assumptions of this analysis would be violated.

The results of this study indicate that the effect of spin on the meridional variables F, δ_1 and τ_s is appreciable whereas with proper nondimensionalization the variation of circumferential properties with spin is very slight.

This analysis will provide a firm basis for solving the problem which has to date been attacked by highly restrictive method. This is the problem of boundary layer flow over a spinning body at angle of attack. The solution to this problem would open the way to a prediction of Magnus forces on spinning projectiles, reentry bodies, launch vehicles, etc. However, even with the establishment of a solution for bodies at zero angle of attack the problems associated with extension of this solution to include angle-of-attack effects include the development of a three dimensional boundary layer solution, and a three dimensional inviscid solution. The latter will have to be capable of account for the second order effects of displacement thickness which becomes a major contributor to Magnus forces.

One potential application of spinning a body at the high rates considered in this report is to generate high boundary layer temperatures. For example, if a 30^{o} half-angle cone with a 1 ft base diameter is placed in a test facility under the conditions previously analyzed, a surface temperature of about 13,500 ^{o}R would result. It would require a moment of about 26.4 ft-lbs. to overcome the frictional torque and about 340 horsepower or 250 kW of power. The solutions presented herein were obtained using a Control Data Corporation (CDC) 6600 computer. The program language is FORTRAN IV. Storage requirements for the program are 140000 core locations and running times are less than 2 minutes per case.

CHAPTER VI. REFERENCES

1. Hannah, D. M.: Forced Flow Against a Rotating Disc. H.R.C. technical report ROM No. 2772, April 1947 (1952).

2. Cochran, W. G.: Flow Due to a Rotating Disc. Cambridge Philosophical Soc. Proceedings, Vol. 30, July 1934.

3. Homann, Von F.: The Effect of High Viscosity on Flow Around a Cylinder and Around a Sphere. Zeitschr. f. angeu. Math. u. Mech., No. 16, Vol. 3, June 1936.

4. Tifford, Arthur N.; and Chu, Sheng To: On the Flow Around a Rotating Disc in a Uniform Stream. U.A.S. Reader Forum, Vol. 19, No. 4, April 1952.

5. Illingsworth, C. R.: The Laminar Boundary Layer of a Rotating Body of Revolution. Phil. Mag., Ser. 7, Vol. 44, No. 351, April 1953.

6. Schlicting, H.: Laminary Flow About a Rotating Body of Revolution in an Axial Stream. NASA TM-1415, February 1956. (1953 in German).

7. Illingsworth, C. R.: Boundary-Layer Growth on a Spinning Body. Phil. Mag., Ser. 7, Vol. 45, P. 1, January 1954.

8. Schmidt, L. E.: The Dynamic Properties of Pure Cones and Cone Cylinders. BRL Report No. 759, January 1954.

9. Kelly, Howard R.: An Analytical Method for Predicting the Magnus Forces and Moments on Spinning Projectiles. NOTS TM-1634, August 1954.

10. Fehrman, Alvin L.: Effect of Spin and Yaw on Boundary Layer Transition Along a Body of Revolution. Thesis presented to California Institute of Tech., 1955.

11. Martin, J. C.: Magnus Characteristics of Finned and Nonfinned Projectiles. AIAA Journal, Vol. 3, No. 1, January 1965.

12. Krahn, E.: The Laminar Boundary Layer on a Rotating Cylinder in Crossflow. NAVORD Report 4022, June 1955.

13. Sedney, R.: Laminar Boundary Layer on a Spinning Cone at Small Angles of Attack. BRL Report No. 991, September 1956.

14. Wood, Robert M.; and Kistler, Ingeborg, B.: The Determination of Twist and Yaw of Projectile Boundary Layers by Photographic Measurements. BRL Report No. 981, September 1956.

15. Fieberg, M.: Laminar Boundary Layer on a Spinning Circular Cone in Supersonic Flow at a Small Angle of Attack. Air Force Office of Scientific Research TN-56-532, June 1956.

16. Martin, J. C.: On Magnus Effects Caused by the Boundary Layer Displacement Thickness on Bodies of Revolution at Small Angles of Attack. J.A.S. Vol. 24, No. 6, June 1957.

17. Sedney, R.: Laminary Boundary Layer on a Spinning Cone at Small Angles of Attack in a Supersonic Flow. J.A.S. Vol. 24, No. 6, June 1957.

18. Schlicting, H.; and Truckenbrodt, E.: The Flow Around a Rotating Disc in a Uniform Stream. J.A.S. Reader Forum, September 1957.

19. Yamaga, V.: An Approximate Solution of the Laminar Boundary Layer on a Rotating Body of Revolution in Uniform Compressible Flow. Proceedings of the 6th Japan National Congress for Applied Mechanics, pp. 295-298, March 1957.

20. Siekmann, V.: The Thermal Laminar Boundary Layer on a Rotating Sphere. AGARD Report 283, April 1960.

21. Tien, C. L.: Heat Transfer by Laminar Flow From a Rotating Cone. Journal of H.T., August 1960.

22. Rubinow, S. I.; and Keller, Joseph B.: The Transverse Force on a Spinning Sphere Moving in a Viscous Fluid. Journal of Fluid Mechanics, Vol. II, pt. 3, November 1961.

23. Bowden, F. P.; and Lord, R. G.: The Aerodynamic Resistance to a Sphere Rotating at High Speed. Proceedings of the Royal Society, No. 1345, Vol. 27, January 1963.

24. Hoskin, N. E.: The Laminar Boundary Layer on a Rotating Sphere. 50 Johne Grenzschichtforschung Herausgegeben von H. Görtler und W. Tollmien, Verlag Friedr. Viewig u. Sohn Braunschweig, 1955.

25. Fox, Jay: Boundary Layer on Rotating Spheres and Other Axisymmetric Shapes. NASA TN D-2491, September 1964.

26. Rott, Nicholas; and Lewellen, W. S.: Boundary Layers in Rotating Flows. Aerospace Corporation, ATN-6A(9227)-6, September 4, 1964.

27. Platou, Anders S.: Magnum Characteristics of Finned and Nonfinned Projectiles. AIAA Journal, Vol. 3, No. 1, January 1965.

28. Koh, J. C.; and Price, J. F.: Nonsimilar Boundary Layer Heat Transfer of a Rotating Cone in Forced Flow. Boeing Scientiic Laboratory. D1-82-0433, April 1965.

29. Tien, C. L.; and Tsuji, I. J.: A Theoretical Analysis of Laminar Forced Flow and Heat Transfer About a Rotating Cone. AMSE Paper No. 64-HT-34, 1964.

30. Moore, F. K. (editor): Theory of Laminar Flows, Princeton Univ. Press, p. 329, 1964.

31. Blottner, F. G.: Chemical Non-Equilibrium Boundary Layer. AIAA Journal, Vol. 2, No. 2, February 1964.

32. Whitehead, C. G.; and Canetti, G. S.: The Laminar Boundary Layer on Solids of Revolution. Phil. Mag., Vol. 41, No. 321, October 1950.

33. Schlicting, H.: Boundary Layer Theory. Sixth edition, McGraw-Hill Book Co., 1968, pp. 181-184.

34. Davis, R. T.; and Flugge-Lotz, I.: Laminar Compressible Flow Part Axisymmetric Blunt Bodies (Results of a Second-Order Theory). Tech. Rept. No. 143, Div. of Eng. Mech., Stanford Univ., Stanford, California, 1963.

35. Flugge-Lotz, I.; and Blottner, F. G.: Computation of the Compressible Laminar Boundary-Layer Flow Including Displacement Thickness Interaction Using Finite Difference Methods. Tech. Rept. No. 151, Div. of Eng. Mech., Stanford Univ., Stanford, California, 1962.

36. Richtmyer, R. D.: Difference Methods for Initial Value Problems. Interscience Publishers, Inc., New York, 1957.

37. Hildebrand, F. B.: Advanced Calculus for Engineers. Prentice-Hall, Inc., 1960.

38. Lomax, H.; and Inouye, M.: Numerical Analysis of Flow Properties About Blunt Bodies Moving at Supersonic Speeds in an Equilibrium Gas. NASA TR R-204, July 1964.

39. Walsh, J. L.; Ahlberg, J. H.; and Nilson, E. N.: Best Approximation Properties of the Spline Fit. Journal of Math. and Mech., Vol. II, No. 2, 1962.

CHAPTER VII. ACKNOWLEDGMENTS

The author is deeply indebted to Dr. R. T. Davis for his many suggestions and criticisms throughout this effort and to the entire committee for their review and comments on this thesis.

The author is also indebted to the NASA and in particular to Mr. Vernon L. Alley for their support and encouragement during this effort.

Thanks are also due to Mrs. Maria Stephens, who programed the computer plotting subroutines from which the figures in chapter V were made, and to Mrs. Yvonne Powell and Mrs. Norma Price who typed the manuscript.

Lastly, I wish to acknowledge my family whose patience during this effort has been outstanding.

The vita has been removed from the scanned document

THE LAMINAR BOUNDARY LAYER ON SPINNING BODIES OF REVOLUTION

By

Ralph John Muraca

ABSTRACT

The subject of this dissertation is the analysis and solution of the equations describing the laminar boundary layer on axisymmetric bodies immersed in an oncoming stream and spinning at a constant rate about their axis of revolution. The flow is allowed to be compressible or incompressible and the geometries for which solutions are obtained include the sphere, cone, paraboloid, hyperboloid and tangent ogive. The only limitation on spin rate involves the assumption that the pressure across the boundary layer remain essentially constant. The method of solution for the set of parabolic nonlinear partial differential equations which describe the boundary layer is an implicit finite difference technique. A study of step size and convergence criteria is included to determine the accuracy of the numerical method. Comparisons with previous approximate methods are also presented in an effort to establish confidence in these results. Boundary layer characteristics in the form of shear stress, heat transfer, velocity and temperature profiles, displacement thickness and frictional drag and moment coefficients are presented for each geometry over a wide range of spin rates.